MEMBERS OF THE *ARABIDOPSIS THALIANA* FL FAMILY ACT WITH ARF MACHINERY TO LOCALIZE PIN1 DURING AUXIN RELATED DEVELOPMENTAL PROCESSES

HOULIN YU
Bachelor of Science, Northwest A&F University, China, 2016

A Thesis
Submitted to the School of Graduate Studies
of the University of Lethbridge
in Partial Fulfilment of the
Requirements for the Degree

MASTER OF SCIENCE

Biological Sciences
University of Lethbridge
LETHBRIDGE, ALBERTA, CANADA

MEMBERS OF THE *ARABIDOPSIS THALIANA* FL FAMILY ACT WITH ARF MACHINERY TO LOCALIZE PIN1 DURING AUXIN RELATED DEVELOPMENTAL PROCESSES

HOULIN YU

Date of Defense: August 8, 2018

Dr. Elizabeth Schultz Supervisor	Associate Professor	Ph.D.
Dr. James Thomas Thesis Examination Committee Member	Professor Emeritus	Ph.D.
Dr. Roy Golsteyn Thesis Examination Committee Member	Associate Professor	Ph.D.
Dr. Steve Wiseman Chair, Thesis Examination Committee	Associate Professor	Ph.D.

DEDICATION

In the loving memory of my grandma Li

ABSTRACT

PINFORMED (PIN) proteins are phytohormone auxin efflux carriers. By polar distribution and dynamic re-localization via the endomembrane vesicle trafficking system, PIN proteins control many auxin-dependent developmental processes. Vesicle trafficking is controlled by protein machineries including small G protein ADP ribosylation factors (ARFs) and their regulators ARF-GTPase activating proteins (ARF-GAPs) and ARF-guanine nucleotide exchange factors (ARF-GEFs). *FORKED1* (*FKD1*) is part of the nine member Arabidopsis *FKD1-LIKE* (*FL*) gene family. My results show that FKD1 and SCARFACE (SFC/FKD2, an ARF-GAP) co-localize with BIGs (ARF-GEFs) and they all co-localize with PIN1 in vesicles. Mutant analysis supports the idea that FKD1, SFC and BIGs are acting in the same secretory pathway, and together with ARFA group, these proteins control PIN1 localization and therefore the auxin transport in leaves, hypocotyls and roots. My results also show that FL3 is acting in a different manner from FKD1, likely in the endocytic pathway.

ACKNOWLEDGMENTS

Wholeheartedly thank my thesis supervisor, Dr. Elizabeth Schultz for her consistent support and patience throughout my program and above all for offering me an opportunity to study abroad. Thank my supervisory committee members, Dr. James Thomas and Dr. Roy Golsteyn for their valuable comments and suggestions.

Thanks to Schultz lab and Helper Hall family, Kurt, Neema, Saabi, Darren, Margaret, Ryan, Ping, Bo, Nuanying, Aki and everyone else who has been cooperative and supportive, especially Kurt who devoted his time and patience to help me to a large extent. Thanks to Grant Duke and Maurice for the technique help and training of the confocal microscope. Thanks to the University of Lethbridge and all supportive departments, offices for providing me a wonderful study atmosphere and financial support.

Thanks to my girlfriend, Le and my parents for their constant love, encouragement and care they had for me. Thanks to my friends, Dun, Emma and Haley for making my grad life easy. Thanks to my friend, Wei for being like my brother all the time.

Finally, I would like to thank all the people who contributed in some way to the production of my thesis.

TABLE OF CONTENTS

LIST OF TABLES

LIST OF FIGURES

LIST OF ANNOTATIONS, ABBREVIATIONS AND GENE SYNONYMS

Annotations

FORKED1 – wild type gene is capitalized and italicized
forked1 – mutant gene is italicized
FORKED1 – protein is capitalized

Abbreviations

AP2 = Adaptor Protein 2
ABRC = Arabidopsis Biological Resource Centre
AGD = ARF-GAP Domain
ARF = ADP Ribosylation Factor
AUX1/LAX = Auxin Resistant1/Like Aux1
BAR = Bin Amphiphysin-Rvs
BEN1 = BFA-VISUALIZED ENDOCYTIC TRAFFICKING DEFECTIVE1
BFA = Brefeldin A
BiFC = Bimolecular Fluorescence Complementation
CC = Columella Cells
BIG = BREFELDIN A INHIBITED ARF GUANINE EXCHANGE FACTOR
CVL1 = COTYLEDON VASCULAR PATTERN 2 LIKE1
CVP2 = COTYLEDON VASCULAR PATTERN 2
DAG = Days After Germination
DNA = Deoxyribonucleic acid
DUF828 = Domain of Unknown function
E.coli = Escherichia coli
EE = Early Endosomes
ER = Endoplasmic Reticulum
EZ = Elongation Zone
FL = FORKED1-LIKE
FKD1 = FORKED1
FM4-64= (*N*-(3-Triethylammoniumpropyl)-4-(6-(4-(Diethylamino) Phenyl) Hexatrienyl) Pyridinium Dibromide
GA = Golgi Apparatus
GAP = GTPase-activating Protein
GEF = Guanine Nucleotide Exchange Factor
GFP = Green Fluorescent Protein
GNL= GNOM LIKE
GUS = β-GLUCORONIDASE
MZ = Meristematic Zone
NAA = 1-Naphthaleneacetic Acid
N. tabacum = Nicotiana tabacum
PA = Phosphatidic Acid
PCC = Pearson's Coefficient of Correlation
PH = Pleckstrin Homology
PI = Phosphoinositides

PIN = PINFORMED
PM = Plasma Membrane
QC = Quiescent Centre
RFP = Red Fluorescent Protein
ROI = Region of Interest
SFC = SCARFACE
ST = Sialyl Transferase
SYP = Syntaxin of Plants
T-DNA = Transfer-DNA
TGN = Trans Golgi Network
VHA = Vacuolar ATPase
VI = Vascular Island
WT = Wild Type
YFP = Yellow Fluorescent Protein

Gene synonyms

BIG2 = BEN3
BIG5 = BEN1 = MIN7
FKD2 = SFC = VAN3
RabF2b = ARA7

1 Introduction

Auxin is involved in almost all aspects of plant development and growth, and allows these processes to respond to different environmental factors. The cellular auxin level, which drives particular developmental processes, is established by auxin transport between neighbouring cells, which is mainly controlled by influx and efflux carriers. One group of the plant-specific efflux carriers is the PIN-FORMED (PIN) family. By polar distribution and dynamic re-localization, PIN proteins control many auxin-dependent developmental processes such as vein patterning and tropisms. Polar localization of proteins such as PINs is achieved through transport in a complicated endomembrane vesicle trafficking system, involving a wide range of protein machineries such as small G protein ADP ribosylation factors (ARFs) and their regulators ARF-GTPase activating proteins (ARF-GAPs) and ARF-guanine nucleotide exchange factors (ARF-GEFs). Leaf vascular patterning is mediated by the auxin positive feedback loop, where PINs, as well as other proteins such as FORKED1 (FKD1), are involved. *FKD1* is one member of a plant-specific gene family, the *FKD1-LIKE* (*FL*) family, whose cellular function is unknown at the molecular level. My study focuses on dissecting the functions of the FL family, working with the ARF-dependent endomembrane trafficking system, in localizing PIN1 in *Arabidopsis thaliana* (Arabidopsis).

1.1 Auxin, its transport and carriers

The phytohormone auxin plays a significant role in plant growth and development, including cell division and polarity (Friml et al., 2003), cell expansion and differentiation (Fukuda, 2004), intracellular membrane trafficking (Paciorek et al., 2005), organogenesis (Weijers et al., 2006), apical dominance and tropisms (Reed, 2001; Woodward and Bartel, 2005). Such developmental processes are influenced by the local accumulation and depletion of auxin (Mockaitis and Estelle, 2008; Vanneste and Friml, 2009).

Auxin balance is maintained through auxin sources created by biosynthesis, gradient establishment by transport, and signal perception and response (Chandler, 2009). Most auxin is synthesized in the shoot apex and young leaves, thus auxin transport from the sites of synthesis (source tissue) such as shoots to the sites of action (sink tissue) such as roots is very important for plant development (Ljung et al., 2001). Auxin is transported in two ways: long-distance transport and short-distance transport (Peer et al., 2011). Long-distance transport through mature phloem is used to transport auxin from young shoot tissues to roots (Petrasek and Friml, 2009). Short-distance transport in a polar direction happens between neighbouring cells via lipophilic diffusion and auxin carriers (Peer et al., 2011). When the extracellular auxin level is high, auxin can enter cells via lipophilic diffusion, while under the circumstance of low extracellular auxin levels, auxin uptake from the environment is mediated by the transmembrane proteins

AUXIN RESISTANT1/LIKE AUX1 (AUX1/LAX) family, which act as auxin influx carriers to develop an auxin sink in cells (Bennett, 1996; Swarup et al., 2001). However, auxin is anionic in the cytosol and cannot go passively through the membrane and thus an efflux carrier is required (Peer et al., 2011).

1.2 PINs, their functions and distributions

Plant-specific PIN-FORMED (PIN) proteins are auxin efflux carriers, which are crucial for the spatiotemporal dynamics of auxin (Petrásek et al., 2006). The PIN nomenclature comes from the 'pin-formed' inflorescence phenotype of loss of function *pin1* (Peer et al., 2011). The PIN family consists of eight members; five members (PIN1, 2, 3, 4 and 7) are full-length plasma membrane (PM) localized proteins, which directly serve as auxin efflux carriers (Petrásek et al., 2006); the other three members (PIN5, 6 and 8) are short-length endoplasmic reticulum (ER) localized proteins, which are involved in homeostatic auxin compartmentalization (Mravec et al., 2009). Fluorescently labeled protein expression and transcription profiling illustrate that PIN1, 3, 4, and 7 are expressed globally during development, but exhibit tissue-specific expression intensity and polarity (Vieten et al., 2005).

The PIN proteins have been identified and characterized as key regulators of auxin-dependent processes, which play diversified roles responsible for different developmental processes. Functions of PIN proteins include axis formation in

embryogenesis (PIN1, 4 and 7), meristem maintenance of root (PIN1, 3, 4 and 7) (Peer et al., 2011) and vascular tissue differentiation and regeneration (PIN1, 5, 6, and 8) (Sawchuk and Scarpella, 2013). Root growth in the direction of gravitational field (*i.e.*, root gravitropism) and shoot growth responding to a light stimulus (*i.e.*, shoot phototropism) are both controlled by auxin asymmetrical distribution, achieved through the action of PIN proteins (Armengot et al., 2016). Gravitropism mainly requires PIN2 and PIN3, whereas phototropism utilizes PIN1 and PIN3 (Peer et al., 2011). Although auxin transport in different tissues is maintained by the different combination of PINs, the loss-of-function mutation in one PIN can be compensated by the ectopic expression of other PIN members (Vieten et al., 2005), indicating their functional redundancy.

PIN proteins control auxin polar transport through their asymmetric distribution. The polar localization of PINs at the single cell level determines the direction of intercellular auxin transport. For example, the apical localization of PIN1 leads to upward auxin transport, whereas the basal localization of PIN1 leads to downward auxin transport (Adamowski and Friml, 2015). During embryogenesis, in the octant stage, PIN1 localizes symmetrically to the PM of all cells, while PIN7 localizes to the apical PM of suspensor cells to maintain a pre-globular stage basal to apical auxin gradient (Friml et al., 2003). Around the globular stage, PIN1 localization shifts to the basal membrane of embryo cells, PIN7 is reversed to the basal membrane of suspensor cells, and PIN4 expression starts at the basal membrane of the embryo provascular cells, which

together support the apical to basal switch of the auxin gradient (Friml et al., 2003). During postembryonic seedling development of roots (see Figure 1 for a summary of auxin transport controlled by PIN proteins), auxin transport is downward in stele and cortex tissues. When auxin reaches the columella cells, it is transported laterally and will finally be taken back to the elongation zone by epidermal upward transport (Vieten et al., 2005). PIN1 predominantly localizes at the basal membrane of stele and endodermal cells and thereby contributes to auxin transport towards the root meristem (Friml et al., 2002a). PIN3 localizes to the basal side of vascular cell membranes and to the lateral sides of pericycle cell membranes in the elongation zone of the root, and PIN7 localizes at lateral and basal membranes of provascular cells in the meristem and elongation zone, both contributing to apical to basal transport of auxin (Friml et al., 2002a; Friml et al., 2002b). PIN2 is basally localized in cortical cells, which contributes to auxin transport towards the root meristem, but its apical localization in root epidermal cells and lateral root cap cells contributes to the shootward transport of auxin from the root meristem towards the elongation zone within peripheral tissues (Friml et al., 2003; Billou et al., 2005; Adamowski and Friml, 2015). PIN3 (Friml et al., 2002b) and PIN7 (Billou et al., 2005) are more or less asymmetrically and overlappingly localized in columella cells. Basal localization of PIN4 in the quiescent center and neighboring cells contribute to auxin transport towards the columella initials (Friml et al., 2002a).

In shoots, PIN1 localizes towards the shoot apex in the epidermis while PIN3 localizes laterally at the inner side of shoot endodermal cells (Grunewald and Friml, 2010). In developing leaf primordia, PIN1 is distally localized in the epidermis (Benková et al., 2003), which may confer the epidermal pavement cell polarity at the early leaf morphogenesis stage. PIN1 is the only PM-localized member expressed early in a series of closed loops of the early ground meristem of leaves, predicting the position of vascular development (Scarpella et al., 2006). Consistent with its importance in vein patterning, *pin1* leaves exhibit vascular defects such as increased marginal vasculature and number of central vascular strands (Mattsson et al., 1999). The unique role of PIN1 in vein formation provides an opportunity to dissect the role of a single PIN on auxin transport and the resultant vascular phenotype.

1.3 Root development

Plant roots are vital for plant development and function in the uptake of water and nutrients and fix the plant in its environment (Petricka et al., 2012). The whole root system patterning is dependent on sensing environmental factors and subsequent morphogenesis response, which is achieved through signaling events (Rymen and Sugimoto, 2012). The plasticity of root morphology provides a variable root entity, which consists of different root-types with varying spatial configuration. In general, the root system maintains at least two types of roots: the primary root, which is developed

during embryogenesis, and lateral roots which are initiated post-embryonically and branch off from the primary roots (John et al., 1995). Also, certain plants can develop adventitious roots, which emerge from non-root tissues, such as stems and leaves (Verstraeten et al., 2014).

The primary root emerges from the seed upon germination and grows gravitropically into the soil by cell division in the meristematic zone and subsequent cell elongation in the elongation zone (Beemster and Baskin, 1998). The meristematic center at the root tip is important to maintain the root growth. This part of root serves as a growth coordinating center and includes quiescent center (QC) cells, which remain undifferentiated and are surrounded by initial cells. Upon asymmetrical divisions, these initial cells differentiate into specific cell types, each with a specific function (Sabatini et al., 2003; Garay-Arroyo et al., 2012). Endogenous auxin accumulates at the root tip to coordinate cell divisions, cell expansion and gravitropic response through PIN3, PIN4 and PIN7 (Friml et al., 2002a; Friml et al., 2002b; Friml et al., 2003; Petersson et al., 2009; Overvoorde et al., 2010). A high level of auxin is able to stimulate cell division, whereas a low level stimulates elongation (Perrot-Rechenmann, 2010). The auxin level in the elongation zone (where cell elongation and differentiation happen) is lower than that in the meristematic zone (where cell division happens) but both have to maintain a balance to coordinate developmental processes (Kong et al., 2018). Such maintenance is mainly achieved by both root-ward transport through basal membrane localized PIN1 and

PIN7 (provascular cells), PIN2 (cortical cells) and PIN3 (vascular cells), and shoot-ward transport through apically localized PIN2 (epidermal cells) between meristematic zone and elongation zone (Billou et al., 2005; Vieten et al., 2005; Keuskamp et al., 2010; Adamowski and Friml, 2015)

Lateral roots develop from pericycle cells at the xylem pole (Beeckman et al., 2001; Casimiro et al., 2003), with corresponding auxin polar accumulation by PIN proteins (Benková et al., 2003). Initially, auxin accumulates at the presumptive founder cells of primordium within the pericycle (Benková et al., 2003). Auxin can induce anticlinal divisions (Dubrovsky et al., 2008). After anticlinal divisions produce short initial cells, auxin accumulates in these cells; following the establishment of outer and inner layers by periclinal divisions, auxin is restricted to the central cells of both layers, where PIN1, PIN3, PIN4 and PIN6 are expressed (Benková et al., 2003). Later on, a gradient of auxin with its maximum at the primordium tip is gradually established. During this process, PIN1 is expressed in derivatives of inner cells; PIN2 is basally localized in outer cells; PIN3 is expressed in the basal part of the primordium and columella precursors; PIN4 is expressed in the same region as PIN3, but its basal cell expression is more restricted to the margin; PIN6 and PIN7 are expressed in the margin (Benková et al., 2003). In the mature lateral root, as in the primary root, auxin is at a maximum in the columella initials and surrounding cells (Benková et al., 2003). The founder cell establishment and subsequent lateral root initiation is dependent on the

recurrent accumulations of auxin in the root meristem (De Rybel et al., 2010; De Smet et al., 2015), which could be manifested by the distance between the root apex and first most distal lateral root initiation point, since the two biological traits are highly correlated. Dynamic auxin transport between the root elongation zone and the meristematic zone by PIN proteins is important for positioning auxin accumulation, an idea that can be supported by affected lateral root primordia development in *pin3*/*pin7* and *pin1*/*pin3*/*pin4* mutants (Benková et al., 2003). As well, treatment with one type of auxin, 1-Naphthaleneacetic acid (NAA), can also induce lateral root development (Benková et al., 2003).

Adventitious roots are roots that develop from non-root tissues, such as hypocotyls and stems (Verstraeten et al., 2014). In the Arabidopsis hypocotyl, adventitious roots originate from a cell layer reminiscent of the pericycle in the primary root and thereby adventitious roots may share developmental characteristics with lateral roots (Negroni and Balliau, 2006; Li et al., 2009). Exogenous auxin or wounding is able to enhance adventitious root formation (Sukumar et al., 2013). Adventitious root formation is a complex process, controlled by multiple factors, including phytohormones, light, wounding, and stress, among which auxin plays a central role (Verstraeten et al., 2014).

1.4 The involvement of PIN1 directed auxin transport in leaf venation

As evolution has proceeded, plants have been developing leaves of certain forms to adjust to various environmental factors and changes and to optimize their life strategies (Malinowski, 2013). Plants equipped with a complex leaf vascular system are more successful in a terrestrial environment, and the acquisition of more complex leaf vascular systems can represent critical stages in plant evolution (Roth-Nebelsick et al., 2001). Leaf venation is one crucial characteristic for plants due to its importance in the transport of photosynthetic substrates and products (Brodribb and Feild, 2010). Higher plants, mostly all angiosperms, tend to have a hierarchical vein pattern, with higher-order veins branching off from lower-order veins, forming a closed vasculature by joining of distal branches (Trivett and Pigg, 1996). The transition from the simple, non-hierarchical pattern of primitive vascular plants including ferns, progymnosperms and most gymnosperms to a reticulate one is thought to be a main driving force for angiosperm success. The hierarchies and meeting of veins create a vascular system with a stronger capability to tolerate both abiotic and biotic stresses (Roth-Nebelsick et al., 2001; Brodribb and Feild, 2010; Feild et al., 2011).

Auxin triggers vascular patterning, through a proposed ‘auxin canalization’ model. Canalization involves a positive feedback mechanism, and thereby the ability of a cell to transport auxin increases with auxin flux level enhancement (Sachs, 1981). In leaves, some cells with high auxin transport rate will drain auxin from neighbors, gradually leading to a file of cells maintaining very high auxin flux level. These high auxin flux

cells become the precursors of veins and will later differentiate to form vasculature (Sachs, 1981). The new vasculature develops towards and unites with the existing vasculature leading to a connected vein pattern (Sachs, 1981). At the cellular level, the localization of PIN1 dynamically changes during different stages of vein patterning, ranging from lateral to apical or basal (For the outline, see Figure 2). Apical localization of PIN1 in the marginal epidermis of the young leaf primordium results in a convergence point and creates an auxin maximum at the leaf apex (Reinhardt et al., 2003). Cells at the convergence point then acquire basal PIN1 localization enabling auxin movement into the inner layers. PIN1 expression is turned on in these layers, and gradually becomes restricted to a single cell file with basal PIN1 localization, which becomes the midvein (Scarpella et al., 2006). In the adjacent cells, PIN1 localizes laterally towards the midvein and thus auxin is drained from the neighboring cells (Scarpella et al., 2006). The formation of secondary veins reiterates this process in provascular tissues, with PIN1 localizing basally, towards the midvein, in most of the loop of cells and apically in those cells that are in the distal loop region. The regions of the loop with different polarities are bridged by a bipolar cell (Scarpella et al., 2006; Hou et al., 2010). The capability of PIN proteins to maintain polarity and quickly redistribute relies on cellular signaling events occurring at the polar PM site where PIN proteins are localized (Gao et al., 2008).

1.5 Endomembrane system and vesicle transport

Cellular localization of proteins such as PIN is achieved through transport in a complicated endomembrane system, which consists of distinct membrane-bound organelles such as endoplasmic reticulum (ER), Golgi apparatus (GA), trans-Golgi network (TGN), lysosomes, endosomes and vacuoles, each of which contains a unique membrane composition and cargo proteins (Bonifacino and Glick, 2004). Independent organelles function in a sequential fashion to control protein transport (Lee et al., 2004).

The endomembrane system mediates the transport of molecules through the secretory and endocytic pathways (Bonifacino and Glick, 2004). The secretory pathway transports proteins targeted to PM via the ER and GA (Jürgens, 2004). Endocytosis includes recycling of PM proteins via early endosomes, and late endosomes are involved in GA to vacuole trafficking (Jürgens, 2004). In plants, there are no distinct endosomes, and the endocytic and secretory pathways merge within the TGN (Viotti et al., 2010) and proteins such as SYP61 are able to label both TGN and EE (Drakakaki et al., 2012). Dynamics of PIN proteins can be dissected into various PIN protein containing vesicle transport processes involving both secretory and endocytosis pathways, where PIN proteins are constitutively recycled between the endomembrane and the PM to maintain or alter their specific polarity (Langowski et al., 2016).

1.6 Phosphoinositides

Phosphoinositides (PIs), those phospholipids with phosphorylated inositol head groups, are found in eukaryotic membranes (Heilmann, 2016) and have been reported to be somehow involved in PIN1 localization to control cell polarities, such as regulating the tip growth of root hairs and pollen tubes (Tejos et al., 2014). Unlike the majority of membrane lipids that serve structural roles, PIs are of a minor abundance and their dynamic formation occurs at very precise locations and times (Heilmann, 2016). PIs are regulatory lipids that exert their influence by acting as ligands for membrane-associated proteins (Heilmann, 2016). One domain which contributes to protein localization via an interaction with PIs is the Pleckstrin Homology (PH) domain (Lemmon, 2007).

In plants, five kinds of PI have been detected, PI3P, PI4P, PI5P, PI(3,5)P_2 and PI(4,5)P_2 (Heilmann, 2016). PI3P and PI(3,5)P_2 are found in the late endosomes and vacuoles, which control the endomembrane trafficking in the context of autophagy and are important for vacuolar/tonoplast functions (Heilmann, 2016). Another two forms of PIs, PI4P and PI(4,5)P_2, have been reported to be involved in the actin-dependent delivery of PIN1 containing vesicles to the root epidermal membrane (Tejos et al., 2014). PI(4,5)P_2 mainly exists on the PM and a gradient of PI4P has been confirmed, with the highest amount at the PM, an intermediate amount in post-Golgi/endosomal compartments, and the lowest amount in the GA (Simon et al., 2014). *COTYLEDON VASCULAR PATTERN 2* (*CVP2*) encodes an inositol polyphosphate 5’ phosphatase that catalyzes the switch from PI(4,5)P_2 to PI4P, and mutation in the gene *CVP2* results in

leaves with discontinuous veins (Carland and Nelson, 2004). *CVP2 LIKE 1* (*CVL1*) is the closest homolog to *CVP2*, and mutation in both genes results in lower PI4P yield, shorter root growth, and more severe vasculature defects, which suggests functional redundancy (Carland and Nelson, 2009; Naramoto et al., 2009).

1.7 ARFs and vesicle transport

The endomembrane trafficking of proteins is controlled by molecular machinery involved in packing cargo proteins into the vesicles as well as formation, recognition, tethering and fusion of vesicles (Bonifacino and Glick, 2004). Guanine nucleotide-binding proteins (G proteins) represent the largest family of signaling machinery in eukaryotes, and are involved in regulation of a wide variety of processes such as cell proliferation, cytoskeletal assembly and intracellular membrane trafficking (Takai et al., 2001). ADP ribosylation factors (ARFs), which comprise one typical G protein family, are important for endomembrane trafficking because of their roles in vesicle coat recruitment and vesicle formation (Bonifacino and Traub, 2003). One type of coat protein mediated by ARFs is the clathrin coat, which consists of the protein clathrin (comprising clathrin heavy chain and clathrin light chain), adaptor protein 2 (AP2) complex and other accessory factors (Bonifacino and Glick, 2004). During vesicle cycling, ARFs cycle through GTP and GDP bound forms. GTP bound ARFs form a stable link with donor membranes through hydrophobic residues at the N-terminus

(Jackson and Casanova, 2000). ARF-GTP sorts trans-membrane cargoes and recruits coat proteins necessary for vesicle budding (Gebbie et al., 2005). A large GTPase named dynamin controls membrane scission (*i.e.* pinching of endocytic vesicles from the membrane) (Luschnig and Vert, 2014). Following budding of the vesicle, GTP undergoes hydrolysis to GDP and a conformation change blocking the hydrophobic residues, and thus destabilizes the association with the membrane (Jackson and Casanova, 2000). Cytosolic ARF-GDP triggers coat dissociation, which must occur prior to docking and fusion of vesicles with new target membranes (Jackson and Casanova, 2000).

ARFs were first discovered in mammals as co-factors in the activation of adenylate cyclase, an enzyme important for the production of a crucial second messenger cAMP (Szopa and Sikorski, 1995). Later, ARFs were identified as GTPases involved in the recruitment of clathrin coat during the formation of vesicles (Bonifacino and Traub, 2003). Mammalian ARFs are classified into three classes based on sequence similarity (Jackson and Casanova, 2000). Class I ARFs (ARF1-3) are the most well characterized and have a known role in vesicle formation at the GA, TGN and endosomal membranes (Jackson and Casanova, 2000; Vernoud et al., 2003). Class I ARFs show high sequence similarity with yeast ARFs 1 and 2, and Arabidopsis ARFA Group (Bonifacino and Traub, 2003). Arabidopsis ARFA1c is able to rescue yeast with mutations in *ARF1* and *ARF2*, which are normally fatal (Gebbie et al., 2005). Class II contains mammalian ARFs 4 and 5, and Class III includes mammalian ARF6 (Jackson and Casanova, 2000). ARF6

acts in endocytosis and membrane recycling with the localization of both PM and endosomes (Jackson and Casanova, 2000), but we still know very little about Class II and III ARFs.

When only Arabidopsis ARF proteins are considered, they can be classified into various subgroups (Vernoud et al., 2003). The ARFA subgroup consists of 6 members (ARFA1a, ARFA1b, ARFA1c, ARFA1d, AtARFA1e, ARFA1f), which are close to mammalian Class I ARFs (ARF1-3) (Jackson and Casanova, 2000); the ARFB subgroup consists of three members (ARFB1a, ARFB1b and ARFB1c), which are close to mammalian ARF Class III (ARF6) (Matheson et al., 2008); the ARFC only consists of one member (ARFC1) and ARFD subgroup consists of two members (ARFD1a and ARFD1b) (Yorimitsu et al., 2014). The large number of family members and thus potential functional redundancy make it quite difficult to uncover the functions of plant ARF proteins (Yorimitsu et al., 2014). The function of the ARFA subclass in plant development is not known as a whole (Yorimitsu et al., 2014), since the six members are ubiquitously expressed and single loss of function mutation in these genes shows no obvious phenotype (Xu and Scheres, 2005). However, this group is one of the best-characterized groups of ARFs in terms of function and localization. ARFA1c localizes to the GA and post-Golgi compartments that bud from the GA (Xu and Scheres, 2005) and also co-localizes with the late endosome marker ARA7/RABF2b (Ueda et al., 2004). ARFA1c is required for post-Golgi trafficking of vacuolar proteins to lytic vacuoles, a

pathway that needs clathrin coat components (Pimpl, 2003). In tobacco epidermal cells, ARFA1f similarly localizes to GA and TGN compartments (Robinson et al., 2011). A line expressing antisense *ARFA1c* (with reduced expression of *ARFA1a, c, d, e* and *f*) has a smaller root system when grown on soil but not on plates, smaller leaves and more infertile siliques (Gebbie et al., 2005). A GTP locked dominant mutant allele of *ARFA1c* has defects in root growth and root hair formation (Xu and Scheres, 2005) and a dominant-negative mutation in *ARF1A1c* affects the exocytosis or recycling of PIN1 to the PM and gravitropism response (Tanaka et al., 2014). Overexpression of this dominant-negative allele causes disorganized cell arrangement of the hypophysis (the basal part of embryos forming the embryonic root) and failure to develop cotyledon primordia (Tanaka et al., 2014). *ARFA1a*, *ARFA1d*, *ARFA1e* and *ARFA1f* are expressed in cotyledons, leaves and roots while *ARFA1b* is only expressed in anthers (Klepikova et al., 2016). Taken together, the ARFA subgroup plays a significant role in both plant root and shoot development.

1.8 Regulators of ARFs

The rate of nucleotide exchange between GDP and GTP of ARFs is slow when ARFs act alone, but can be enhanced by ADP ribosylation factor-guanine nucleotide exchange factors (ARF-GEFs) that mediate the formation of ARF-GTP, and by ADP

ribosylation factor-GTPase activating proteins (ARF-GAPs) which mediate the hydrolysis to ARF-GDP (Scheffzek et al., 1998).

1.8.1 ARF-GAP

ARF-GAPs activate GTP hydrolysis of ARF proteins, triggering vesicle coat dissociation and allowing for fusion with target membranes (Gebbie et al., 2005). SCARFACE (SFC) is one of the ARF-GAPs which is capable of acting on yeast ARF1 to stimulate GTP hydrolysis (Koizumi et al., 2005). SFC has four domains, PH, Bin–Amphiphysin–Rvs (BAR), ARF-GAP, and two Ankyrin repeats (Sieburth et al., 2006), all of which may have roles in protein-protein interaction or membrane docking (Peter et al., 2004; Koizumi et al., 2005; Sieburth et al., 2006; Naramoto et al., 2009), consistent with the idea that the ARF-GAP controls localization of the ARF.

Mutation in *SFC* results in a discontinuous vein pattern with many vascular islands (VIs) (Deyholos et al., 2000; Koizumi et al., 2005), which is strongly correlated with the inability to maintain proper PIN1 expression domains (Scarpella et al., 2006). Mutation in *SFC* together with three other ARF-GAP genes, which are the closest homologs to SFC (*ARF-GAP DOMAIN1* (*AGD1*), *AGD2* and *AGD4*), cause defects in lateral root primordia and cotyledon formation (Naramoto et al., 2010), although the *agd1*/*agd2*/*agd4* triple mutant did not show any remarkable defect (Sieburth et al., 2006). In addition, the *sfc* phenotype was similar to *cvp2*/*sfc* double mutants, as well as

cvp2/*cvl1*/*sfc* triple mutants (Carland and Nelson, 2009; Naramoto et al., 2009), suggesting that SFC acts in the same pathway as CVP2 and CVL1. SFC co-localizes with TGN marker SYP41 and unidentified organelles, but its localization becomes nuclear and cytoplasmic in the absence of SFC PH domain (Naramoto et al., 2009). As well, SFC becomes completely cytosolic in the *cvp2*/*cvl1* double mutant (Naramoto et al., 2009). As for PI binding affinity, the PH domain of SFC shows the highest affinity for PI4P *in vitro*, as well as weak binding to PI(4, 5)P_2 (Koizumi et al., 2005). Strong activation of SFC ARF-GAP activity by PI4P, weak stimulation by PI(4,5)P_2 and phosphatidic acid (PA), as well as the compromised activity in the absence of the PH domain even with PI(4)P, indicates that the affinity of the PH domain for a specific phospholipid (likely PI4P) is important for the ARF-GAP activity (Naramoto et al., 2009). Since ARFs are capable of recruiting various coat proteins in different cellular areas, the specific function and localization of a given ARF are likely conferred through an interaction with a specific ARF-GAP domain (Naramoto et al., 2009).

1.8.2 ARF-GEF

ARF-GEFs activate the switch in ARFs from GDP to GTP bound form, which has a stable link with donor membranes and recruits coat proteins for vesicle budding (Jackson and Casanova, 2000; Gebbie et al., 2005). The steps of PIN1 vesicle transport

have been dissected partially through analysis of ARF-GEFs that are required in vesicle coat formation.

ARF-GEFs can be sorted into two groups based on their sensitivity to fungal toxin brefeldin A (BFA) (Geldner et al., 2003b). BFA functions by binding to hydrophobic residues of ARF-GEF Sec7 domain, which can destabilize the association of ARF-GEF and ARF-GDP at the donor membrane, thus preventing conversion to ARF-GTP (Jackson and Casanova, 2000; Gebbie et al., 2005). Also, BFA treatment can cause endomembrane as well as protein localization changes. GA is one of the BFA action sites in plant cells, and BFA treatment results in the formation of various GA-derived structures, including ER–GA hybrids (Nebenfuhr et al., 2002), BFA compartments and aggregates (Baldwin et al., 2001; Tse et al., 2004) and loss of the Golgi cis-cisternae (Hess et al., 2000). Tracking changes in the fluorescent protein-labeled endosomal compartments in response to BFA has been developed as a useful tool for studying protein localization and trafficking in plant endocytic and secretory pathways (Lam et al., 2009). For example, in root cells, BFA treatment causes PIN1 or PIN2 switching from the PM to aggregated endomembrane compartments, which also co-localize with the internalized endocytic marker FM4-64 (Geldner et al., 2001; Baluska, 2002; Samaj et al., 2004; Dettmer et al., 2006). Similarly, an early endosome (EE) or TGN labeled by the vacuolar ATPase subunit VHA-a1 was induced to form aggregates by treatment of BFA in root cells (Dettmer et al., 2006).

Arabidopsis has eight ARF-GEFs, GNOM and its two homologs GNOM LIKE 1 (GNL1) and GNL2, as well as BREFELDIN A INHIBITED ARF GUANINE EXCHANGE FACTOR1-5 (BIG1-5) (Geldner et al., 2003b). Five ARF-GEFs, including GNOM, GNOM-LIKE2 (GNL2), BIG1, BIG2 and BIG4 are inhibited by BFA (Geldner et al., 2003b). A critical role for ARF-GEF GNOM in the cycling of PIN1 (Richter et al., 2007; Naramoto et al., 2010), is suggested by the random localization of PIN1 in *gnom* null allele mutant embryos (Steinmann et al., 1999). Loss of function mutation in *GNOM* results in shorter primary root growth, fewer lateral roots and perturbed gravitropism response (Geldner et al., 2003a). The secretion of *de novo* synthesized PIN1 to the PM is BFA sensitive, and BIG2 serves as a crucial target component of such BFA action (Kitakura et al., 2017). BIG2 co-localizes with TGN/EE marker SYP61 and BIG5/BEN1/MIN7 (Kitakura et al., 2017). BIG4 co-localizes with ARFA1c, and TGN marker VHA-a1 (Jonsson et al., 2017).

PIN1 targeting to different membrane faces has been designated to different trafficking routes. Prolonged BFA treatment results in redistribution of internalized PIN1 to the apical membrane. Together with the continued apical localization of PIN1 in the absence of GNOM function, this result suggests that GNOM is primarily working in basal PIN1 localization, whereas BFA resistant ARF-GEFs (GNL1, BIG3 and BIG5) may be involved in apical PIN1 localization (Geldner et al., 2003a; Kleine-Vehn and Friml, 2008). Mutation in *GNL1*, a GNOM homolog with a function in vesicle cycling

between the ER and GA (Richter et al., 2007), shows defects in PIN1 internalization following treatment with BFA, which was interpreted as indicating that GNL1 may contribute to PIN1 recycling from the plasma membrane through a role in endocytosis (Naramoto et al., 2010). Although *gnl1* mutant plants are viable and fertile, the double mutant *gnom*/*gnl1* lacking both ARF-GEF activities, is gametophytic lethal (Richter et al., 2007). This indication of functional redundancy is supported by a later finding that GNOM and GNL1 work in an early secretory pathway localizing newly synthesized PIN1 to the basal PM (Doyle et al., 2015). Mutation in *BEN1*/*BIG5* also shows defects in PIN1 internalization, suggesting its function in endocytosis (Tanaka et al., 2009). BIG5/BEN1 localizes with TGN marker SYP61 and VHA-a1 (Tanaka et al., 2009) and with ARFA1c (Tanaka et al., 2014). BIG5/BEN1 is also important for PIN1 recycling to PM (Tanaka et al., 2014), which together with the polarized callose deposition defects in *MIN7/BIG5* knock-out mutant (Nomura et al., 2006), suggests that BIG5 also plays a role in the secretory pathway. Some *ben1* mutants have been reported to have disconnected distal parts of veins (Tanaka et al., 2009), which indicates that BEN1/BIG5 plays a role in vein patterning. Whereas *big3* mutants do not show any striking phenotype, following BFA treatment, which inhibits BIG1, BIG2, BIG4, GNOM and GNL2 (Geldner et al., 2003b), the *big3* mutant shows seed germination and short root defects, and lateral root primordia initiation defects with treatment by one type of auxin NAA (Richter et al.,

2014; Kitakura et al., 2017), suggesting a functional redundancy of ARF-GEF in plant root and shoot development.

1.9 FKD1 and its Family

The discontinuous vasculature phenotype of *fkd1* indicates a crucial role of FKD1 in vein patterning (Steynen and Schultz, 2003). The *GUS* reporter gene driven by the *FKD1* promoter (*pFKD1:GUS*) is expressed throughout the vasculature of developing leaves, floral organs, root precursors, mature roots, and stems (Hou et al., 2010). Similar to *PIN1*, expression of *pFKD1:GUS* in leaves is initially in a wide group of cells, and then gradually narrows to a single cell file that develops a closed loop (Hou et al., 2010). As well, *FKD1* is transcriptionally activated by auxin (Hou et al., 2010). This evidence indicates that the expression of *FKD1*, in a fashion similar to *PIN1*, is likely influenced by auxin canalization, suggesting its involvement in the same positive feedback mechanism (Hou et al., 2010). In *fkd1*, PIN1 narrowing is delayed compared with wild-type, and cells with apical PIN1 localization or those with bipolar PIN1 localization are absent in 90% of *fkd1* secondary veins (Hou et al., 2010). Abnormal PIN1 polarity in *fkd1* suggests that the lack of vein meeting most likely results from defective PIN1 dependent auxin canalization (Hou et al., 2010).

FKD1 is one member of the *FKD1-LIKE (FL)* family (Prabhakaran Mariyamma et al., 2018). Phylogenetic analysis places the *FL* gene family, which includes nine

members (FKD1 and FL1-8) into three groups (Groups 1, 2 and 3). Group 1 includes *FKD1* and three closely related genes *FL1*, *FL2* and *FL3*; Group 2 includes *FL4* and *FL8*; Group 3 includes *FL5*, *FL6* and *FL7* (Prabhakaran Mariyamma et al., 2018). The *FL* genes encode proteins with DUF828 and PH or PH_2 domains. DUF828 is a plant-specific domain, and its expansion can be correlated with key evolutionary events of the plant kingdom (Prabhakaran Mariyamma et al., 2018). The presence of a single DUF828 coding gene within the genome of the liverwort *Marchantia polymorpha* and the moss *Physcomitrella patens* indicates the coincident origin of the family with the occurrence of terrestrial plants about 443-490 million years ago (Douzery et al., 2004). The emergence of a reticulate vein pattern in the basal angiosperm *Amborella trichopoda* (Takhtajan 2009), can be correlated with the emergence of a single gene that falls within Group 1 (Prabhakaran Mariyamma et al., 2018). Knocking-out all four Group 1 genes in Arabidopsis results in failure to form a reticulate vein pattern, supporting the idea that the emergence of the Group I homologous gene in *Amborella* may have played an important role in reticulate vein patterning of angiosperms (Prabhakaran Mariyamma et al., 2018)

All *FL* Group 1 genes have predicted upstream auxin response factor binding sequences, suggesting that they may be together involved in the same auto-regulatory system (Prabhakaran Mariyamma et al., 2018). The severity of the disconnected vein phenotype of *fkd1* can be increased by mutating more members of Group 1, but not Group 3 (Prabhakaran Mariyamma et al., 2018). PIN1 localization in provascular cells is

more asymmetric in the Group 1 triple mutant *fkd1*/*fl2*/*fl3* than in the *fkd1* single mutant, indicating that these genes act redundantly to control vein meeting by localizing PIN1 to the proper position (Prabhakaran Mariyamma et al., 2018). As well, the Group 1 triple mutant (*fkd1*/*fl2*/*fl3)* has reduced root growth and a less sensitive gravitropic response, both of which are PIN related auxin transport defects. Since PIN1 localization in the triple mutant root does not show a difference compared with PIN1 localization in a wild-type background, localization of other PIN members such as PIN2 and PIN3 may be disturbed in *fkd1*/*fl2*/*fl3* root (Prabhakaran Mariyamma et al., 2018). FL1 and FL3 partially co-localize with FKD1, and the incomplete co-localization indicates that FL1 and FL3 may have functions distinct from FKD1 (Prabhakaran Mariyamma et al., 2018).

The targeting of PIN1 proteins to specific compartments is mediated by a wide range of proteins involved in the vesicle trafficking system. The mislocalization of PIN1 in *fkd1*/*fl2*/*fl3* triple mutants (Prabhakaran Mariyamma et al., 2018) suggests that members of FL Group 1 are candidates for such helper proteins. FKD1 localizes with TGN marker SYP61-YFP (Prabhakaran Mariyamma et al., 2017), where the endocytic and secretory pathways merge (Dettmer et al., 2006). FKD1 co-localizes weakly with GA marker ST-RFP and the endocytic tracer FM-64, but strongly with secretory markers RABA1e and RABA4b which are involved in tethering of vesicles; FKD1 compartments are insensitive to BFA; collectively, the localization pattern indicates that FKD1 mainly works in the BFA insensitive secretory pathway (Prabhakaran Mariyamma et al., 2017).

The moderate to strong co-localization with ARFA group members (ARFA1a, ARFA1c, ARFA1d and ARFA1e), suggests that FKD1 may also work in an ARFA positive pathway (Prabhakaran Mariyamma et al., 2017). The co-localization of FL1 and FL3 proteins with the TGN marker SYP61 and secretory pathway marker RABA1c but not GA marker ST-RFP is similar to FKD1 localization, indicating they all act in the RABA positive secretory pathway (Prabhakaran Mariyamma et al., 2018). The Group 3 FL proteins, FL5 and FL6 co-localize with ST-RFP whereas FL7 co-localizes weakly with ST-RFP and SYP61 but strongly with RABA1c (Prabhakaran Mariyamma et al., 2018). However, there is no cellular or phenotypic information about FL4 and FL8.

The FKD1 Pleckstrin Homology_2 (PH_2) domain has been suggested to bind membrane localized PI4P (Naramoto et al., 2009). Additional evidence for the association is the more frequent cytosolic localization of FKD1 in the double mutant *cvp2*/*cvl1* (Prabhakaran Mariyamma et al., 2017). FKD1 and SFC have been reported to interact with each other (Naramoto et al., 2009). The vein phenotype of *fkd1*/*fkd2* (*fkd2* is a weak allele of *sfc*) double mutant is more severe than either single mutant, indicating that two genes may work together (Steynen and Schultz, 2003). This is supported by the interaction of the two proteins in yeast two-hybrid assay and bimolecular fluorescence complementation (BiFC) (Naramoto et al., 2009), as well as strong co-localization in both heterologous system and in Arabidopsis (Naramoto et al., 2009; Prabhakaran Mariyamma et al., 2017). Either the FKD1 PH_2 domain or the SFC PH domain is

sufficient for localization of both proteins (Naramoto et al., 2009). Like FKD1, SFC also localizes to a BFA-insensitive RABA (RABA1b and RABA1c)-positive compartments, which partially overlaps with TGN marker SYP61 (Prabhakaran Mariyamma et al., 2017).

In summary, FKD1 and one ARF-GAP, SFC, are proposed to work together to mediate the localization of PIN1 to a specific membrane face of provascular cells by interacting with PI4P. I hypothesize that Group 1 of the FL family and SFC work with ARF-GEF BIG family members to enable PIN1 localization.

My experimental predictions are described as: A) Because FKD1 co-localizes strongly with SFC (Prabhakaran Mariyamma et al., 2017) and partially with members of FL family (FL1 and FL3), together with the fact that members of FL family act redundantly to localize PIN1 to control vein patterning (Prabhakaran Mariyamma et al., 2018), I predict that members of FL family (FL1 and FL3) will co-localize with SFC. B) Mutations in members of *FL* family (Steynen and Schultz, 2003; Hou et al., 2010; Prabhakaran Mariyamma et al., 2018), *SFC* (Steynen and Schultz, 2003; Sieburth et al., 2006) or *ARF-GEF* (*BIG5*) (Tanaka et al., 2009) show vein patterning defects, and, based on the possibility that they may work with each other, I predict that members of FL family and SFC co-localize with ARF-GEFs (BIGs). C) Mutations in members of the *FL* family, *SFC* or *ARF-GEF* (*BIG5*) show PIN1 polarity defects, and based on the possibility that they may control PIN1 polarity, I predict that FL family, proteins, SFC and ARF-GEF (BIG5) co-localize with PIN1. D) Mutations in the genes that are involved

in the proposed pathway may show defects that are similar to the reported auxin transport related developmental defects in mutants of *FL* family, *SFC* or *ARF-GEF* (*BIG5*) (Steynen and Schultz, 2003; Sieburth et al., 2006; Tanaka et al., 2009; Hou et al., 2010; Prabhakaran Mariyamma et al., 2018). Thus, I predict that mutations in *BIG3*, *BIG5* or *ARFA* group show auxin transport related developmental defects.

2 Materials and Methods

2.1 Seeds and lines generated

The Columbia (Col-0) ecotype of Arabidopsis, obtained from Dr. George Haughn, University of British Columbia, was used as a wild-type (WT) control in all experiments. Alleles of the *FKD1-LIKE* gene family are as described previously (Prabhakaran Mariyamma et al., 2018). T-DNA insertion line (Alonso et al., 2003) for *BIG5* (Salk_012013; AtMIN7 KO#3) was described in Nomura et al., 2006, and is referred to as *big5-1* allele. T-DNA insertion lines for members of *ARFA* gene family as well as two ARF-GEF genes are from the Arabidopsis Biological Resource Centre (ABRC) at Ohio State University, USA. T-DNA insertion lines include the following: At1G23490/*ARFA1a* (Salk_107987; *arfa1a*), At5G14670/*ARFA1b* (Salk_027659; *arfa1b*), At1G70490/*ARFA1d* (Salk_039612; *arfa1d*), At3G62290/*ARFA1e* (Salk 130670, *arfa1e*), At1G01960/*BIG3* (Salk_044617; *big3*) (Table 1). Double mutants for *CVP2* and *CVL1* were described previously (Carland and Nelson, 2009). Seeds of *Nicotiana tabacum* (*N. tabacum*) were obtained from Michigan State University, USA.

The *ARFA* subgroup quadruple mutant was selected by PCR using gene-specific primers from the population of a line homozygous for *arfa1a, arfa1e* but segregating for *arfa1b* and *arfa1d*. Mutants with multiple genes mutated in *FL* family members, including *fkd1/fl1-2*, *fkd1/fl2*, *fkd1/fl3*, *fkd1/fl2/fl3* and *fkd1/fl1-2/fl2/fl3* and the PUBQ10:FL3-YFP expressing line are as described in Prabhakaran Mariyamma et al.,

2018. *fkd1, fkd2* (a weak *sfc* allele) and *fkd1*/*fkd2* were described previously (Steynen and Schultz, 2003). Double mutants of *fkd1*/*big3, fkd1*/*big5-1, fkd2*/*big3* were generated by crossing single mutant lines and screening F3 lines for those homozygous for *fkd1* or *fkd2* by phenotype and homozygous for T-DNA insertion by PCR amplification using primers specific to either *big3* or *big5* T-DNA insertion junctions (see section 2.3 for details).

2.2 Growth Conditions

Seeds of Arabidopsis were sown on pots of soil (potting mix and vermiculite in the ratio of 3:1) with 9 seeds per pot, or on petri dishes of Arabidopsis growth medium (AT medium) (Ruegger et al., 1998) with 15 or 20 seeds per plate. Pots, covered with saran wrap, or plates were left at 4 ºC for 3 days for stratification, and then were transferred to the growth chamber. The date of transfer was considered 0 days after germination (DAG). Plants were grown in growth chambers at 22ºC with continuous light, intensity approximately 130 mmol photons per m^2 per sec obtained from Sylvania Cool White, Grow Lux and 60W frosted incandescent bulbs (Osram Sylvania Inc, Danvers, USA). At 7 DAG, saran wrap was removed and after that plants were maintained at 60% humidity. *N. tabacum* seeds were sown on soil and treated in the same way as the Arabidopsis until 14 DAG. *N. tabacum* seedlings were transplanted into pots

at 14 DAG with one plant per pot, and were later grown at 16 h of light at 22°C and 8 h of dark at 18°C with 60% relative humidity.

2.3 Identification of plants homozygous for T-DNA insertions

DNA was isolated from leaf tissue of 21-day-old plants using the CTAB DNA extraction protocol (Allen et al., 2006). Three to four young leaves were ground in liquid nitrogen and incubated in 300 µl DNA total extraction buffer (Appendix I) for 1 hour at 65ºC. The supernatant was extracted by adding 300 µl of chloroform and phase separated by centrifugation at 18000 × g for 10 min. DNA in the aqueous phase was precipitated by adding 2/3 volume of isopropanol, incubating for two hours/overnight at 4ºC and centrifuging at 20000 × g m for 10 min. The pellet was washed twice with 70% ethanol, air-dried and finally re-suspended in 40 µl sterile water. Plants homozygous for T-DNA insertion were identified by PCR, using the primers listed (Table 2). PCR was done using a combination of forward (left, L) and reverse (right, R) gene-specific primers and also the left border T-DNA primers. Wild-type plants with no insertions should produce a product only with L and R gene-specific primers (Figure 3). Homozygous lines with insertions in both chromosomes should give the product only with the left border T-DNA and the gene-specific primers (Figure 3). The PCR products of T-DNA junctions in *fl1-2*, *fl2* and *fl3* alleles were sequenced to confirm the insertion position (Figure 4).

2.4 Preparation of competent cells

Escherichia coli (*E. coli*) cells and *Agrobacterium* strain GV3101 were previously made competent in the Schultz laboratory. To make electrocompetent cells of *Agrobacterium* strain EHA105, a starter culture was made by inoculating a single colony of strain EHA105 into 2 ml of LB liquid media (Appendix I) supplemented with antibiotic (25 µg/ml rifampicin) and incubated at 28°C with shaking at 260 rpm overnight. The starter culture was used to inoculate 200 ml of LB liquid media and the culture was shaken at 260 rpm at 28°C until an OD_{600} of 0.3 was reached. *Agrobacterium* cells were then spun down at 4°C at 2700 × g for 10 min and the pellet was re-suspended in 20 ml ice-chilled sterile water; pelleting and resuspension was repeated three times. Finally, the pellet was re-suspended in 2 ml of ice-chilled 10% glycerol and stored as 80 µl aliquots at -80°C for future use.

2.5 Bacterial constructs obtained and generation

The p35S:BIG5/MIN7-dsRED vector was described in Nomura et al., 2011. Vectors of pMDC7(estradiol-induced):PIN1-RFP, pGII:BIG3-YFP and pUBC:BIG4-YFP were described previously (Richter et al., 2014). Vectors of pUBQ10:RABA4b-eYFP, pUBQ10:RFP-RABF2a and pUBQ10:YFP-RABF2b (Geldner et al., 2009), pSAT4A-mCherry-N1 (pE3279) and pPZP-RCS2-ocs-bar-RI (pE3519) (details of vectors are available at Dr. Stanton Gelvin's laboratory's website, Purdue University,

USA: https://www.bio.purdue.edu/people/faculty/gelvin/nsf/protocols_vectors.htm) were obtained from ABRC. Vector of p35S:SYP61–YFP was obtained from Dr. Federica Brandizzi, Michigan State University, USA (Stefano et al., 2010). Vectors of p35S:SFC-YFP, p35S:FKD1-GFP, pUBQ10:FL1-YFP, pUBQ10:FL3-YFP, pUBQ10:FL5-YFP, pUBQ10:FL6-YFP and pUBQ10:FL7-YFP were described in Prabhakaran Mariyamma et al., 2018. To generate the p35S:SFC-mCherry construct, SFC cDNA was amplified by PCR from full-length cDNA (obtained from Dr. Carland and Dr. Nelson, Yale University, USA). After purification using EZ-10 Spin Column PCR purification Kit (Bio Basic Inc.), the PCR product was then ligated into the pJET1.2/blunt vector using CloneJET PCR Cloning Kit (Thermo Fisher Scientific, Waltham, USA). The SFC cDNA was then ligated into pSAT4A-mCherry-N1 (pE3279) vector, which had been cut with EcoR-I and BamH-I restriction enzymes. The SFC-mCherry containing part of the vector was next ligated into pPZP-RCS2-ocs-bar-RI (pE3519) vector, and the final product was confirmed by PCR amplification using primers that spanned the ligated junction. Products of ligation were immediately transformed into *E. coli* cells (described in section 2.6). A single colony was picked into LB liquid medium and DNA was extracted from an overnight culture using a commercial mini-prep kit (Bio Basic Inc., Markham, ON) and checked by restriction digestion and sequencing. FL4 cDNA was synthesized and ligated into pSAT4A-mCherry-N1 (pE3279) vector (Bio Basic Inc., Markham, ON) and

p35S:FL4-mCherry was produced following the same procedure as described for p35S:SFC-mCherry.

2.6 Transformation

Transformations of different vectors into *E. coli* (p35S:SFC-mCherry and p35S:FL4-mCherry), *Agrobacterium strain* GV3101 (pMDC7:PIN1-RFP and pUBC:BIG4-YFP), *Agrobacterium strain* GV3101 containing pSOUP vector (pGII:BIG3-YFP) and *Agrobacterium strain* EHA105 (p35S:SFC-mCherry, p35S:FL4-mCherry and p35S:FKD1-GFP) were conducted as follows.

For *E. coli* transformation, vector DNA (300 ng) was added to 80 µl of thawed *E. coli* competent cells on ice. The mixture was transferred to an ice-chilled electroporation cuvette and pulsed at 2.5 kV in an electroporator (Eppendorf electroporator 2510). Ice-chilled LB liquid medium (500 µl) was immediately added to the electroporated cells in the cuvette and the cell mixture was transferred to a 1.5 ml tube and incubated with shaking (120 rpm) at 37°C for 1 hour. After incubation, 100 µl of cell mixture was plated onto LB media (Appendix I) supplemented with spectinomycin for p35S:SFC-mCherry or p35S:FL4-mCherry selection, and incubated at 37°C overnight for transformed cell colonies to grow. The positive colonies were picked, restreaked and grown in liquid cultures.

For *Agrobacterium* transformation, vector DNA (600 ng) was added to 80µl of thawed *Agrobacterium* cells on ice. The reaction mixture was transferred to an ice-chilled electroporation cuvette and pulsed at 1.8 kV in an electroporator (Eppendorf electroporator 2510). Ice-chilled LB liquid medium (500 µl) was immediately added to the electroporated cells in the cuvette and the cell mixture was transferred to a 1.5 ml Eppendorf tube and incubated with shaking (120 rpm) at 28°C for 4 hours. The cell mixture (200 µl) was plated onto LB media supplemented with appropriate antibiotics (25 µg/ml rifampicin to select for *Agrobacterium*; 50 µg/ml spectinomycin to select for the plasmid p35S:SFC-mCherry, p35S:FL4-mCherry, pMDC7:PIN1-RFP or pUBC:BIG4-YFP; 50 µg/ml kanamycin to select for the plasmid p35S:FKD1-GFP or pGII:BIG3-YFP) and incubated at 28°C for 48-72 hours for transformed colonies to grow. The positive colonies were picked, restreaked and grown in liquid cultures.

2.7 Transient expression

The protein co-localization of products from the following constructs were analyzed by transient expression in *N. tabacum*: a) pMDC7:PIN1-RFP with p35S:FKD1-GFP, p35S:SFC-YFP, pUBC:BIG4-YFP, pUBQ10:FL1-YFP, pUBQ10:FL3-YFP, pUBQ10:FL5-YFP or pUBQ10:FL7-YFP; b) p35S:SFC-mCherry with pGII:BIG3-YFP, pUBC:BIG4-YFP, pUBQ10:FL1-YFP or pUBQ10:FL3-YFP; c) p35S:BIG5-dsRED with p35S:FKD1-GFP, pUBQ10:FL1-YFP or pUBQ10:FL3-YFP; d) p35S:FKD1-GFP with

pGII:BIG3-YFP or pUBC:BIG4-YFP; e) pUBQ10:RFP-RABF2a with pUBQ10:FL1-YFP or pUBQ10:FL3-YFP; f) p35S:FL4-mCherry with p35S:SYP61-YFP, pUBQ10:RABA4b-eYFP or pUBQ10:YFP-RABF2b. To assess co-localization of fluorescence-tagged proteins by transient expression, *N. tabacum* plants were injected with various *Agrobacterium* strains harbouring appropriate vectors following the protocol of Batoko et al., 2000 about 5 weeks after sowing seeds. *Agrobacterium* cultures were grown in LB liquid with antibiotics at 28°C overnight. 1 ml of each culture was centrifuged at 1700 × g for 5 min at 20°C and the supernatant was discarded. The pellet was re-suspended in 1 ml of infiltration buffer (Appendix I) and re-centrifuged. The supernatant was discarded and the pellet was re-suspended in 1 ml of infiltration buffer again. Re-suspended culture (200 µl) was mixed with 800 µl of infiltration buffer and OD at 600 nm was measured using an Ultraspec 1100 Amersham Pharmacia Biotech spectrophotometer. The diluted culture was then further diluted with infiltration buffer to reach a final OD_{600} value of 0.05. The inoculum was injected using a 5 ml syringe into the *N. tabacum* leaves through the abaxial epidermis. For any co-localization involving pMDC7:PIN1-RFP, 20 µM β-estradiol was injected into the same area 24 hours after the *Agrobacterium* injection.

2.8 Confocal imaging and analysis

For transient expression analysis, pieces of *N. tabacum* leaves 3 days post-

Agrobacterium injection were mounted in water. For stable expression analysis, Arabidopsis roots at 2.5 DAG were mounted in water or 50 µM BFA solution. Tissues were viewed under a 60X oil-immersion objective using an Olympus Fluoview FV1000 confocal microscope. For co-localization experiments with the combination GFP/YFP and RFP/mCherry/dsRED, fluorophores were excited with 473 nm (emission filters 485–585 nm) and 559 nm (emission filters 570–670 nm) lasers, respectively. For co-localization experiments combining GFP and YFP, they were excited with 458 nm (emission filters 470-496 nm) and 515 nm lasers (emission filters 530–600 nm), respectively. Imaging was carried out using the line-sequential scanning mode, and all images used in comparisons were taken at the same confocal settings. For all co-localization analyses, at least 15 samples were observed and analyzed for each experiment. NIH Image J software (developed at the US National Institutes of Health and available at http://rsb.info.nih.gov/nih-image/) with PSC co-localization plugin (French et al., 2008) was used to assess the co-localization. Pearson's coefficient of correlation (PCC) values were obtained using the PSC co-localization plugin in Image J, from a selected region of interest (ROI), which can eliminate background noise. In the tobacco leaf epidermis, the ROI selected was a single epidermal cell, while in Arabidopsis roots, the ROI selected was a single cell file. Images shown in the figure are representative of co-localization patterns whenever possible. Images were processed with Adobe Photoshop Elements version 5.0 software (Adobe Systems).

2.9 BFA and FM4-64 treatment in confocal microscopy

BFA treatment was done by incubating 2.5 DAG seedlings expressing p35S:FKD1-GFP, p35S:SFC-YFP or pUBQ10:FL3-YFP in 50 µM BFA for 1 hour and viewing roots immediately by confocal microscope. A BFA wash-out experiment was performed on pUBQ10:FL3-YFP following the protocol of Geldner et al., 2001, in which, following a 1 hour BFA treatment, seedlings were washed free of BFA using two rinses of water and the root cells were imaged after 2 h water incubation. For FM4-64 labeling, seedlings of a homozygous line expressing pUBQ10:FL3-YFP at 2.5 DAG were labeled with 16 µM FM4-64 for 15 min, rinsed in water twice and then viewed after a further 15, 30 and 45 min. For combining FM4-64 labeling with BFA treatment, pUBQ10:FL3-YFP and p35S:SFC-YFP were treated with 50 µM BFA for 15 minutes and then with BFA and FM4-64 simultaneously for 15 minutes. After rinsing twice in water, the roots were observed by confocal microscope 30 minutes after mounting in 50 µM BFA solution. All treatments were done at room temperature.

2.10 Leaf vein characterization

For analysis of cotyledon and first leaf vein pattern under untreated conditions, cotyledons and first leaves were taken from plants grown on soil at 14 DAG and 21 DAG respectively from wild-type and homozygous mutant lines including *fkd1*, *fkd2*, *big3*,

big5-1, *fkd1*/*big3*, *fkd1*/*big5-1*, *fkd2*/*big3* and *arfa1a*/*b*/*d*/*e*. For analysis of cotyledons with BFA treatment, cotyledons were taken at 10 DAG from wild-type and homozygous mutant lines including *fkd1*, *fl1*, *fl2*, *fl3*, *fkd1*/*fl1*, *fkd1*/*fl2*, *fkd1*/*fl3*, *fkd1*/*fl2*/*fl3*, *fkd1*/*fl1-2*/*fl2*/*fl3*, *fkd2*, *fkd1*/*fkd2*, *arfa1a*/*b*/*d*/*e* and *cvp2*/*cvl1* that were grown on AT plate supplemented with BFA at the concentration of 0, 10 and 20 µM. The following treatments are the same for both cotyledons and first leaves, except the safranin staining step. All cotyledons and leaves were cleared using 5% NaOH solution for 3 hours. After rinsing with water, 50% bleach was added to the cotyledons and first leaves for 20 s, followed by water rinsing again. Cotyledons and first leaves were taken through an ethanol series (30%, 50%, 70% and 100%). The next step is different between cotyledons and first leaves: cotyledons were covered in 1% safranin overnight followed by destaining in 400 µL 100% ethanol containing 3-6 drops of 37% HCl (a method adapted from Vasco et al., 2014) and first leaves were covered in 1% safranin for 10 minutes. After that, cotyledons and first leaves were brought back to the water through a reverse ethanol dilution series (100%, 70%, 50%, 30%) and left in distilled water. Cleared cotyledons and first leaves were mounted in 66% glycerol and images were taken using a Nikon Cool Pix 990 camera mounted on Leica MZ8 microscope.

For cotyledon vein pattern analysis, vein numbers (total and non-meeting) and VIs were counted using Image J, and pattern was categorized using a method adapted from Tanaka et al., 2009 (shown in Figure 5): Pattern 1 (P1)- secondary veins meet

distally with either the midvein (upper loops) or the upper secondary veins (lower loops). P2- upper loops met distally but at least one of the lower loops did not meet distally. P3- at least one upper loop did not meet distally. If the cotyledon only had one loop layer, it was considered as upper loop. For first leaf vein pattern analysis, number of secondary veins, number of non-meeting secondary veins, number of VIs, number of tertiary and quaternary veins, number of non-meeting tertiary and quaternary veins, leaf area, number of non-meeting secondary veins/leaf area, number of tertiary and quaternary veins/leaf area and number of non-meeting tertiary and quaternary veins/leaf area were counted and calculated.

2.11 Root analysis of mutant lines

For root analysis, seedlings of wild-type, *fkd1*, *fkd2*, *fl1*, *fl2*, *fl3*, *fkd1*/*fl1*, *fkd1*/*fl2*, *fkd1*/*fl3*, *fkd1*/*fl2*/*fl3*, *fkd1*/*fl1-2*/*fl2*/*fl3*, *fkd2*, *big3*, *big5-1*, *fkd1*/*fkd2*, *fkd1*/*big3*, *fkd1*/*big5-1*, *fkd2*/*big3*, *arfa1a*/*b*/*d*/*e* and *cvp2*/*cvl1* were grown vertically on petri plates with AT medium at a density of 15 plants per plate. At 9 DAG, roots were mounted in water, and total primary root length and tip to first distal lateral root initiation point distance were directly measured under Leica MZ8 microscope, during which process adventitious root number and lateral root number were counted. Number of lateral roots/total primary root length (lateral root density) and tip to first distal lateral root initiation point distance/total primary root length were then calculated. Images showing adventitious roots of *fkd1*/*fl1*-

2/fl2/fl3, *fkd1*/*big5-1* and *arfa1a*/*b*/*d*/*e*, and the same region of WT were taken using a Nikon Cool Pix 990 camera mounted on Leica MZ8 microscope.

2.12 Statistical analysis

Shapiro–Wilk test was used for testing data normality. Since all parameters except the area of first leaf compared included data that were not normal, a nonparametric Kruskal–Wallis test was used for all the data comparisons. The mean values were tested by post-hoc test (Dunn test) to determine if the compared samples were significantly different ($p<0.05$) from each other. All statistical tests were conducted using R studio software, version 0.99.484 (RStudio Inc., http://www.rstudio.com/ 2015).

3 Results

3.1 SFC-YFP, BIG4-YFP and FL family co-localize with PIN1

The transport of PIN1 is dependent on various protein machineries. Based on our hypothesis that FL family acts with the ARF-dependent system to enable PIN1 localization, fluorescently tagged protein representatives of ARF-GAPs (p35S:SFC-YFP), ARF-GEFs (pUBC:BIG4-YFP) and FL family (p35S:FKD1-GFP, pUBQ10:FL1-YFP, pUBQ10:FL3-YFP, pUBQ10:FL5-YFP, pUBQ10:FL6-YFP and pUBQ10:FL7-YFP) were tested for co-localization with estradiol-induced pMDC7:PIN1-RFP using transient expression (*N. tabacum*) system (tobacco epidermal pavement cells). Quantification of different proteins with PIN1 co-localization is given (Table 3). Co-localization of pMDC7:PIN1-RFP was positively associated with p35S:SFC-YFP (average PPC=0.20 ± 0.15), pUBC:BIG4-YFP (average PPC=0.27 ± 0.16), p35S:FKD1-GFP (average PPC=0.28 ± 0.15), pUBQ10:FL1-YFP (average PPC=0.28 ± 0.15) and pUBQ10:FL3-YFP (average PPC=0.45 ± 0.13) (Table 3 and Figure 6), whereas it was negatively associated with pUBQ10:FL5-YFP (average PPC=-0.04 ± 0.13), pUBQ10:FL6-YFP (average PPC=-0.04 ± 0.15) and pUBQ10:FL7-YFP (average PPC=-0.19 ± 0.08) (Table 3 and Figure 7). There was a clear difference between those proteins that partially associate with PIN1 (SFC, BIG4, FKD1, FL1 and FL3) and those that never associate with PIN1 (FL5, FL6 and FL7), suggesting a) FKD1, SFC, BIG4, FL1 and FL3 are potential PIN1 transport machineries and b) FL5, FL6 and FL7 are likely not involved in

PIN1 transport (thus not considered further for co-localization study and phenotypic analysis). Interestingly, none of these PPC values of co-localization with PIN1 was above 0.3, indicating a fairly low frequency of association, suggesting a very complicated transport system for PIN1 with potentially abundant proteins involved.

3.2 SFC does not co-localize with FL1 or FL3

Previous evidence shows that FKD1 co-localizes strongly with SFC (Naramoto et al., 2009; Prabhakaran Mariyamma et al., 2017), and the proteins interact based on yeast two hybrid and bimolecular complementation (Naramoto et al., 2009). SFC and Group 1 members (FKD1, FL1 and FL3) of FL family showed co-localization with PIN1 (Section 3.1). As well, FL1 and FL3 partially co-localized with FKD1 (Prabhakaran Mariyama et al., in press). Together, the co-localizations suggest that SFC may co-localize with FL1 and FL3. Because the FL proteins are all tagged with YFP, and the fluorescencely tagged SFC previously described by our lab is p35S:SFC-YFP (Prabhakaran Mariyama et al., 2017), I made p35S:SFC-mCherry to perform co-localization between FL proteins and SFC (see section 2.5). First, to confirm that the localization of p35S:SFC-mCherry protein is representative, I tested the association between newly made p35S:SFC-mCherry and previously made p35S:SFC-YFP. As expected, the localization pattern of p35S:SFC-mCherry and p35S:SFC-YFP was very similar (average PPC=0.70 ± 0.19) (Table 4 and Figure 8 A-D). Next, p35S:SFC-mCherry was tested for co-localization

with pUBQ10:FL1-YFP and pUBQ10:FL3-YFP. Very surprisingly, there was no association of SFC with FL1 (average PPC=0.04 ± 0.16) or with FL3 (average PCC=-0.06 ± 0.17) (Table 4 and Figure 8).

3.3 FKD1, but not FL1 and FL3, co-localizes with BIG5

FKD1 and BIG5 both partially co-localize with ARFA1c (Tanaka et al., 2014; Prabhakaran Mariyamma et al., 2017), which suggests that FKD1 may work together with BIG5. The co-localization experiment showed that p35S:FKD1-GFP and p35S:BIG5-dsRED associated relatively strongly (average PCC=0.70 ± 0.28) (Table 4 and Figure 9 A-D). FKD1 partially co-localizing with FL1 and FL3 (Prabhakaran Mariyama, in press) also led to the question of whether FL1 or FL3 are associated with BIG5. The co-localization study of BIG5 with FL1 or FL3 showed that neither FL1 (average PCC=-0.21 ± 0.19) (Table 4 and Figure 9 E-H) nor FL3 (average PCC=-0.02 ± 0.28) (Table 4 and Figure 9 I-L) showed any co-localization with BIG5, which is also surprising but interesting.

3.4 FKD1 and SFC co-localize with BIG4 and BIG3

My finding that FKD1, SFC and BIG4 all localized with PIN1 positive transport vesicles (Section 3.1) suggested that they may act in the same pathway and co-localize with each other. The strong association between FKD1 and SFC (Naramoto et al., 2009;

Prabhakaran Mariyamma et al., 2017) has been reported, thus the respective association of FKD1 and SFC with BIG4 was proposed and a co-localization test was conducted by expressing p35S:FKD1-GFP with pUBC:BIG4-YFP, and p35S:SFC-mCherry with pUBC:BIG4-YFP in tobacco epidermal cells. As shown in Table 4 and Figure 10, p35S:FKD1-GFP and pUBC:BIG4-YFP co-localized relatively strongly (average PCC=0.64 ± 0.27) and p35S:SFC-mCherry showed partial co-localization with pUBC:BIG4 (average PCC=0.27 ± 0.19). I was not able to co-localize FL1 and FL3 with BIG4, as these proteins are fused to YFP. The functional redundancy of BIGs (Richter, 2014) led me to investigate if FKD1 and SFC co-localize with BIG3 as well. As may be expected, the association between FKD1 and BIG3 (average PCC=0.43 ± 0.13), and between SFC and BIG3 (average PCC=0.78 ± 0.23) were both relatively strong (Table 4 and Figure 10). Collectively, the co-localizations support the idea that FKD1 and SFC may work together with BIG3 and BIG4 to transport PIN1 protein.

3.5 Co-localization with FM4-64 and RABAF2a suggests a role of FL3 in endocytosis

FM4-64 is a lipophilic dye that is incorporated into the PM, and can then track the endocytic vesicles (Bolte et al., 2004). Both FKD1 and SFC co-localize weakly in vesicles with FM4-64 (Prabhakaran Mariyamma et al., 2017). Together with the strong co-localization with secretory markers RABA group, this led to the suggestion that their

primary roles are in the secretory pathway rather than the endocytic pathway (Prabhakaran Mariyamma et al., 2017). FL3 also co-localizes strongly with RABA1c, suggesting a role in the secretory pathway (Prabhakaran Mariyamma et al., 2018). Considering that FL3 co-localizes with FKD1 (Prabhakaran Mariyamma et al., 2018) and PIN1 (Section 3.1) but not FKD1 associated proteins SFC (Section 3.2) and BIG5 (Section 3.3), I was interested in the co-localization between FL3 and FM4-64. Following the method that is described in Section 2.9, I observed the expression pattern of FL3 and the FM4-64 dye 15 min, 30 min and 45 min after staining and subsequent water rinse. As can be seen in Table 5 and Figure 11, FL3 and FM-64 co-localized to dot-like structures starting even at 15 min (average PCC=0.14 ± 0.24), suggesting that FL3 is in early endocytic vesicles. The increasing PCC value over time can be explained by FL3 localizing to early and late endocytic vesicles. To confirm that FL3 works in late endosomes, FL3 was co-localized with a maker that labels late endosomes, RABF2a. Consistently, FL3 co-localized with RABF2a (average PCC = 0.34 ± 0.17) (Table 6 and Figure 12). Next, FL1 was also checked for co-localization with RABF2a and the expression of two markers were negatively associated (average PCC = -0.19 ± 0.21) (Table 6 and Figure 12). My results suggest that besides the secretory pathway, there is also a strong potential that FL3 works in the endocytic pathway.

3.6 Cellular compartmentation of FL3 is BFA sensitive

Cellular compartmentation of FKD1 and SFC are both resistant to BFA (Prabhakaran Mariyamma et al., 2017). Although FL3 is partially co-localized and functions redundantly with FKD1 (Prabhakaran Mariyamma et al., 2018), its lack of co-localization with SFC and BIG5 but positive co-localization with FM4-64 vesicles led me to check its BFA sensitivity. After 1 hour BFA incubation, I observed clear pUBQ10:FL3-YFP labeled compartmentation changes, but not after treatment with DMSO control solution (Figure 13 A-F). Interestingly, following BFA treatment, FL3 was mostly aggregated into two big compartments per cell (Figure 13 D-F) and appeared very similar to PIN1 BFA compartments (Geldner et al., 2003a). After washing out the BFA by 2 hours incubation in water, the FL3 labeled BFA compartments disappeared (Figure 13 G-I). Because the BFA compartments include endocytic vesicles, FM4-64 and PIN1 aggregate into the BFA compartments (Sancho-Andrés et al., 2016). To test if FL3 also co-localizes with FM4-64 following BFA treatment, I treated pUBQ10:FL3-YFP expressing roots with BFA and FM4-64 together following the method described early (Section 2.9). Consistently, FL3 and FM4-64 co-localized strongly within the BFA compartments (average PCC= 0.65 ± 0.16) (Table 5 and Figure 13 J-M).

3.7 FL4 co-localizes with both secretory and endocytic markers

FL4 is one of the three members (FL2, FL4 and FL8) within FL family that have not yet been characterized at the cellular level. cDNA of FL4 was synthesized and cloned

into the mCherry containing vector (described in Section 2.5). When p35S:FL4-mCherry was co-localized with TGN marker p35S:SYP61-YFP, they associated quite strongly in vesicles (average PCC = 0.70 ± 0.21) (Table 7 and Figure 14). Cellular co-localization between p35S:FL4-mCherry with secretory marker pUBQ10:RABA4b-eYFP (average PPC = 0.33 ± 0.26) and late endocytic marker pUBQ10:YFP-RABF2b (average PPC = 0.30 ± 0.19) (Table 7 and Figure 14) suggests that FL4 acts in both secretory and late endocytic pathway. Taken together, FL4 acts in a manner somewhat similar to FL3.

3.8 SFC is sensitive to BFA in the root elongation zone

Mutation to *SFC* causes PIN1 labeled BFA compartments to change from two big compartments per cell into several smaller compartments (Sieburth et al., 2006), which suggests that SFC is somewhat involved in the PIN1 compartmentalization induced by BFA. However, there is no observable change of PIN1 BFA compartments in the *fkd1*/*fl2*/*fl3* background (Prabhakaran Mariyamma et al., 2018). It seems that there is a difference between SFC and FKD1 in terms of BFA action; however, SFC and FKD1 compartments are both reported to be BFA resistant (Prabhakaran Mariyamma et al., 2017). The experiment in Prabhakaran Mariyamma et al., 2017 was done by observing p35S:SFC-YFP and p35S:FKD1-GFP in the meristematic zone of roots following treatment with 50 μM BFA, while the experiment in Sieburth et al., 2006 was done by observing PIN1-GFP in *sfc* in the root elongation zone treated with 50 μM BFA. Cells in

the elongation zone and meristematic zone are undergoing very different processes. Cells of the meristematic zone are isodiametric and undergo division, while cells of elongation zone undergo rapid longitudinal expansion (Maloof, 2004). Morphological and physiological differences between these two zones can be correlated with cellular differences in gene expression and molecular signaling (Billou et al., 2005; Brady et al., 2007). For example, BIG1-4 are involved in trafficking of both endocytosed and newly synthesized proteins to the cell–division plane during cytokinesis (Richter et al., 2014), a process that exists in the meristematic zone but not in the elongation zone. Therefore, I asked if SFC and FKD1 are insensitive to BFA in the elongation zone of the roots. In the meristematic zone, neither p35S:SFC-YFP nor p35S:FKD1-GFP aggregated into BFA compartments following treatment with 50 μM BFA. In the elongation zone, FKD1 was still localized to distinct, small punctae in untreated roots and roots treated with 50 μM BFA. In contrast, following 50 μM BFA treatment, p35S:SFC-YFP localized to larger and brighter dots in cells of the elongation zone, which could not be observed without BFA treatment (Figure 15). These results suggest that whereas in the meristematic zone, SFC is acting in a BFA resistant transport route, in the elongation zone, it acts in a BFA sensitive pathway, which is supported by the PIN1 compartmentalization defect in the *sfc* background shown in Sieburth et al., 2006.

3.9 Mutations in *FKD1, SFC, ARF-GEFs* and *ARFA* genes affect vein patterning

Mutation in the *FKD1* gene results in cotyledons and leaves with open venation due to lack of distal junctions between secondary and tertiary veins (Steynen and Schultz, 2003). As well, mutations in *SFC* and *BIG5*/*BEN1* both result in discontinuous vein phenotype (cotyledon and leaf vein phenotypes of *sfc* and cotyledon vein phenotype of *ben1*) (Deyholos et al., 2000; Tanaka et al., 2009) while no vein pattern defects of *BIG3* and *ARFA* members have been reported. This led me to investigate in more depth the roles of FKD1 and ARF system on vein development by mutant analysis. To gain some knowledge about actions of various proteins in provascular cells, number of total secondary veins, non-meeting secondary veins, meeting secondary veins and VIs were scored in cotyledons and representative pictures are shown (Table 8 and Figure 16). When compared with WT, there were more non-meeting secondary veins in *fkd1*, *fkd1*/*big3*, *fkd1*/*big5-1*, and *arfa1a*/*b*/*d*/*e* (all differences are significant), but there was no significant difference between *fkd1* and either *fkd1*/*big3* or *fkd1*/*big5-1*. *fkd1*/*big3* and *fkd2*/*big3* showed a very low frequency of VIs (1/39; 2.6% and 1/25; 4%, respectively), which I did not see in any other lines. Although *fkd2* and *ben1* (an allele of *big5*) were both previously reported to be defective in vein formation (Deyholos et al., 2000; Tanaka et al., 2009), they showed no difference from WT when non-meeting secondary veins are compared. A categorizing method that is similar to the one used in Tanaka et al., 2009, by which the vein defect of *ben1* (an allele of *big5*) was defined, was also used (Section 2.10 and Figure 5). All the WT that were scored fall into Pattern 1 (P1) (n=39). Although

there was no significant difference of non-meeting secondary veins of *fkd2* and *big5-1* compared with WT, 20.5% of *fkd2* cotyledons (n=28) and 11.5% of *big5-1* cotyledons (n=26) fell into P2 and 10.3% of *fkd2* cotyledons (n=28) and 11.5% of *big5-1* cotyledons (n=26) fell into P3. The pattern analysis for cotyledons of *fkd1*, and *arfa1a*/*b*/*d*/*e* compared with WT was also consistent with 'non-meeting secondary vein' data, with most falling into either P2 or P3. Interestingly, like *fkd2* and *big5-1*, *big3* also showed a pattern change, with 20.5% P2 and 10.3% P3, suggesting its role in vein formation. However, introduction of *big3* or *big5-1* into *fkd1* did not change the pattern so much, although slightly more double mutant cotyledons fell into P2 and less into P3. After introduction of *big3* into *fkd2*, plants tended to have more cotyledons with two distal open veins (1/28; 3.6% in *fkd2* and 5/25; 20% in *fkd2*/*big3*, respectively).

In first leaves, number of total secondary veins, non-meeting secondary veins, VIs, tertiary and quaternary veins and non-meeting tertiary and quaternary veins, as well as leaf area, number of non-meeting secondary veins/leaf area, number of tertiary and quaternary veins/leaf area, number of non-meeting tertiary and quaternary veins/leaf area were scored and representative pictures are shown (Table 9 and Figure 17). Both *fkd1* and *fkd2* had more non-meeting secondary veins and VIs than WT, which is consistent with the evidence in Steynen and Schultz, 2003. Besides, a significantly less tertiary and quaternary vein density of *fkd1* and *fkd2* than WT was found, which is indicative of a simpler vein pattern. When *big3* and *big5-1* were compared with WT, no significant

difference was found between *big5-1* and WT among all parameters, whereas in *big3* the significantly fewer secondary, tertiary and quaternary veins but no change in leaf area compared with WT resulted in a simpler vein pattern. However, neither mutation in *BIG3* nor *BIG5* made *fkd1* significantly more severe in any parameter compared. Similarly, mutation in *BIG3* did not make *fkd2* significantly more severe. *arfa1a*/*b*/*d*/*e* had a simpler vein pattern with significantly fewer secondary veins, tertiary and quaternary veins, non-meeting tertiary and quaternary veins, which was correlated with a smaller leaf.

I also planted seeds of various genotypes on AT media without BFA and with 10 uM or 20 uM BFA and assessed difference of the cotyledon vein patterns. *fl2, fl3, cvp2*/*cvl1* and *arfa1a*/*b*/*d*/*e* showed significantly more VIs after 10 µM BFA treatment compared to the VIs following treatment without BFA (APPENDIX II). WT, *fl2, fl3, fkd1*/*fl2, fkd1*/*fl3, fkd1*/*fl1-2*/*fl2*/*fl3* and *cvp2*/*cvl1* showed significantly more VIs after 20 µM BFA treatment compared to the VIs following treatment without BFA (APPENDIX II). WT, *fl2, fl3* and *fkd1*/*fl2* showed significantly more VIs after 20 µM BFA treatment compared to the VIs following treatment with 10 µM (APPENDIX II). The results indicate that WT, *fl2*, *fl3, cvp2*/*cvl1*, *arfa1a*/*b*/*d*/*e* are sensitive to BFA at different concentrations.

3.10 Mutations in members of *FL* family and *ARF* system result in root defects

Several mutants were reported to have root elongation defects including *sfc*, *cvp2*/*cvl1*, *fkd1*/*fl2*/*fl3* and *fkd1*/*fl1-2*/*fl2*/*fl3*, with *fkd1*/*fl1-2*/*fl2*/*fl3* being more extreme than *fkd1*/*fl2*/*fl3* (Carland and Nelson, 2009; Prabhakaran Mariyamma et al., 2018). Single and double mutants of *FL* family were not analyzed in Prabhakaran Mariyamma et al., 2018. To determine to what extent the single and multiple mutations affect root development, the total primary root length, lateral root number and density, distance between root tip and most distal lateral root emergence point and its ratio to the total primary root length were compared between WT and mutant lines *fkd1*, *fkd2*, *fl1*, *fl2*, *fl3*, *fkd1*/*fl1*, *fkd1*/*fl2*, *fkd1*/*fl3*, *fkd1*/*fl2*/*fl3*, *fkd1*/*fl1-2*/*fl2*/*fl3*, *fkd2*, *big3*, *big5-1*, *fkd1*/*fkd2*, *fkd1*/*big3*, *fkd1*/*big5-1*, *fkd2*/*big3*, *arfa1a*/*b*/*d*/*e* and *cvp2*/*cvl1* (Table 10 and Appendix III).

Interestingly, all mutant lines showed significantly less primary root elongation than WT except *big3* and *arfa1a*/*b*/*d*/*e* (Table 10 and Appendix III). The significant difference between *fkd1*/*fl2*/*fl3* and all single mutants, and between *fkd1*/*fl1-2*/*fl2*/*fl3* and all triple, double and single mutant, suggests a functional redundancy amongst Group 1 members of FL family in root elongation. A more severe root elongation defect in *fkd1*/*fkd2* than *fkd1* (significantly different) and *fkd2* (not significantly different) also support the idea that FKD1 and FKD2/SFC proteins work together. Interestingly, *fkd2*/*big3* double mutant had an intermediate root growth phenotype between *fkd2* and *big3*, suggesting SFC and BIG3 may work in an opposite direction to control root

elongation, which can be related to the opposite roles of ARF-GAPs and ARF-GEFs on ARFs. The short root length of *fkd1*, *big5-1* and *fkd1*/*big5-1* compared to WT, and no significant difference between any two of these three mutants, suggests that FKD1 and BIG5 may work in the same pathway.

Compared to WT, lateral root number was different in all mutants except *big3*, *big5-1*, *fkd1*/*big5-1*, *fkd2*/*big3* and *arfa1a*/*b*/*d*/*e*. Those that had fewer lateral roots also had shorter roots, which may explain the lower number. To account for different lateral root number caused by various primary root elongation rates, lateral root density was compared (Table 10 and Appendix III). *fkd1*/*fl2*, *fkd1*/*fl3*, *fkd2* and *fkd1*/*fkd2* have significantly lower lateral root density than WT, and more severe lateral root density phenotype in *fkd1*/*fkd2* than *fkd1* (significant) were observed. Surprisingly, *fkd1*/*fl1*/*fl2*/*fl3* had significantly higher lateral root density than any other *FL* single or multiple mutants tested. Interestingly, similar to the primary root elongation defect, the lateral root density phenotype of *fkd2* could be recovered by introducing mutation to *BIG3* into the *fkd2* genotype.

Adventitious roots are normally not observed emerging from the hypocotyl in WT growing under untreated conditions at a relatively early stage (Verstraeten et al., 2014), and my observation of WT was consistent with this idea. Adventitious roots were not seen in *fkd1*, *fkd2* and *fkd1*/*fkd2*. Interestingly, I did see occasional adventitious roots

in most of the mutant lines (*fl1*, *fl2*, *fl3*, *fkd1*/*fl1-2*, *fkd1*/*fl3*, *fkd1*/*fl2*/*fl3*, *fkd1*/*fl1-2*/*fl2*/*fl3*, *fkd1*/*big3*, *fkd1*/*big5-1*, *fkd2*/*big3*, *arfa1a*/*b*/*d*/*e* and *cvp2*/*cvl1*), while only *fkd1*/*fl1-2*/*fl2*/*fl3*, *fkd1*/*big5-1* and *arfa1a*/*b*/*d*/*e* were significantly different than WT (Table 10 and Figure 18). There was a significant difference between *fkd1*/*fl1-2*/*fl2*/*fl3* and all other *FL* single or multiple mutants tested, and between *fkd1*/*big5-1* and the two single mutants, suggesting functional redundancy.

4 Discussion

4.1 FKD1 and SFC co-localize with BFA sensitive and resistant ARF-GEFs

Because FKD1 and SFC localize to BFA insensitive vesicles, they are proposed to work with BFA insensitive ARF-GEFs, BIG3 and BIG5 (Geldner et al., 2003b; Prabhakaran Mariyamma et al., 2017). BIG5 co-localizes with TGN markers SYP61 and VHA-a1 and co-localizes with ARFA1c (Tanaka et al., 2009). FKD1 co-localizes with SYP61 and ARFA1c (Prabhakaran Mariyamma et al., 2017). My results show that FKD1 co-localizes strongly with BIG5. Both *ben1* (an allele of *big5*) and *fkd1* show a non-meeting cotyledon vein phenotype (Steynen and Schultz, 2003; Tanaka et al., 2009) but *big5* does not make the *fkd1* vein pattern more severe. As well, a relatively strong co-localization of FKD1 and BIG3, a cotyledon non-meeting vein phenotype in *big3* and *big3* not making *fkd1* vein phenotype more severe were observed. The co-localization and the double mutant phenotype are both consistent with BIG3, BIG5 and FKD1 acting in the same pathway and being closely related. A similar logic was used to propose that SFC acts in the same pathway as CVP2 and CVL1, since the *sfc* phenotype was similar to *cvp2*/*sfc* double mutants, as well as *cvp2*/*cvl1*/*sfc* triple mutants (Carland and Nelson, 2009; Naramoto et al., 2009), and was also later supported by the more cytosolic localization of SFC in *cvp2*/*cvl1* (Carland and Nelson, 2009).

The very strong association between one ARF-GAP, SFC and one ARF-GEF, BIG3 suggests that the two proteins likely work on the same ARF(s), which can be

supported by the intermediate root elongation phenotype seen in double mutants. An example of mutations in both ARF-GAP and ARF-GEF having an intermediate phenotype is that when *SFC* and *GNOM* are both mutated, the double mutant shows an intermediate vein defect (Sieburth et al., 2006). Unlike *gnom* which shows a more connected vein pattern than WT, the *big3* single mutant does not have longer root elongation than WT. SFC is localized to TGN but GNOM is localized to GA (Naramoto et al., 2014; Prabhakaran Mariyamma et al., 2017). The different localization of GNOM and SFC and an intermediate phenotype in the double mutant suggests that they are acting in different but opposing steps. BIG3 co-localizes with FM4-64 (Richter et al., 2014), which suggests its possible localization to TGN/early endosomes, like SFC, and BIG3 and SFC may work in the opposing but same step. The co-localization between BIG3 and TGN marker SYP61 needs to be further done to support this hypothesis. The root elongation of *big3* is less than WT, although not significantly, so it is possible that BIG3 and SFC both catalyze GDP-GTP change of the same ARF(s) and either mutation suppresses the same ARF's normal function. Considering the functional redundancy between ARFA group members (Billou et al., 2005), however, it is possible that when both *BIG3* and *SFC* are mutated, but not when only one is mutated, other ARFs that are not associated with both BIG3 and SFC will take over the defective functions of the ARF(s) with which both BIG3 and SFC are associated. SFC was suggested to be able to activate yeast ARF1 (Koizumi et al., 2005), which is close to ARFA subclass in

Arabidopsis (Bonifacino and Traub, 2003) and further co-localization studies between members of ARFA and SFC or BIG3 need to be done to support the idea that they share the same ARF target(s). As well, it will be interesting to check the localization of SFC and FKD1 in *big3* and *big5* mutants, or BIG3 and BIG5 in *fkd1* and *sfc* mutants, since deletion of one protein may change the localization pattern of its associated protein.

Both FKD1 and SFC co-localize with BIG4, a BFA sensitive member of the ARF-GEFs (Geldner et al., 2003b). This is somewhat surprising, but still, such co-localization is consistent with the observation that both BIG4 and FKD1 co-localize with ARFA1c and TGN markers (VHA-a1 for BIG4 and SYP61 for FKD1) (Jonsson et al., 2017; Prabhakaran Mariyamma et al., 2017) and SFC co-localizes with TGN markers SYP41 and SYP61 and has activity *in vitro* on yeast ARF1 protein (Koizumi et al., 2005; Naramoto et al., 2009; Prabhakaran Mariyamma et al., 2017). Such observations suggest that BFA sensitivity is not a good way to predict the association of different proteins under non BFA treated condition, which also can be seen in those proteins with different sensitivity which co-localize without BFA but end up totally or partially in different compartments following treatment with BFA (*e.g.* the association pattern between SFC and SYP61 and between SFC and RABA1c in Prabhakaran Mariyamma et al., 2017). Also, since both FKD1 and SFC are associated with BIG4, it will also be interesting to check the cotyledon and leaf vein phenotypes of *big4*.

BIG3 is insensitive to BFA, and knocking-out *BIG3* makes the plant become super sensitive to BFA so that it shows defects in germination even at a relatively low BFA concentration (Richter et al., 2014). BIG4 is normally BFA sensitive, but introducing a genetically engineered BFA resistant BIG4 is able to recover the defects caused by a low concentration of BFA in *big3*, which suggests a functional redundancy among BIGs in plant development (Richter et al., 2014). This idea is supported by my result that both BIG3 and BIG4 co-localize with SFC or FKD1 in vesicles.

Previous studies showed that FKD1 and SFC not only co-localize strongly but also interact in the yeast two hybrid assay and BiFC test (Naramoto et al., 2009; Prabhakaran Mariyamma et al., 2017). Relatively strong co-localization between BIGs and FKD1 or SFC suggests that these proteins may interact; however, the experiments that can confirm protein interactions such as BiFC, yeast two hybrid or pull-down assay need to be done.

4.2 BIG4, SFC and FKD1 co-localize with PIN1

Co-localization between one BIG protein, BIG4, and SFC or FKD1 suggests their association, and furthermore, they all co-localize with PIN1 in dot-like structures. This is consistent with the observation that PIN1 localization is disrupted in provascular cells of *sfc* and *fkd1* (Scarpella et al., 2006; Hou et al., 2010) and PIN1 compartmentation after BFA treatment is disturbed in *ben1* (an allele of *big5*), *ben3* (an allele of *big2*) (Tanaka et

al., 2009) and *fkd2* (Sieburth et al., 2006), which suggests that BIGs, SFC and FKD1 play key roles in PIN1 transport. The previous studies of PIN protein transport are mostly based on the expression of PIN proteins in a mutant/inhibitory background (Geldner et al., 2003b; Tanaka et al., 2009). PIN1 co-localization with the proteins that are reported to be important for PIN1 dynamics and plant development may also provide a way to test the interplay of various proteins with PIN1, in addition to expressing PIN1 in a mutant background or treated with inhibitors.

4.3 FL family Group 1 and 3 show distinct co-localization with PIN1

Members of FL Group 1 but not Group 3 partially co-localize with PIN1, suggesting that only Group 1 is involved in PIN1 trafficking. The more severely disconnected vein phenotype in plants with null mutations in all members of *FL* Group 1 compared to the *fkd1* single mutation, together with more compromised PIN1 polar localization in leaf provascular cells in *fkd1*/*fl2*/*fl3* than in *fkd1*, suggested that there is a functional redundancy for Group 1 of FL family proteins in PIN1 polar localization during vein development (Prabhakaran Mariyamma et al., 2018), which can also be supported by my observation that FKD1, FL1 and FL3 partially co-localize with PIN1. Previous literature reported the non-meeting vein pattern of *fkd1*/*fl6*/*fl7* is no more severe than *fkd1* (Prabhakaran Mariyamma et al., 2018). Meanwhile, the negative association of FL5, FL6 and FL7 with PIN1 suggests that they are not involved in PIN1 transport and

thus have no role in the PIN1 canalization that occurs in leaf provascular tissue to control vein patterning. Taken all together, positive co-localization of PIN1 and those proteins that are important for PIN1 traffic, but negative association between PIN1 and non-proposed interactors supports an alternative and more straightforward way to dissect the PIN1 transport pathway- directly testing protein co-localization.

Members of FL Group 1 are co-localized with PIN1 (Section 3.1) and act redundantly to maintain PIN1 polarity in leaf provascular tissues to control vein patterning (Prabhakaran Mariyamma et al., 2018), which suggests their key roles in auxin transport. The primary root elongation rate over a 24 hour period between 4 and 5 DAG of WT, *fkd1*, *fkd1*/*fl2*/*fl3* and *fkd1*/*fl1-2*/*fl2*/*fl3* were previously compared (Prabhakaran Mariyamma et al., 2018), while in my study, more single and multiple mutant lines in this group were tested. Similar to the vein pattern defects (Prabhakaran Mariyamma et al., 2018), more severe of root growth defects are shown as more members of Group 1 are removed from *fkd1*, suggesting the functional redundancy of the Group 1 members of FL family in primary root elongation.

Auxin also controls lateral root initiation in root pericycle cells and adventitious root initiation in hypocotyl of Arabidopsis (Benková et al., 2003; Verstraeten et al., 2014). Interestingly, *fkd1*/*fl2* and *fkd1*/*fl3* show significantly lower lateral root density and reduced primary root elongation defects, while *fkd1*/*fl1*/*fl2*/*fl3* shows reduced primary root elongation but significantly higher lateral root density and significantly

more adventitious roots. Adventitious roots are normally not seen in WT without any stimuli (Verstraeten et al., 2014). The phenotype of unexpected adventitious roots may indicate auxin transport defects, where auxin fails to be transported properly to the root and accumulates in the hypocotyl tissue. The primary root elongation defects can be explained by auxin defects in either or both the meristematic zone where cell divisions happen and the elongation zone where cell elongation and differentiation happen (Verbelen et al., 2006), and the auxin transport mechanism can be quite different than in the hypocotyl region. The spatiotemporal distribution of different PIN proteins within the root gives different characteristics of each root region in term of auxin transport. Variation of phenotypes in terms of primary root elongation, lateral root initiation and adventitious root initiation may be correlated with the disruption of different PIN protein combinations in different regions. Also, the threshold of the mutation effects may be different in different regions.

4.4 Members of FL family Group 1 do not co-localize with SFC or BIG5

FKD1 co-localizes strongly with SFC (Naramoto et al., 2009; Prabhakaran Mariyamma et al., 2017), and partially with FL1 and FL3 (Prabhakaran Mariyamma et al., 2018). SFC, FKD1, FL1 and FL3 were observed to co-localize with TGN markers (SYP41 and SYP61 for SFC and SYP61 for FKD1, FL1 and FL3) and secretory markers (RABA1b and RABA1c for SFC, RABA1e and RABA4b for FKD1, and RABA1c for

FL1 and FL3) (Naramoto et al., 2009; Prabhakaran Mariyamma et al., 2017; Prabhakaran Mariyamma et al., 2018), suggesting that SFC may co-localize with FL1 and FL3. However, no co-localization was found, which suggests that FL1 and FL3 may function independently of SFC. SFC has three close homologs in ARF-GAP family, AGD1 (expressed primarily in root, co-localized with late endosome marker ARA7/RABF2b), AGD2 (expressed in both leaf and root, co-localized with late endosome marker ARA7/RABF2b) and AGD4 (expressed in both leaf and root) (Naramoto et al., 2010; Naramoto et al., 2016), so it is possible that FL1 and FL3 work with one of these proteins instead of SFC. Although, like BIG5 (Tanaka et al., 2009), FL1 and FL3 co-localize with TGN marker SYP61 (Prabhakaran Mariyamma et al., 2018), they are not co-localized with BIG5. Except for BIG5, it is possible that FL1 and FL3 co-localize with other BIG family members.

4.5 FL3 localization suggests a role in endocytosis

F1 and FL3 co-localize with TGN marker SYP61, as well as RABA1c, suggesting a role in the secretory pathway (Prabhakaran Mariyamma et al., 2018). FKD1 and SFC co-localize weakly with FM4-64, but strongly with RABA members, suggested they are mainly involved in a secretory pathway instead of an endocytic pathway (Prabhakaran Mariyamma et al., 2017). Incomplete co-localization with FKD1 together with no association with SFC or BIG5 suggested that FL3 may be involved in a different

pathway. FM4-64, a lipophilic styryl dye (Bolte et al., 2004), labels the PM and is then taken into the cell interior by endocytosis, after which it gradually labels the entire endocytic pathway (Bolte et al., 2004; Tse et al., 2004; Ueda et al., 2004; Dettmer et al., 2006). The increasing co-localization with FM4-64 indicates that FL3 co-localizes with both early and late endosomes, in a different fashion than FKD1 which is weakly associated with FM4-64 (Prabhakaran Mariyamma et al., 2017). As well, FKD1 co-localizes weakly with a late endosome marker RABF2b (Prabhakaran Mariyamma et al., 2017) but the co-localization between another late endosome marker RABF2a and FL3 is relatively strong, which supports the idea that FL3 works in the late endocytic pathway. Although FL3 does not co-localize with SFC, it is possible that FL3 co-localizes with SFC homologs AGD1 or AGD2, both of which co-localize with late endosome marker ARA7/RABF2b (Naramoto et al., 2017). As well, the co-localization between FL3 and BIG1-4 has not been tested yet. BIG2 co-localizes with FM4-64 labeled vesicles and TGN marker SYP61 (Kitakura et al., 2017), which is similar to FL3, indicating their potential association.

The PH domain is important for protein localization via an interaction with PIs (Lemmon 2007). SFC has a PH domain and FKD1 has a PH_2 domain and PI4P was suggested to be crucial for proper cellular localization of both proteins (Naramoto et al., 2009; Prabhakaran Mariyamma et al., 2017). Both FL1 and FL3 have PH_2 domains (more than 60% similarity in terms of amino acids to FKD1 PH_2 domain), suggesting

their binding to PIs (Prabhakaran Mariyamma et al., 2018). However, the correlation between the protein PH/PH_2 domain sequences and specific PI binding ability of domains is unknown, and thus the sequence similarity amongst PH_2 domains cannot be used to predict the PI4P binding of FL1 or FL3 (Lemmon, 2007; Prabhakaran Mariyamma et al., 2018). Meanwhile, PI3P and PI(3,5)P_2 are the PIs that label the late endosomes (Heilmann, 2016) and the co-localization of FL3 with late endosome marker RABF2a suggests its localization may be partially PI3P or PI(3,5)P_2 dependent.

4.6 Different genetic interplay between *FL* family and *ARF* system in auxin related development

SFC shows different BFA sensitivity in root meristematic and elongation zones, as compartmentation of SFC is BFA sensitive in the elongation zone but not in the meristematic zone. FKD1 is consistently BFA resistant in both regions (Prabhakaran Mariyamma et al., 2017 and my results). Since BFA did not clearly change the strong association between SFC and FKD1 in the meristematic zone (Prabhakaran Mariyamma et al., 2017), it will be interesting to see if their association will be disturbed in elongation zone by BFA treatment. As well, SFC co-localizes with BIG3 and BIG4 in a transient expression system. BIG1-4 are involved in trafficking of both endocytosed and newly synthesized proteins to the cell–division plane during cytokinesis in the meristematic zone, a process that does not exist in the elongation zone (Richter et al.,

2014) and the BFA sensitivity of SFC could be correlated with the different roles of BIG family in different root zones. The different BFA sensitivity of SFC in different root zones suggests that protein associations/biological functions can be quite variable in different systems (organisms/tissues/cells) and thus a) the association of Arabidopsis proteins in a heterologous system (epidermal cells of tobacco) may not always happen in Arabidopsis or may only happen in certain tissues/cells; b) mutant phenotypes can be quite variable in different tissues due to the different interactions of proteins.

Transient expression in tobacco leaf epidermis shows that FKD1, SFC and BIGs are partially in the same transport vesicles as PIN1. However, how this system is applicable to Arabidopsis different tissues/cells remain to be determined. Clearly, the protein dynamics and interactions are not the same in all plant tissues. It seems FKD1, SFC, BIGs and ARFs work to control PIN1-dependant auxin transport and its related phenotypes. Such redundancy varies amongst different tissues of leaf and root, as the phenotypic difference between multiple mutants and single mutants differs in distinct tissues (cotyledon veins, first leaf veins, primary roots, lateral roots and seedling hypocotyls).

The significantly more non-meeting secondary veins of cotyledons, especially non-distal meetings in *arafa1a*/*b*/*d*/*e* compared to WT provide the first direct evidence that members of ARFA groups play important roles in vein patterning. However, the non-meeting secondary vein defect is only seen in cotyledons, and the first leaf vein

pattern has no change in vein meeting, although fewer veins and smaller leaf area were observed. Also, the primary root elongation defects were not observed in *arafa1a*/*b*/*d*/*e*. One possibility is that the ARFA subclass is primarily expressed earlier in development, which can be supported by the overexpression of a dominant-negative allele of *ARFA1c* causing disorganized cell arrangement of the hypophysis (the basal part of embryos forming the embryonic root) and failure to develop cotyledon primordia (Tanaka et al., 2014). Another explanation is that both *ARFA1c* and *ARFA1f* are expressed in leaves and roots (Klepikova et al., 2016), which may be enough for maintaining primary root elongation and first leaf vein meeting, but not the cotyledon vein meeting. The non-meeting vein phenotypes of *big3* and *big5-1* in cotyledons but not in first leaves is the same as defects of *arafa1a*/*b*/*d*/*e*, suggesting that ARF-GEF BIGs and ARFA members are functionally highly correlated for vein patterning. BFA inhibits the function of sensitive ARF-GEFs (Geldner et al., 2003b). Compartmentation of FL3 is sensitive to BFA, and the sensitivity of *fl2*, *fl3*, *cvp2*/*cvl1* and *arfa1a*/*b*/*d*/*e* suggests that FL2, FL3, PI4P and ARFA group are all involved in a redundant BFA sensitive network for vein patterning. According to this idea, mutation to additive components of the BFA sensitive system will result in vein defects in the presence of BFA.

BFA treated *big3* shows a severe defect in primary root elongation, suggesting ARF-GEFs are redundantly important for primary root elongation (Richter et al., 2014), which is also supported by the observation that both *big3* and *big5-1* show shorter root

elongation than WT in my experiment. Adventitious root defects in *fkd1*/*big5-1* and *arfa1a*/*b*/*d*/*e*, but not in *big5-1* and *fkd1* single mutants were observed. BIGs and ARFA1c were reported to be important for the secretion of the auxin influx carrier AUX1 to the PM from the TGN during hypocotyl apical hook development (Jonsson et al., 2017). Taken together, FKD1, BIG4 and ARFA group proteins are very important for maintaining proper auxin transport in the hypocotyl by their influence on auxin transport carriers such as AUX1 and PIN proteins.

5 Conclusions

1. Introducing mutations in *ARF-GEF*s that are important for vein patterning does not make *fkd1* or *fkd2* cotyledon vein defects more severe. These results indicate that FKD1 and FKD2/SFC work together with members of ARF-GEFs, which is supported by the moderate to strong co-localization between FKD1 or SFC with members of ARF-GEFs.

2. FL Group 1 members, ARF-GAP (SFC) and ARF-GEF (BIG4) all co-localize with PIN1, supporting their roles in PIN1 transport, and their importance in auxin transport in leaves, hypocotyls and root.

3. The cellular localization and BFA response of FL3 is very different from FKD1. The co-localization with endocytic markers suggests that FL3 works in the endocytic pathway to affect PIN1 distribution.

4. Group 3 members of the FL family do not co-localize with PIN1, and therefore are unlikely to be involved in PIN1 trafficking.

Table 1: Gene name, AGI designation (annotated locus code), allele name, seed line with SALK T-DNA insertion (Alonso et al., 2003) and position of T-DNA insertion. * indicates that the allele information was provided by ABRC and the position of T-DNA insertion was predicted by high-throughput sequencing (Alonso et al., 2003). ** indicates that the allele was further confirmed by sequencing (see Figure 4). *** indicates that the allele was further confirmed by Richter et al., 2014. **** indicates that the allele was further confirmed by Nomura et al., 2006.

Gene name	AGI designation	Allele name	Seed line	Position of T-DNA insertion
FL1	At5G43870	*fl1-2*	Salk_064024	Intron 2 of 6**
FL2	At3G22810	*fl2*	Salk_026656	Exon 4 of 7**
FL3	At4G14740	*fl3*	Salk_013371	Exon 2 of 7**
ARFA1a	At1G23490	*arfa1a*	Salk 107987	5'UTR*
ARFA1b	At5G14670	*arfa1b*	Salk 027659	5'UTR*
ARFA1d	At1G70490	*arfa1d*	Salk_039612	Exon 2 of 5*
ARFA1e	At3G62290	*arfa1e*	Salk 130670	Promoter*
BIG3	At1G01960	*big3*	Salk_044617	Exon 7 of 11***
BIG5	At3G43300	*big5-1*	Salk_012013	Exon 18 of 32****

Table 2: Primers used in PCR reactions for identifying T-DNA insertions and constructing SFC-mCherry vector. Primers used for amplifying junction regions are in bold. * indicates that the T-DNA left border primer used was CGTCCGCAATGTGTTATTAAG; ** indicates that the T-DNA left border primer used was ATTTTGCCGATTTCGGAAC; *** indicates that the T-DNA left border primer used was ATAATAACGCTGCGGACATCTACATTTT.

allele	Left Primer	Right Primer
fl1-2	GCTCATTCACCGACAGTCCTCCG	**GGCTGTTGAGATAGACCGTTGTG***
fl2	**CACTGCAACAACTACACAGTCC****	**CGTGAAGGTCCCTCCTACATGC****
fl3	GTATCACCAAGAACATCTGGTCGGC	**CGTGAATCTGAGCGTTATGAGCCCG***
arfa1a	CTGGAGAGAACTCGTTGTTGG	GCGAGAACTCCAAATGTTGAC**
arfa1b	GTCCGGTTCACAGTAGAGCAG	ACATCCCAAACAGTGAAGCTG**
arfa1d	TCTGTGATGAAAACGATGCAG	CAAGCTCGGAGAGATTGTCAC**
arfa1e	AGTGAGCTCTCCTTCTTTGGG	GTTGTGGAAGCCAGAGATGAG**
big3	CTCCGTGATGTGTGGGAAGT	ATCTCTTGGGGGAAGGAGCG**
big5-1	CTACATTTGCTCCCTCTGTGC	TTCTTCTCTGCTGTCAGGCTC**
T-DNA left border	CGTCCGCAATGTGTTATTAAG* ATTTTGCCGATTTCGGAAC** ATAATAACGCTGCGGACATCTACATTTT***	
SFC cDNA amplifying	TATTAGAATTCATGCATTTCACTAAGCTTG	ATAATGGATCCCGCACTGTCTGTGATTGTA
SFC-mCherry junction amplifying	TGGAGAGGACGTCGAGAGTT	GCGAAAGCAATGTCCCCATC

Table 3: Correlation of expression between pMDC7:PIN1-RFP and members of ARF-GAP, ARF-GEF or FL family fused to YFP or GFP in transiently transformed (*N. tabacum*) leaf epidermis. PCC is the mean of PCC from all merged images and determined using co-localization plugin in NIH Image J. Sample size is number of individual cells analyzed.

pMDC7:PIN1-RFP co-localized with	Sample size	Mean PPC ± standard deviation
p35S:SFC-YFP	17	0.20 ± 0.15
pUBC:BIG4-YFP	24	0.27 ± 0.16
p35S:FKD1-GFP	27	0.28 ± 0.15
pUBQ10:FL1-YFP	20	0.28 ± 0.15
pUBQ10:FL3-YFP	20	0.45 ± 0.13
pUBQ10:FL5-YFP	21	-0.04 ± 0.13
pUBQ10:FL6-YFP	17	-0.04 ± 0.15
pUBQ10:FL7-YFP	15	-0.19 ± 0.08

Table 4: Correlation of expression between A) p35S:SFC-mCherry and p35S:SFC-YFP, pUBQ10:FL1-YFP or pUBQ10:FL3-YFP; B) p35S:BIG5-dsRED and p35S:FKD1-GFP, pUBQ10:FL1-YFP or pUBQ10:FL3-YFP; C) pGII:BIG3-YFP and p35S:FKD1-GFP or p35S:SFC-mCherry and D) pUBC:BIG4-YFP and p35S:FKD1-GFP or p35S:SFC-mCherry in transiently transformed (*N. tabacum*) leaf epidermis. PCC is the mean of PCC from all merged images and determined using co-localization plugin in NIH Image J. Sample size is number of individual cells analyzed.

A) Co-localization of p35S:SFC-mCherry with	Sample size	Mean PPC ± standard deviation
p35S:SFC-YFP	23	0.70 ± 0.19
pUBQ10:FL1-YFP	20	0.04 ± 0.16
pUBQ10:FL3-YFP	18	-0.06 ± 0.17
B) Co-localization of p35S:BIG5-dsRED with		
p35S:FKD1-GFP	31	0.70 ± 0.28
pUBQ10:FL1-YFP	18	-0.21 ± 0.19
pUBQ10:FL3-YFP	16	-0.02 ± 0.28
C) Co-localization of pGII:BIG3-YFP with		
p35S:FKD1-GFP	23	0.43 ± 0.13
p35S:SFC-mCherry	24	0.78 ± 0.23
C) Co-localization of pUBC:BIG4-YFP with		
p35S:FKD1-GFP	16	0.64 ± 0.27
p35S:SFC-mCherry	23	0.27 ± 0.19

Table 5: Correlation of expression between pUBQ10:FL3-YFP and FM4-64 with and without BFA treatment in Arabidopsis root at different time intervals. PCC is the mean of PCC from all merged images and determined using co-localization plugin in NIH Image J. n is the number of root cell files.

	FM4-64 (15 mins)	FM4-64 (30 mins)	FM4-64 (45 mins)
pUBQ10:FL3-YFP	0.14 ± 0.24 (n=30)	0.28 ± 0.21 (n=38)	0.33 ± 0.24 (n=25)
pUBQ10:FL3-YFP (with BFA)		0.65 ± 0.16 (n=21)	

Table 6: Correlation of expression between pUBQ10:RFP-RABF2a and pUBQ10:FL1-YFP or pUBQ10:FL3-YFP in transiently transformed (*N. tabacum*) leaf epidermis. PCC is the mean of PCC from all merged images and determined using co-localization plugin in NIH Image J. Sample size is number of individual cells analyzed.

pUBQ10:RFP-RABF2a co-localized with	Sample size	Mean PPC ± standard deviation
pUBQ10:FL1-YFP	16	-0.19 ± 0.21
pUBQ10:FL3-YFP	18	0.34 ± 0.17

Table 7: Correlation of expression between p35S:FL4-mCherry and p35S:SYP61-YFP, pUBQ10:RABA4b-eYFP or pUBQ10:YFP-RABF2b in transiently transformed (*N. tabacum*) leaf epidermis. PCC is the mean of PCC from all merged images and determined using co-localization plugin in NIH Image J. Sample size is number of individual cells analyzed.

Co-localization of FL4-mCherry with	Sample size	Mean PPC ± standard deviation
p35S:SYP61-YFP	23	0.70 ± 0.21
pUBQ10:RABA4b-eYFP	26	0.33 ± 0.26
pUBQ10:YFP-RABF2b	29	0.30 ± 0.19

Table 8: Cotyledon vein characteristics of different Arabidopsis genotypes after 14 days of growth. Values reported are means ± standard deviations, or percentages of the whole sample. VI is vascular island. P refers to the vein pattern, P1, P2 and P3 are shown in Figure 5. [a] is significantly different from WT, [bi] is significantly different from the corresponding single mutant labeled as [*bi*]. '% VI' is the percentage of the cotyledons showing VI(s). '1 open' refers to the cotyledon has only one distal non-meeting upper loop, '2 open' refers to the cotyledon has two distal non-meeting upper loops.

Genotype	Sample size	#Secondary veins	#Non-meeting secondary veins	#Meeting secondary veins	% VI	% P1	% P2	% P3	% P3 1 open	% P3 2 open
WT	39	3.9 ± 0.6	0.8 ± 0.8	3.2 ± 0.9	0	100	0	0	-	-
fkd1	37	3.4 ± 0.8[a]	2.7 ± 1.2[a]	0.7 ± 0.7[a]	0	8.1	2.7	89.2	48.6	40.6
fkd2	28	2.4 ± 0.7[a]	1.0 ± 1.0	1.5 ± 0.7[a]	0	39.3	17.9	42.9	39.3	3.6
big3[*b1*]	39	3.7 ± 0.6	1.2 ± 0.9	2.5 ± 0.9[a]	0	69.2	20.5	10.3	7.7	2.6
big5-1[*b2*]	26	3.8 ± 0.6	0.8 ± 0.8	3.0 ± 0.7	0	76.9	11.5	11.5	11.5	0
fikd1/big3	39	3.2 ± 0.7[a,b1]	2.2 ± 1.2[a,b1]	1.0 ± 1.1[a,b1]	2.6	12.8	10.3	77.0	28.2	48.8
fkd1/big5-1	22	3.5 ± 0.7[a]	2.6 ± 0.9[a,b2]	0.9 ± 0.7[a,b2]	0	0	18.2	81.8	50.0	31.8
fkd2/big3	25	2.6 ± 0.7[a,b1]	1.3 ± 1.2	1.2 ± 1.0[a,b1]	4	32.0	36.0	32.0	12.0	20.0
arfa1a/b/d/e	42	4.1 ± 0.7	1.7 ± 0.9[a]	2.3 ± 0.7[a]	0	45.2	42.9	11.9	11.9	0

Table 9: First leaf characteristics of different Arabidopsis genotypes after 21 days of growth. Values reported are means ± standard deviations. [a] is significantly different from WT, [bi] is significantly different from the corresponding single mutant labeled as [*bi*].

Genotype	Sample size	#Secondary veins	#Non-meeting secondary veins	#VI	# Tertiary and quaternary veins	# Non-meeting tertiary and quaternary veins	Leaf area (mm^2)	# Non-meeting secondary veins / Leaf area ($veins/mm^2$)	# Tertiary and quaternary veins / leaf area ($veins/mm^2$)	# Non-meeting tertiary and quaternary veins / leaf area ($veins/mm^2$)
WT	40	4.6 ± 0.8	0.3 ± 0.5	0	14.2 ± 3.3	6.9 ± 2.5	18.3 ± 4.6	0.0 ± 0.0	0.8 ± 0.2	0.4 ± 0.1
fkd1	34	3.9 ± 0.8[a]	2.1 ± 1.0[a]	2.6 ± 1.6[a]	6.0 ± 1.7[a]	5.2 ± 1.3[a]	13.6 ± 3.2[a]	0.2 ± 0.1[a]	0.5 ± 0.1[a]	0.4 ± 0.1
fkd2[*b3*]	45	3.4 ± 0.7[a]	1.8 ± 0.9[a]	2.9 ± 1.7[a]	5.0 ± 1.8[a]	4.6 ± 1.7[a]	12.2 ± 1.7[a]	0.1 ± 0.1[a]	0.4 ± 0.1[a]	0.4 ± 0.1
big3[*b1*]	44	4.0 ± 0.8[a]	0.5 ± 0.7	0	9.8 ± 2.9[a]	6.1 ± 2.1	18.3 ± 3.4	0.0 ± 0.0	0.5 ± 0.1[a]	0.3 ± 0.1
big5-1[*b2*]	27	4.3 ± 0.8	0.7 ± 1.1	0	13.1 ± 4.0	7.2 ± 2.6	19.7 ± 4.6	0.0 ± 0.0	0.7 ± 0.2	0.4 ± 0.2
fkd1/*big3*	59	4.1 ± 0.9[a]	1.9 ± 1.1[a,b1]	1.7 ± 1.2[a,b1]	5.3 ± 2.9[a,b1]	4.8 ± 2.5[a,b1]	12.1 ± 3.1[a,b1]	0.2 ± 0.1[a,b1]	0.4 ± 0.2[a,b1]	0.4 ± 0.2[b1]
fkd1/ *big5-1*	30	4.2 ± 0.7	2.7 ± 1.0[a,b2]	2.1 ± 1.3[a,b2]	5.3 ± 2.3[a,b2]	4.8 ± 1.9[a,b2]	11.7 ± 3.5[a,b2]	0.2 ± 0.1[a,b2]	0.5 ± 0.2[a,b2]	0.4 ± 0.2
fkd2/*big3*	38	4.0 ± 0.9[a,b3]	2.2 ± 1.2[a,b1]	3.3 ± 1.7[a,b1]	5.9 ± 1.9[a,b1]	5.5 ± 1.8	12.7 ± 3.0[a,b1]	0.2 ± 0.1[a,b1]	0.5 ± 0.2[a]	0.4 ± 0.2
arfa1a/*b*/*d*/*e*	41	3.7 ± 0.7[a]	0.4 ± 0.6	0.2 ± 0.4	9.8 ± 2.8[a]	5.2 ± 2.2[a]	13.0 ± 3.6[a]	0.0 ± 0.0	0.8 ± 0.3	0.4 ± 0.2

Table 10: Root parameters of different Arabidopsis genotypes after 9 days of growth. Values reported are means ± standard deviations. [a] indicates significantly different from WT, [bi] indicates significantly different from the corresponding single mutant labelled as *[bi]*, [c] indicates significantly different from both single mutants, [d] indicates significantly different from the other member labelled as *[d]*, [e1] indicates significantly different from all mutants that include *fl* members, [e2] indicates significantly different from *fkd1*/*fl2*, [e3] indicates significantly different from *fl3*. Since not all seedlings have lateral roots, sample size is indicated within the parenthesis for tip to first distal lateral root initiation point distance (Tip to distal LR distance) and tip to first distal lateral root initiation point distance/total primary root length (Tip to distal LR distance/Total PR length).

Genotype	Sample size	Total primary root length (mm)	Lateral roots number	Lateral Root Density (roots/cm)	Adventitious root number	Tip to distal LR distance (mm)	Tip to distal LR distance/Total PR length
WT	27	52.6 ± 10.7	8.0 ± 3.7	1.4 ± 0.5	0	29.0 ± 4.2 (26)	0.5 ± 0.1 (26)
fkd1	20	42.0 ± 9.0[a,*b1*,*d*]	5.0 ± 3.6[a,*b2*]	1.1 ± 0.6[*b1*]	0	24.3 ± 3.9[a,*b1*,*b2*] (19)	0.6 ± 0.1 (19)
fl1	42	42.6 ± 10.3[a]	5.1 ± 3.0[a]	1.1 ± 0.6	0.0 ± 0.2	25.5 ± 3.7 (38)	0.6 ± 0.1 (38)
fl2	34	42.0 ± 11.0[a,*d*]	5.4 ± 3.3[a,*b1*]	1.2 ± 0.6	0.1 ± 0.2	26.2 ± 3.5[*d*] (31)	0.6 ± 0.1 (31)
fl3	32	42.9 ± 12.4[a,*d*]	4.8 ± 3.6[a]	1.0 ± 0.7	0.1 ± 0.2	20.2 ± 4.4[a] (27)	0.5 ± 0.1[*b1*,*d*,*e3*] (27)
fkd1/*fl1-2*	33	40.6 ± 12.5[a]	5.4 ± 4.6[a]	1.2 ± 0.8	0.0 ± 0.2	23.9 ± 4.2[a] (28)	0.6 ± 0.2 (28)
fkd1/*fl2*	26	31.7 ± 8.9[a,c]	2.7 ± 2.5[a,b1]	0.7 ± 0.6[a]	0	22.4 ± 6.3[a] (18)	0.6 ± 0.2 (18)
fkd1/*fl3*	31	37.1 ± 9.8[a]	4.2 ± 3.6[a]	1.0 ± 0.7[a]	0.0 ± 0.2	23.2 ± 4.1[a] (28)	0.6 ± 0.1[b1] (28)
fkd1/*fl2*/*fl3*	39	34.7 ± 8.8[a,d]	3.9 ± 3.1[a]	1.1 ± 0.8	0.2 ± 0.4	22.0 ± 4.5[a,d] (26)	0.7 ± 0.2[a,d] (36)
fkd1/*fl1-2*/*fl2*/*fl3*	32	21.8 ± 5.4[a,e1]	4.9 ± 2.7[a,e2]	2.2 ± 1.1[e1]	1.0 ± 0.7[a,e1]	13.0 ± 3.9[a,e1] (31)	0.6 ± 0.2[e3] (31)
fkd2	28	30.3 ± 6.7[a]	2.5 ± 2.2[a,*b4*]	0.7 ± 0.6[a,*b2*]	0	20.3 ± 3.8[a] (20)	0.6 ± 0.2 (20)
big3	36	46.0 ± 8.9[*b2*]	6.7 ± 3.2[*b3*]	1.4 ± 0.5	0.1 ± 0.3	21.6 ± 4.7[a] (36)	0.5 ± 0.2[*b2*] (36)
big5-1	33	44.2 ± 6.9[a]	6.4 ± 2.8	1.4 ± 0.5	0	25.5 ± 4.5 (33)	0.6 ± 0.1 (33)
fkd1/*fkd2*	24	20.4 ± 7.0[a,b1]	0.8 ± 1.3[a,b2]	0.3 ± 0.4[a,b1]	0	17.8 ± 5.0[a,b1] (9)	0.7 ± 0.1 (9)
fkd1/*big3*	26	36.4 ± 11.3[a,b2]	4.5 ± 3.5[a,b3]	1.1 ± 0.6	0.2 ± 0.4	19.0 ± 5.4[a,b2] (23)	0.5 ± 0.1 (23)
fkd1/*big5-1*	24	42.8 ± 8.4[a]	7.1 ± 4.3	1.7 ± 1.0	0.5 ± 0.7[a,c]	23.0 ± 5.5[a] (24)	0.5 ± 0.1 (24)
fkd2/*big3*	68	40.7 ± 8.2[a,c]	6.1 ± 3.2[b4]	1.5 ± 0.9[b2]	0.1 ± 0.4	25.0 ± 7.6[a,c] (66)	0.6 ± 0.1[b2] (66)
arfa1a/*b*/*d*/*e*	33	54.0 ± 6.7	7.2 ± 3.1	1.3 ± 0.6	0.3 ± 0.5[a]	27.2 ± 6.1 (33)	0.5 ± 0.1 (33)
cvp2/*cvl1*	31	19.2 ± 5.1[a]	2.0 ± 1.7[a]	1.0 ± 0.7	0.2 ± 0.5	14.6 ± 3.7[a] (27)	0.7 ± 0.1[a] (27)

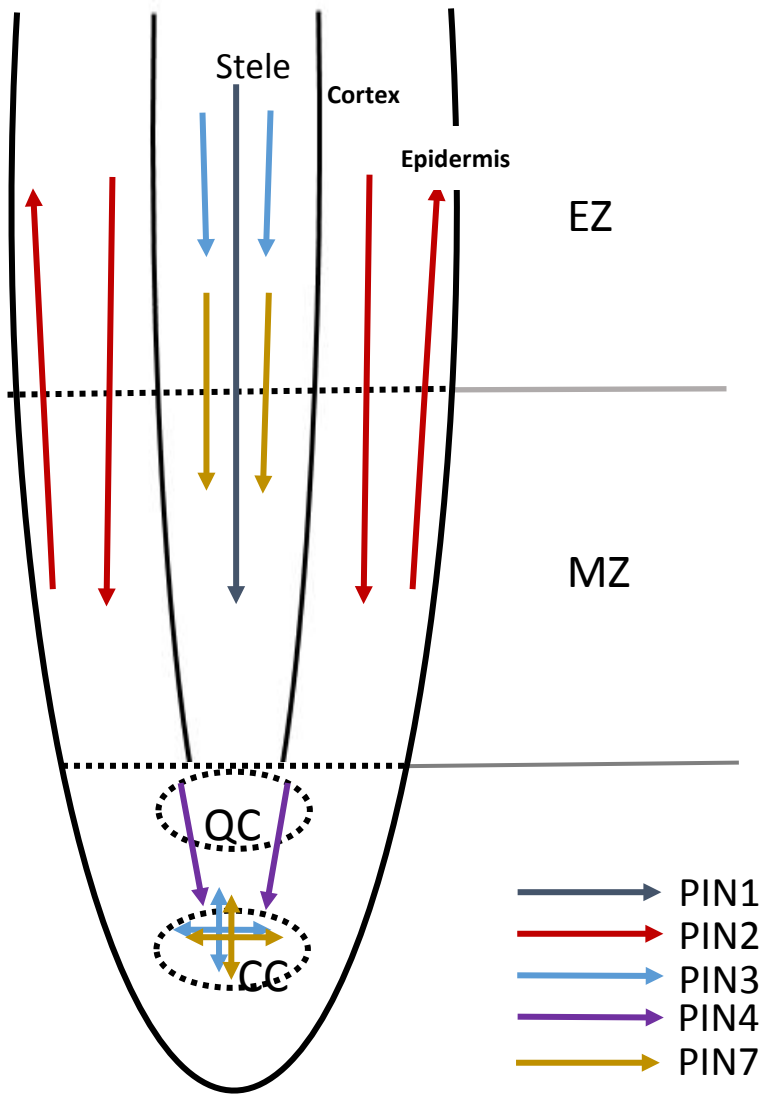

Figure 1: A summary of auxin transport flow directed by PIN proteins in seedling primary root. Arrows indicate presumed directions of auxin transport. EZ is elongation zone. MZ is meristematic zone. QC is quiescent center. CC is columella cells. Figure is adapted from Vieten et al., 2005.

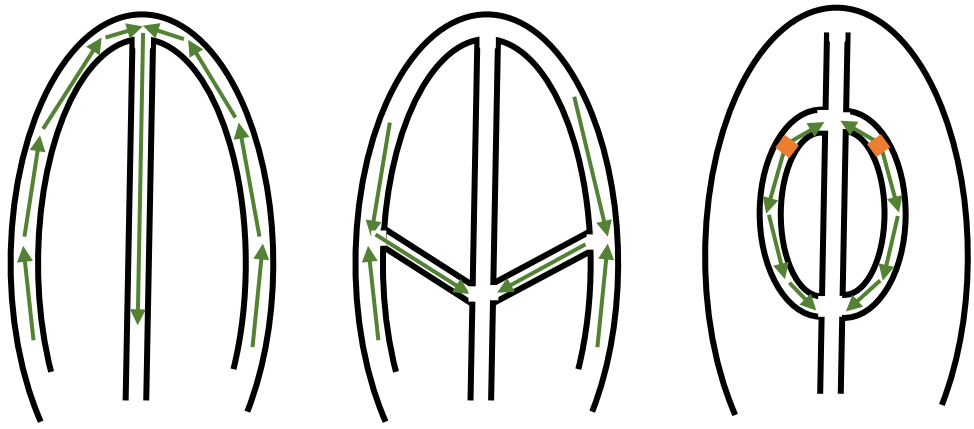

Figure 2: An outline of auxin transport as predicted by PIN1 localization during vein patterning. (A) Apical localization of PIN1 in the marginal epidermis of the young leaf primordium results in a convergence point at the distal tip and basal movement of auxin into the inner layers. (B) and (C) The formation of secondary veins reiterates this process in provascular tissues. Orange square is the cell with PIN1 localized on both apical and basal membranes.

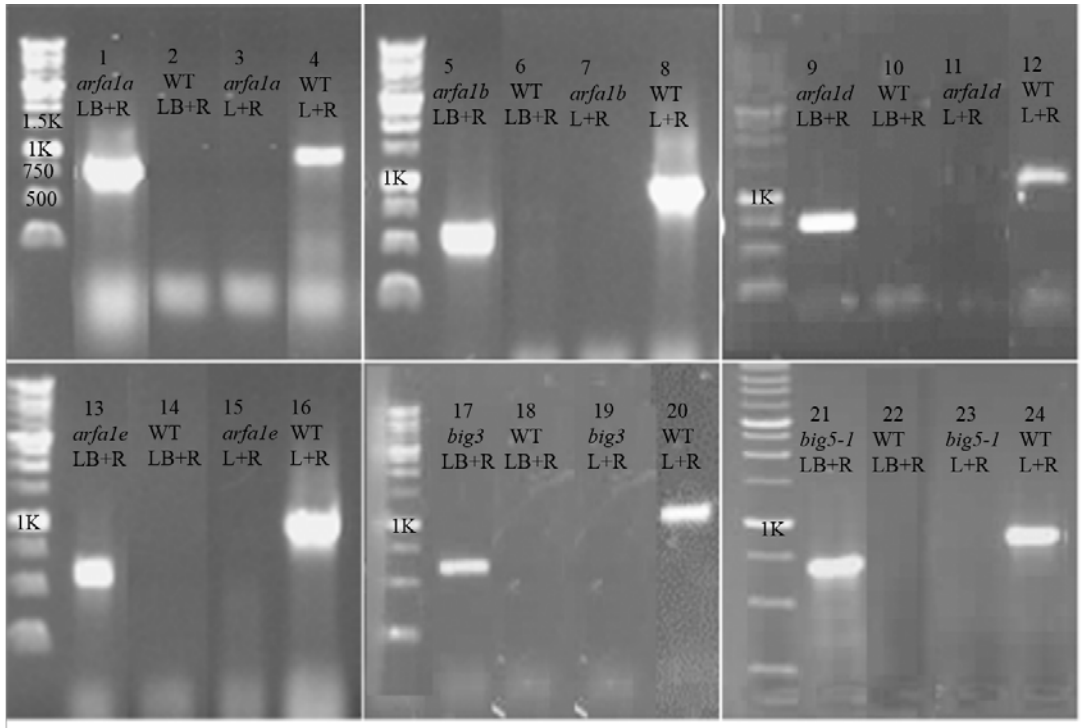

Figure 3: Genotyping of T-DNA insertion lines using PCR. DNA from wild-type (WT, used as a control) and various mutant lines (*arfa1a*, *arfa1b*, *arfa1d*, *arfa1e*, *big3* and *big5-1*) was amplified with 24 sets of primers. (1, 3), (5, 7), (9, 11), (13, 15), (17, 19) and (21, 23) are using mutant DNA as template (indicated in Table 1); (2, 4), (6, 8), (10, 12), (14, 16), (18, 20) and (22, 24) are using WT as template; (1, 2), (5, 6), (9, 10), (13, 14), (17, 18) and (21, 22) are using R primer and one of LB primers (indicated in Table 2); (3, 4), (7, 8), (11, 12), (15, 16), (19, 20) and (23, 24) are using L and R primers (indicated in Table 2). DNA electrophoresis was conducted on 0.8 % agarose gel at 150 volts for 15 min. DM3100 ExcelBand 1 KB DNA Ladder is used (informative bands were labeled in bp).

Figure 4: Position of T-DNA insertions in alleles *fl1-2*, *fl2*, *fl3* of *FL* gene family members. For each gene, the transcribed region and area immediately 5' of the transcriptional start-site is drawn. Exons are indicated as boxed regions, with translated sequences shaded and untranslated sequences open. Introns are indicated as lines. Position of left border (LB) is shown on insertion; number adjacent to insertion indicates position of insertion relative to transcription start site. Note that *fl2* has two adjacent insertions in opposite orientations.

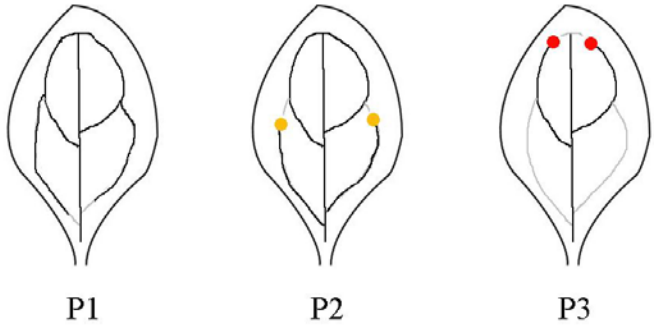

Figure 5: A method to distinguish different vein patterns for Arabidopsis cotyledon after 14 days of growth: Pattern 1 (P1)- secondary veins meet distally with either the midvein (upper loops) or the upper secondary veins (lower loops). P2- upper loops meet distally but at least one of the lower loops does not meet distally. P3- At least one upper loop does not meet distally. If the cotyledon only had one loop layer, it was considered as upper loop.

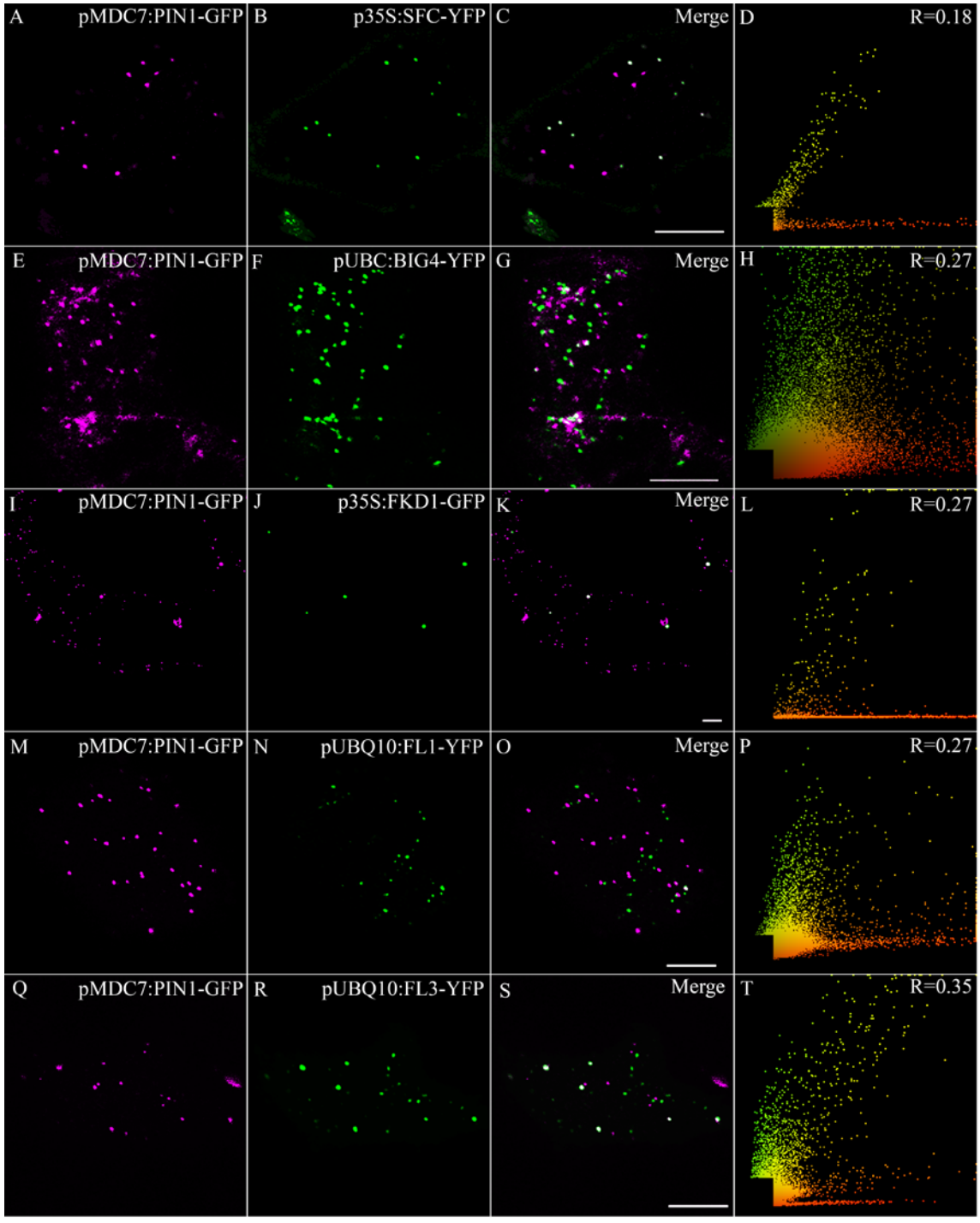
A pMDC7:PIN1-GFP
B p35S:SFC-YFP
C Merge
D R=0.18
E pMDC7:PIN1-GFP
F pUBC:BIG4-YFP
G Merge
H R=0.27
I pMDC7:PIN1-GFP
J p35S:FKD1-GFP
K Merge
L R=0.27
M pMDC7:PIN1-GFP
N pUBQ10:FL1-YFP
O Merge
P R=0.27
Q pMDC7:PIN1-GFP
R pUBQ10:FL3-YFP
S Merge
T R=0.35

Figure 6: Subcellular localization of estradiol induced pMDC7:PIN1-RFP with various proteins transiently expressed in *N. tabacum* leaf epidermal cells. Co-localization of pMDC7:PIN1-RFP with p35S:SFC-YFP (A-D), pUBC:BIG4-YFP (E-H), p35S:FKD1-GFP (I-L), pUBQ10:FL1-YFP (M-P) and pUBQ10:FL3-YFP (Q-T). A, E, I, M and Q are pMDC7:PIN1-RFP alone; B, F, J, N and R are p35S:SFC-YFP, pUBC:BIG4-YFP, p35S:FKD1-GFP, pUBQ10:FL1-YFP and pUBQ10:FL3-YFP, respectively; C, G, K, O and S are merged images. D, H, L, P and T are scatter plots of the merged image with Pearson's coefficient of Correlation (R) values. Scale bar: 10μm.

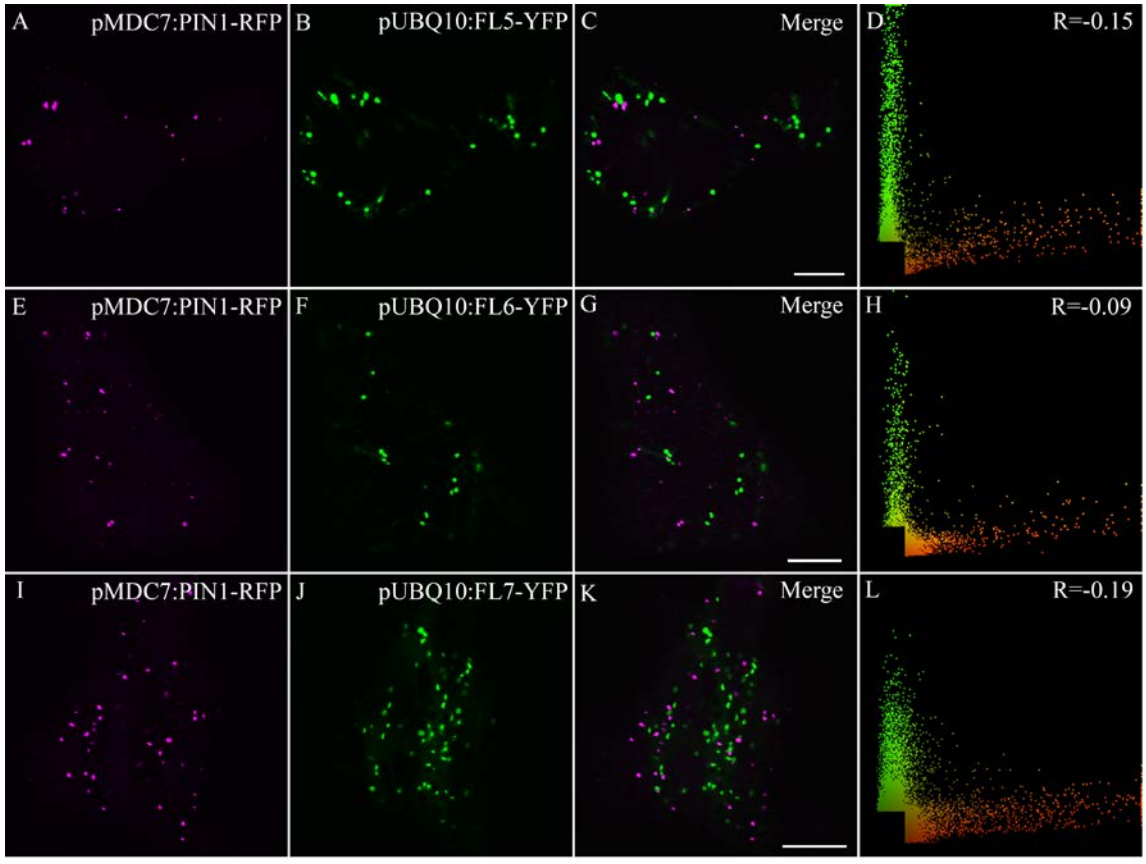

Figure 7: Subcellular localization of estradiol induced pMDC7:PIN1-RFP with various proteins transiently expressed in *N. tabacum* leaf epidermal cells. Co-localization of pMDC7:PIN1-RFP with pUBQ10:FL5-YFP (A-D), pUBQ10:FL6-YFP (E-H) and pUBQ:FL7-GFP (I-L). A, E and I are pMDC7:PIN1-RFP alone; B, F and J are pUBQ10:FL5-YFP, pUBQ10:FL6-YFP and pUBQ10:FL7-YFP, respectively; C, G and K are merged images. D, H and L are scatter plots of the merged image with Pearson's coefficient of Correlation (R) values. Scale bar: 10 μm.

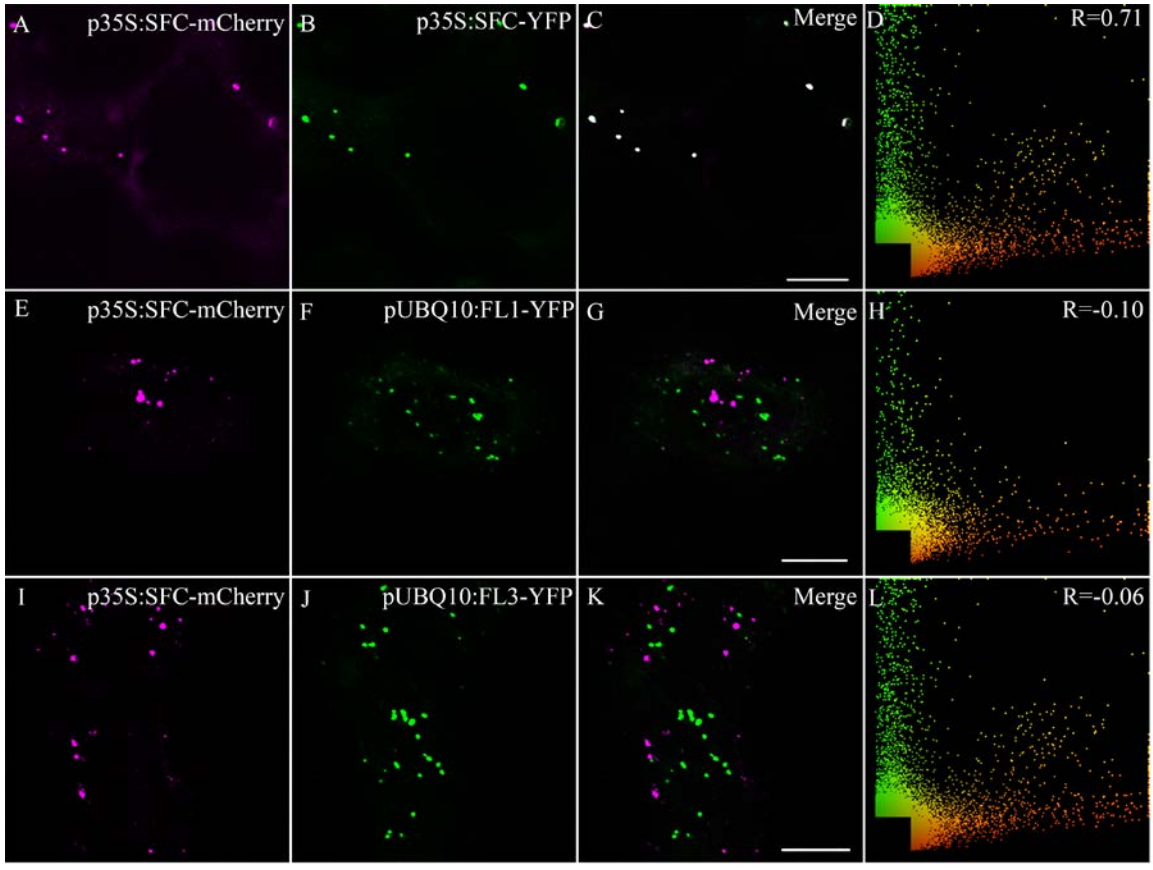

Figure 8: Subcellular localization of p35S:SFC-mCherry with various proteins transiently expressed in *N. tabacum* leaf epidermal cells. Co-localization of p35S:SFC-mCherry with p35S:SFC-YFP (A-D), pUBQ10:FL1-YFP (E-H) and pUBQ10:FL3-GFP (I-L). A, E and I are p35S:SFC-mCherry alone; B, F and J are p35S:SFC-YFP, pUBQ10:FL1-YFP and pUBQ10:FL3-YFP, respectively; C, G and K are merged images. D, H and L are scatter plots of the merged image with Pearson's coefficient of Correlation (R) values. Scale bar: 10 μm.

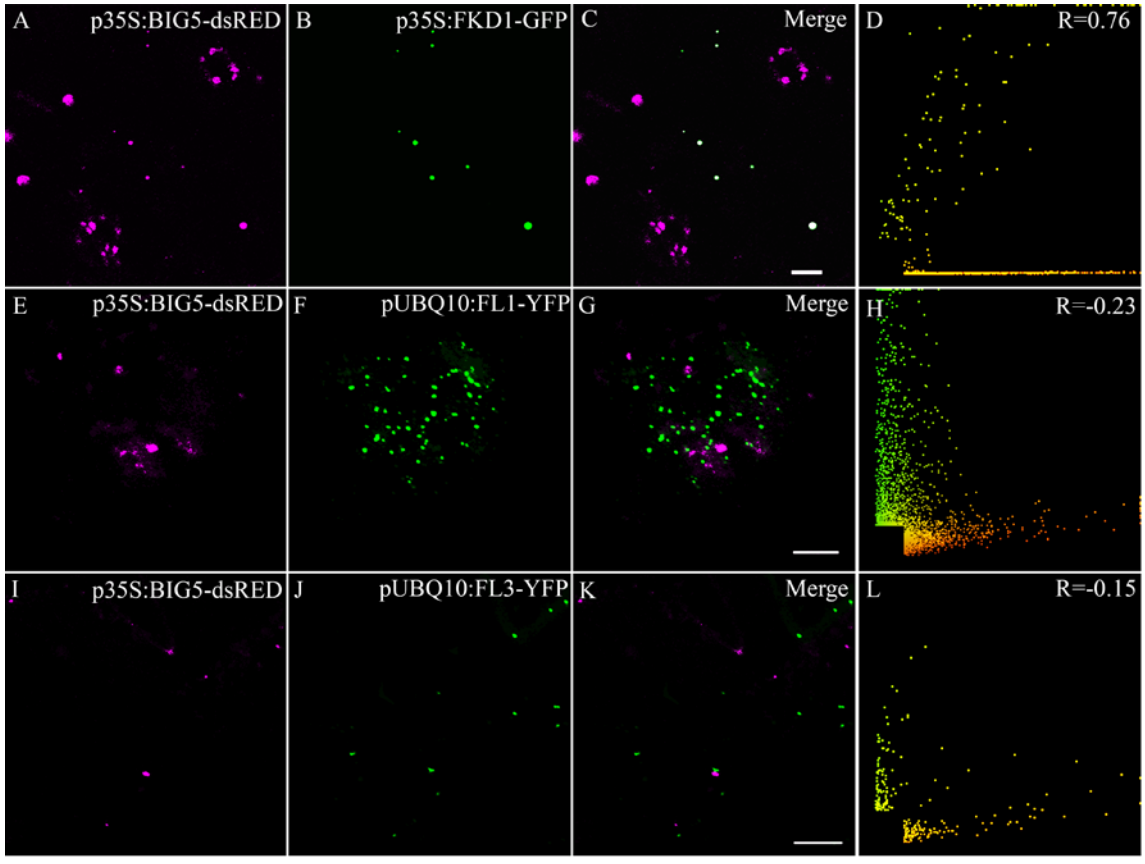

Figure 9: Subcellular localization of p35S:BIG5-dsRED with members of FL family transiently expressed in *N. tabacum* leaf epidermal cells. Co-localization of p35S:BIG5-dsRED with p35S:FKD1-GFP (A-D), pUBQ10:FL1-YFP (E-H), pUBC:FL3-GFP (I-L). A, E and I are p35S:BIG5-dsRED alone. B, F and J are p35S:FKD1-GFP, pUBQ10:FL1-YFP and pUBQ10:FL3-YFP, respectively; C, G and K are merged cells. D, H and L are scatter plots of the merged image with Pearson's coefficient of Correlation (R) values. Scale bar: 10 μm.

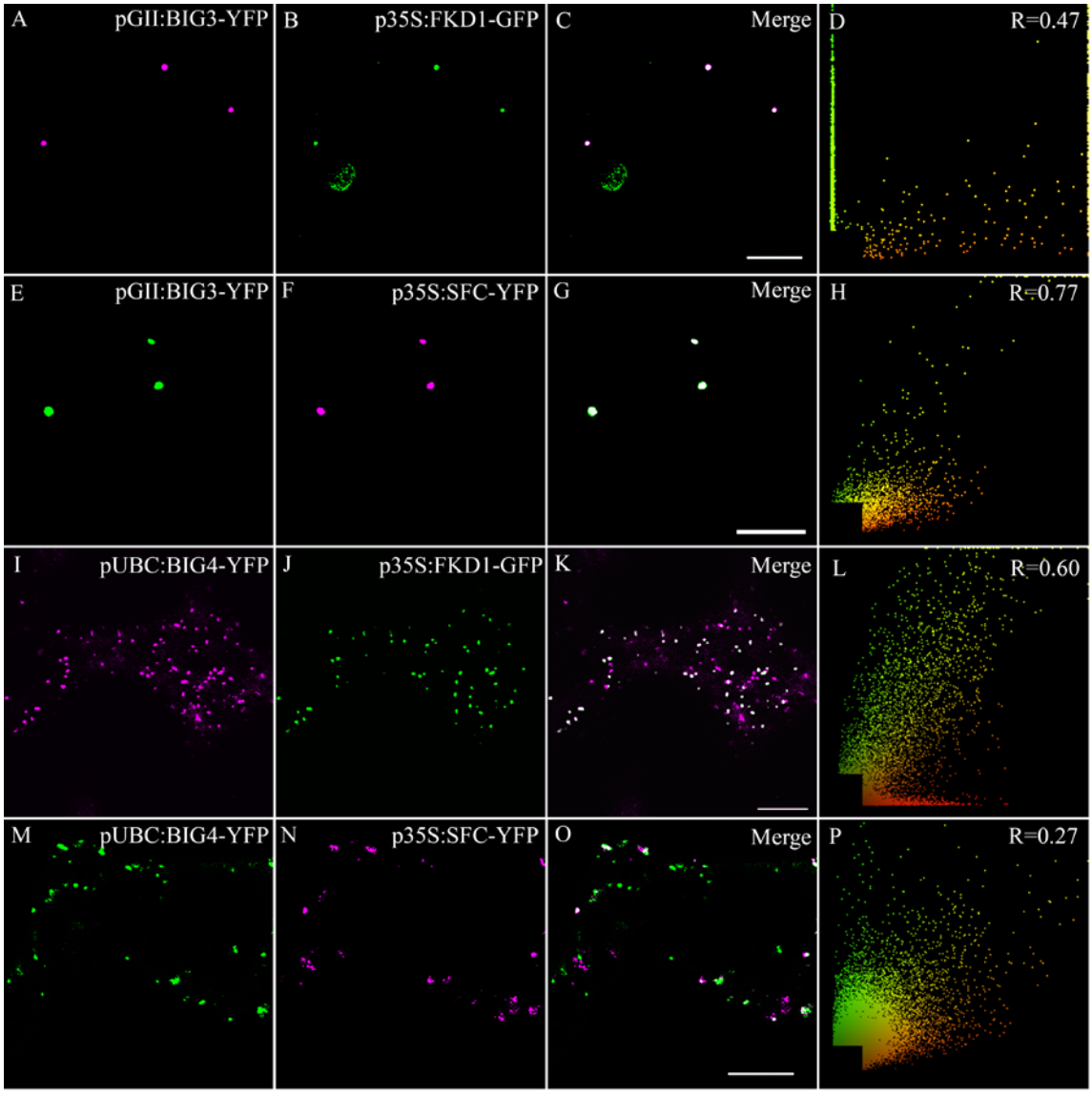

Figure 10: Subcellular localization of pGII:BIG3-YFP and pUBC:BIG4-YFP with p35S:FKD1-GFP or p35S:SFC-YFP transiently expressed in *N. tabacum* leaf epidermal cells. Co-localization of pGII:BIG3-YFP with p35S:FKD1-GFP (A-D) and p35S:SFC-mCherry (E-H). Co-localization of pUBC:BIG4-YFP with p35S:FKD1-GFP (I-L) and p35S:SFC-mCherry (M-P). A and E are pGII:BIG3-YFP. I and M are pUBC:BIG4-YFP. B and J are p35S:FKD1-GFP. F and N are p35S:SFC-mCherry. C, G, K and O are merged cells. D, H, L and P are scatter plots of the merged image with Pearson's coefficient of Correlation (R) values. Scale bar: 10 μm.

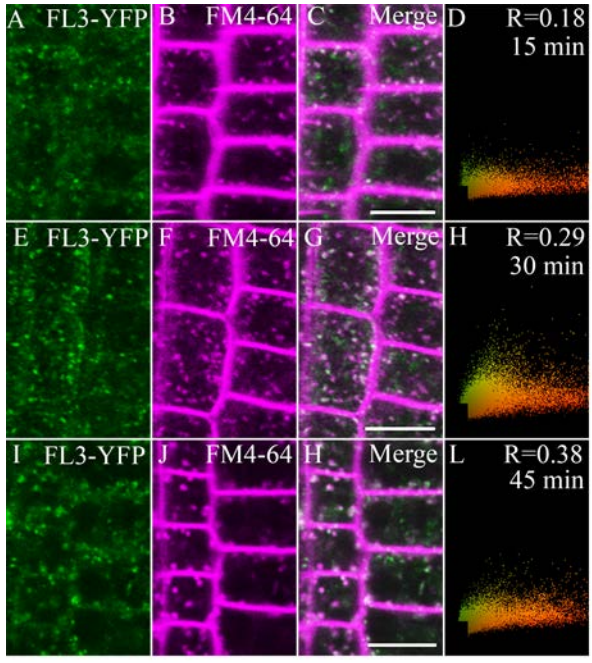

Figure 11: Co-localization of pUBQ10:FL3-YFP with FM4-64 at different time intervals. Epidermal cells in the root expressing pUBQ10:FL3-YFP (A–L) stained with the endocytic tracer FM4-64 after 15 min (A–D), 30 min (E–H), and 45 min (I–L). (A), (E), and (I) are pUBQ10:FL3-YFP alone; (B), (F) and (J) are FM4-64 alone; (C), (G) and (K) are merged images; (D), (H), and (L) are scatter plots of the merged images with Pearson's coefficient of correlation (R) values. Scale bars:10 μm.

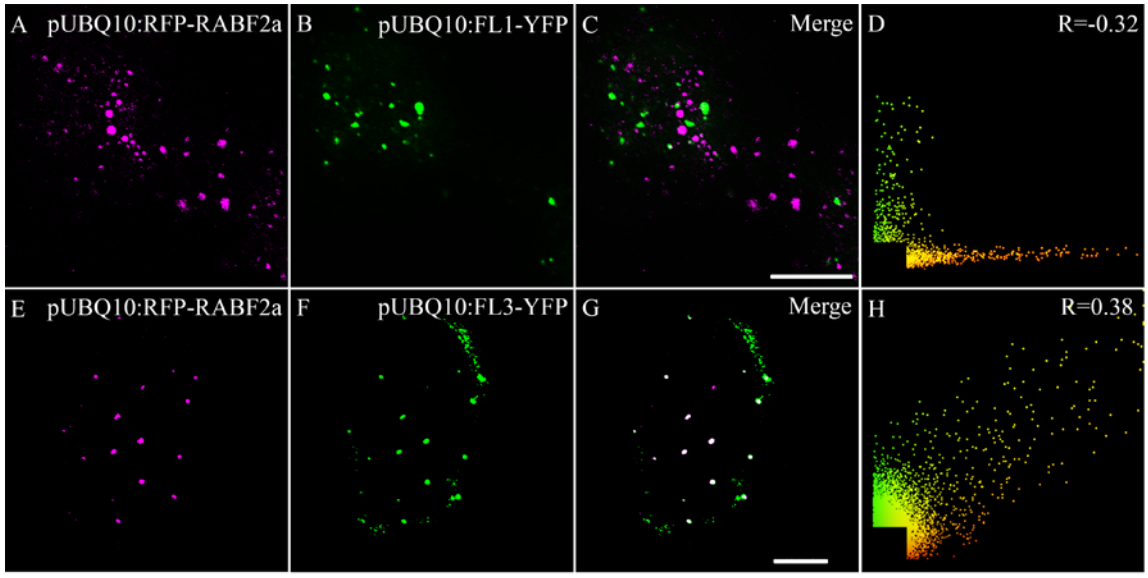

Figure 12: Subcellular localization of pUBQ10:RFP-RABAF2a with pUBQ10:FL1-YFP or pUBQ10:FL3-YFP transiently expressed in *N. tabacum* leaf epidermal cells. Co-localization of pUBQ10:RFP-RABAF2a with pUBQ10:FL1-YFP (A-D), pUBQ10:FL3-YFP (E-H). A and E are pUBQ10:RFP-RABAF2a alone; B and F are pUBQ10:FL1-YFP and pUBQ10:FL3-YFP, respectively; C and G are merged images. D and H are scatter plots of the merged image with Pearson's coefficient of Correlation (R) values. Scale bar: 10 μm.

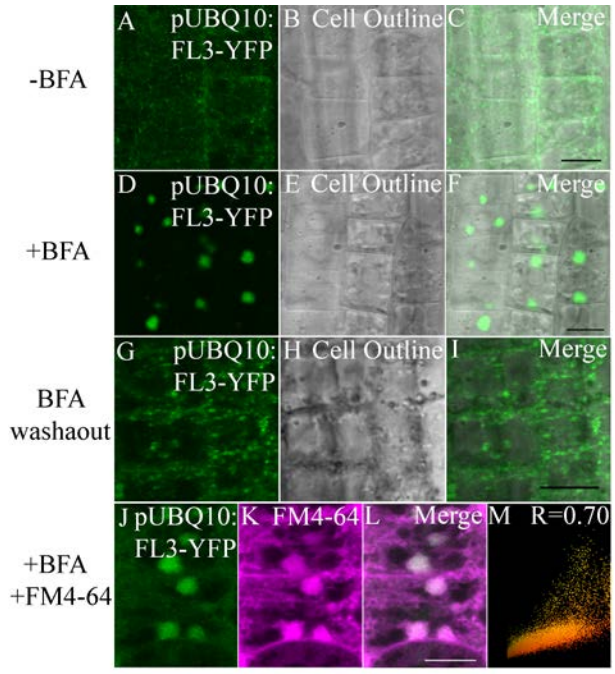

Figure 13: pUBQ10:FL3-YFP compartments are affected by BFA treatment. Expression pattern of pUBQ10:FL3-YFP in Arabidopsis root epidermal cells treated with DMSO (A-C), 50 μM BFA in DMSO (D-F), washout of BFA (G-I) and treated with BFA and FM4-64 (J-M) (methods described in Section 2.9). (A), (D), (G) and (J) are pUBQ10:FL3-YFP alone. (B), (E) and (H) are images showing the cell outlines. (K) is FM4-64. (C), (F), (I) and (L) are merged images. (M) is scatter plot of merged images with Pearson's coefficient of correlation (R) values. Scale bars: 10 μm.

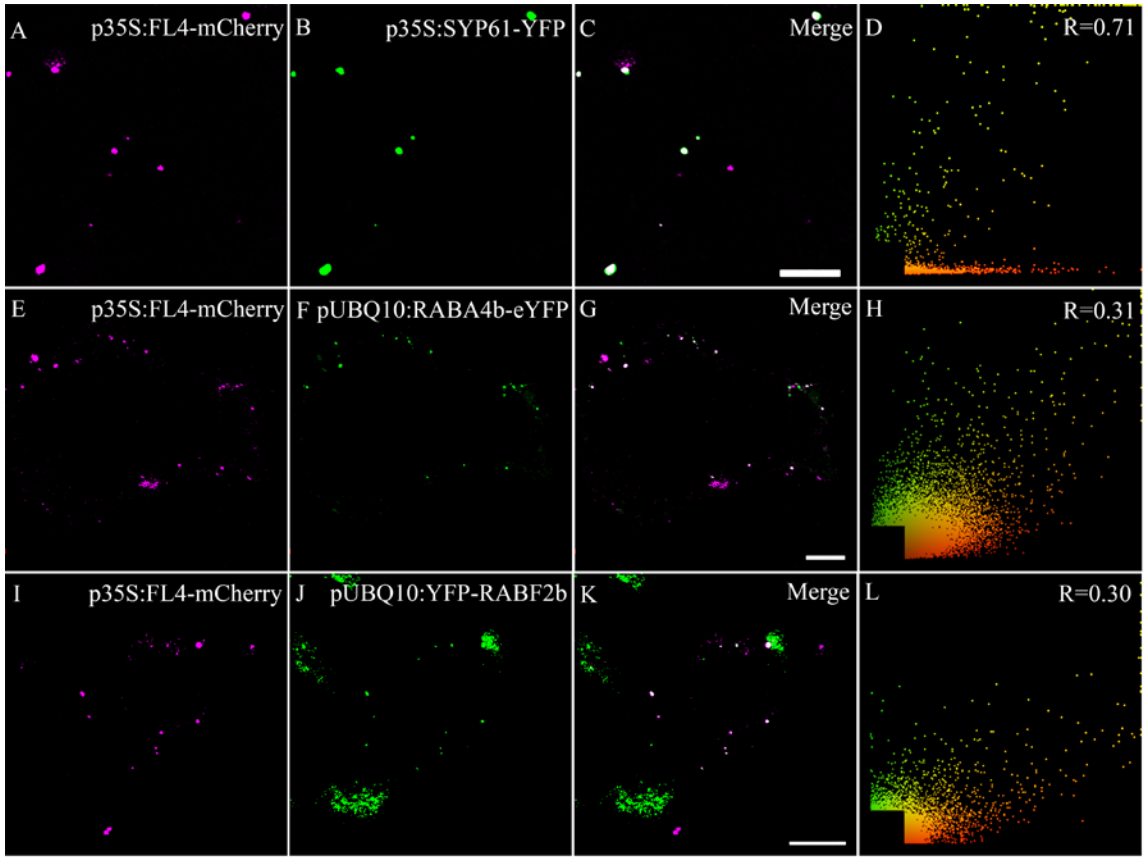

Figure 14: Subcellular localization of p35S:FL4-mCherry with p35S:SYP61-YFP, pUBQ10:RABA4b-eYFP or pUBQ10:YFP-RABF2b transiently expressed in *N. tabacum* leaf epidermal cells. Co-localization of p35S:FL4-mCherry with p35S:SYP61-YFP (A-D), pUBQ10:RABA4b-eYFP (E-H) and pUBQ10:YFP-RABF2b (I-L). A, E and I are p35S:FL4-mCherry alone. B, F and J are p35S:SYP61-YFP, pUBQ10:RABA4b-eYFP and pUBQ10:YFP-RABF2b respectively; C, G and K are merged images. D, H and L are scatter plots of the merged image with Pearson's coefficient of Correlation (R) values. Scale bar: 10 μm.

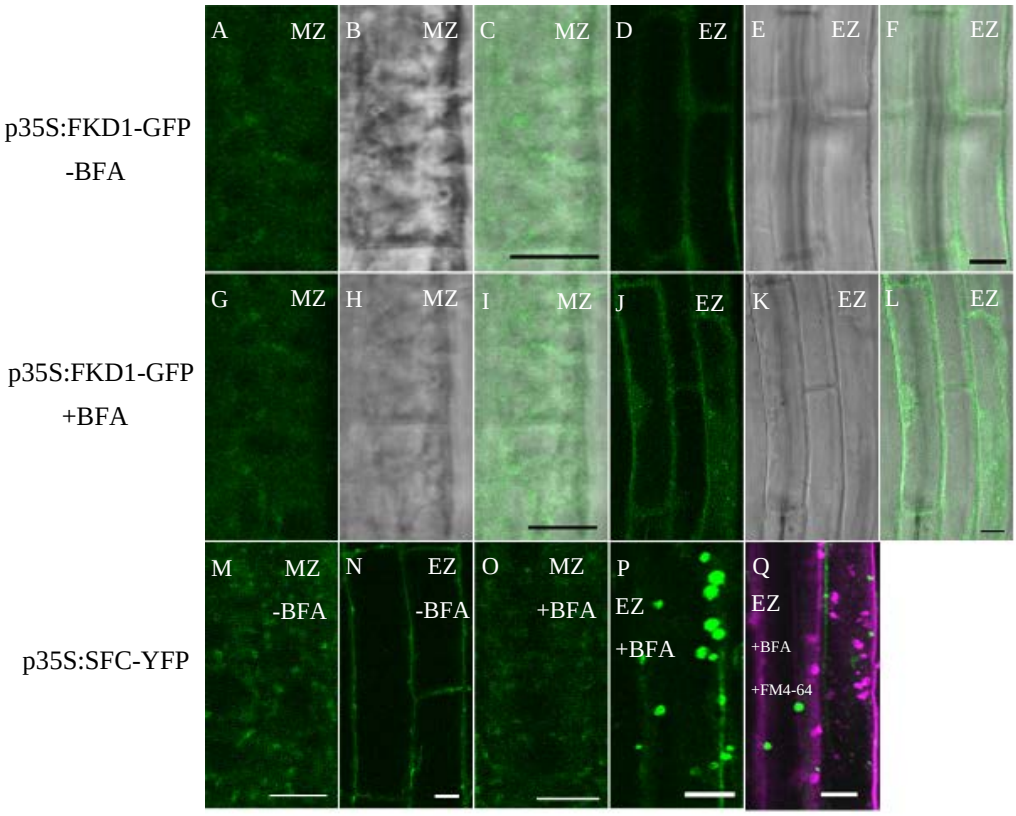

Figure 15: Sensitivity of FKD1 and SFC compartments in root meristematic and elongation zone. Expression pattern of p35S:FKD1-GFP in Arabidopsis root epidermal cells treated with DMSO in root meristematic zone (indicated as MZ) (A-C) and elongation zone (indicated as EZ) (D-F). Expression pattern of p35S:FKD1-GFP in Arabidopsis root epidermal cells treated with 50 µM BFA in DMSO in the meristematic zone (G-I) and elongation zone (J-K). (A), (D), (G) and (J) are p35S:FKD1-GFP alone. (B), (E), (H) and (K) are images showing the cell outlines. (C), (F), (I) and (L) are merged images. Expression pattern of p35S:SFC-YFP treated with DMSO in root meristematic region (M) and elongation region (N). Treated with 50 µM BFA in DMSO in the meristematic zone (O) and elongation region (P). Elongation region stained with FM4-64 together with BFA treatment (Q). Scale bars:10 µm.

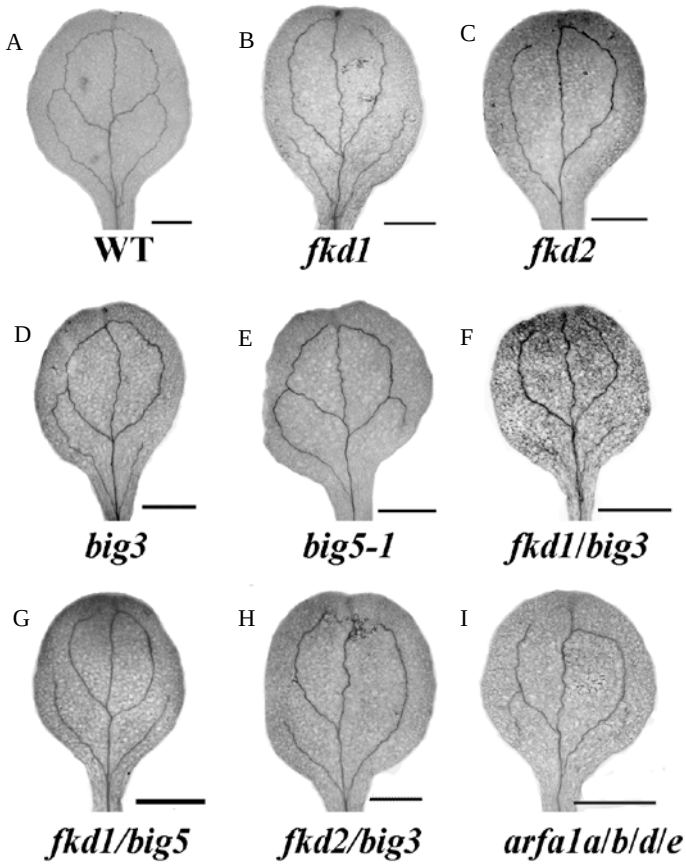

Figure 16: Vascular patterns of cotyledons of various genotypes grown on soil at 14 DAG. (A) WT; (B) *fkd1*; (C) *fkd2*; (D) *big3*; (E) *big5-1*; (F) *fkd1*/*big3*; (G) *fkd1*/*big5-1*; (H) *fkd2*/*big3*; (I) *arfa1a*/*b*/*d*/*e*. Scale bars: 1 mm.

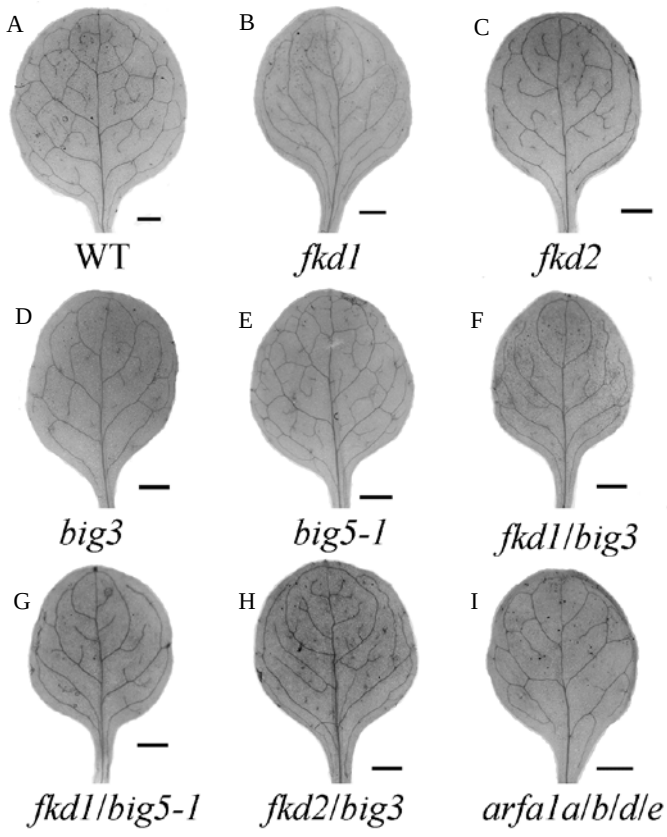

Figure 17: Vascular patterns of first leaves of various genotypes grown on soil at 21 DAG. (A) WT; (B) *fkd1*; (C) *fkd2*; (D) *big3*; (E) *big5-1*; (F) *fkd1*/*big3*; (G) *fkd1*/*big5-1*; (H) *fkd2*/*big3*; (I) *arfa1a*/*b*/*d*/*e*. Scale bars: 1mm.

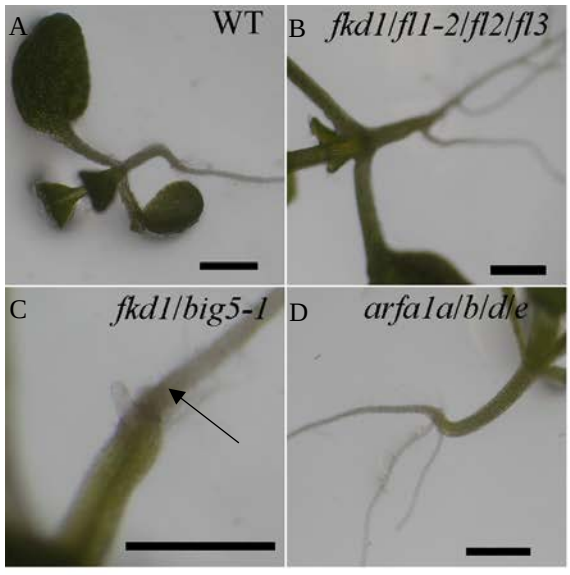

Figure 18: Emergence of adventitious roots from hypocotyls of various genotypes grown on plates at 9 DAG. (A) WT; (B) *fkd1*/*fl1-2*/*fl2*/*fl3* (C) *fkd1*/*big5-1*; (D) *arfa1a*/*b*/*d*/*e*. Scale bars: 1mm. Arrow indicates hypocotyl (with green pigmentation) and root (without green pigmentation) boundary.

References

Adamowski M, Friml J (2015) PIN-Dependent Auxin Transport: Action, Regulation, and Evolution. Plant Cell **27**: 20–32

Allen GC, Flores-Vergara MA, Krasynanski S, Kumar S, Thompson WF (2006) A modified protocol for rapid DNA isolation from plant tissues using cetyltrimethylammonium bromide. Nat Protoc **1**: 2320–2325

Alonso JM, Stepanova AN, Leisse TJ, Kim CJ, Chen H, Shinn P, Stevenson DK, Zimmerman J, Barajas P, Cheuk R, et al (2003) Genome-Wide Insertional Mutagenesis of Arabidopsis thaliana. Science **301**: 653–657

Armengot L, Marquès-Bueno MM, Jaillais Y (2016) Regulation of polar auxin transport by protein and lipid kinases. J Exp Bot **67**: 4015–4037

Baldwin TC, Handford MG, Yuseff MI, Orellana A, Dupree P (2001) Identification and characterization of GONST1, a golgi-localized GDP-mannose transporter in Arabidopsis. Plant Cell **13**: 2283–2295

Baluska F, Hlavacka A, Samaj J, Palme K, Robinson DG, Matoh T, McCurdy DW, Menzel D, Volkmann D (2002) F-Actin-Dependent Endocytosis of Cell Wall Pectins in Meristematic Root Cells. Insights from Brefeldin A-Induced Compartments. Plant Physiol **130**: 422–431

Batoko H, Zheng H, Hawes C, Moore I (2000) A Rab1 GTPase Is Required for Transport between the Endoplasmic Reticulum and Golgi Apparatus and for Normal Golgi Movement in Plants. Plant Cell **12**: 2201–2218

Beeckman T, Burssens S, Inzé D (2001) The peri-cell-cycle in *Arabidopsis*. J Exp Bot **52**: 403–411

Beemster GTS, Baskin TI (1998) Analysis of Cell Division and Elongation Underlying the Developmental Acceleration of Root Growth in *Arabidopsis thaliana*. Plant Physiol **116**: 1515–1526

Benková E, Michniewicz M, Sauer M, Teichmann T, Seifertová D, Jürgens G, Friml J (2003) Local, Efflux-Dependent Auxin Gradients as a Common Module for Plant Organ Formation. Cell **115**: 591–602

Bennett KD (1996) Determination of the number of zones in a biostratigraphic sequence. New Phytol **132**: 155–170

Billou I, Xu J, Wildwater M, Willemsen V, Paponov I, Frimi J, Heldstra R, Aida M, Palme K, Scheres B (2005) The PIN auxin efflux facilitator network controls growth and patterning in Arabidopsis roots. Nature **433**: 39–44

Bolte S, Talbot C, Boutte Y, Catrice O, Read ND, Satiat-Jeunemaitre B (2004) FM-dyes as experimental probes for dissecting vesicle trafficking in living plant cells. J Microsc **214**: 159–173

Bonifacino JS, Glick BS (2004) The Mechanisms of Vesicle Budding and Fusion. Cell **116**: 153–166

Bonifacino JS, Traub LM (2003) Signals for Sorting of Transmembrane Proteins to Endosomes and Lysosomes. Annu Rev Biochem **72**: 395–447

Brady SM, Orlando DA, Lee J, Wang JY, Koch J, Dinneny JR, Mace D, Ohler U, Benfey PN (2007) A High-Resolution Root Spatiotemporal Map Reveals Dominant Expression Patterns. Science **80**: 801–806

Brodribb TJ, Feild TS (2010) Leaf hydraulic evolution led a surge in leaf photosynthetic capacity during early angiosperm diversification. Ecol Lett **13**: 175–183

Carland F, Nelson T (2004) Cotyledon vascular pattern2-mediated inositol (1,4,5) triphosphate signal transduction is essential for closed venation patterns of Arabidopsis foliar organs. Plant Cell **16**: 1263–1275

Carland F, Nelson T (2009) CVP2- and CVL1-mediated phosphoinositide signaling as a regulator of the ARF GAP SFC/VAN3 in establishment of foliar vein patterns. Plant J **59**: 895–907

Casimiro I, Beeckman T, Graham N, Bhalerao R, Zhang H, Casero P, Sandberg G, Bennett MJ (2003) Dissecting Arabidopsis lateral root development. Trends Plant Sci **8**: 165–171

Chandler JW (2009) Local auxin production: A small contribution to a big field. BioEssays **31**: 60–70

De Rybel B, Vassileva V, Parizot B, Demeulenaere M, Grunewald W, Audenaert D, Van Campenhout J, Overvoorde P, Jansen L, Vanneste S, et al (2010) A novel Aux/IAA28 signaling cascade activates GATA23-dependent specification of lateral root founder cell identity. Curr Biol **20**: 1697–1706

De Smet S, Cuypers A, Vangronsveld J, Remans T (2015) Gene Networks Involved in Hormonal Control of Root Development in Arabidopsis thaliana: A Framework for Studying its Disturbance by Metal Stress. Int J Mol Sci **16**: 19195–19224

Dettmer J, Hong-Hermesdorf A, Stierhof Y-D, Schumacher K (2006) Vacuolar H^+-ATPase Activity Is Required for Endocytic and Secretory Trafficking in Arabidopsis. Plant Cell **18**: 715–730

Deyholos MK, Cordner G, Beebe D, Sieburth LE (2000) The SCARFACE gene is required for cotyledon and leaf vein patterning. Development **127**: 3205–3213

Douzery EJP, Snell EA, Bapteste E (2004) The timing of eukaryotic evolution : Does a relaxed molecular clock reconcile proteins and fossils. Proc Natl Acad Sci **101**: 15386–15391

Doyle SM, Haeger A, Vain T, Rigal A, Viotti C, Łangowska M, Ma Q, Friml J, Raikhel N V., Hicks GR, et al (2015) An early secretory pathway mediated by GNOM-LIKE 1 and GNOM is essential for basal polarity establishment in *Arabidopsis thaliana*. Proc Natl Acad Sci **112**: 806–815

Drakakaki G, Van De Ven W, Pan S, Miao Y, Wang J, Keinath NF, Weatherly B, Jiang L, Schumacher K, Hicks G, et al (2012) Isolation and proteomic analysis of the SYP61 compartment reveal its role in exocytic trafficking in Arabidopsis. Cell Res **22**: 413–424

Dubrovsky JG, Sauer M, Napsucialy-Mendivil S, Ivanchenko MG, Friml J, Shishkova S, Celenza J, Benkova E (2008) Auxin acts as a local morphogenetic trigger to specify lateral root founder cells. Proc Natl Acad Sci **105**: 8790–8794

Feild TS, Brodribb TJ, Iglesias A, Chatelet DS, Baresch A, Upchurch GR, Gomez B, Mohr BAR, Coiffard C, Kvacek J, et al (2011) Fossil evidence for Cretaceous escalation in angiosperm leaf vein evolution. Proc Natl Acad Sci **108**: 8363–8366

French AP, Mills S, Swarup R, Bennett MJ, Pridmore TP (2008) Colocalization of fluorescent markers in confocal microscope images of plant cells. Nat Protoc **3**: 619–628

Friml J, Benková E, Blilou I, Wisniewska J, Hamann T, Ljung K, Woody S, Sandberg G, Scheres B, Jürgens G (2002a) AtPIN4 mediates sink-driven auxin gradients and root patterning in Arabidopsis. Cell **108**: 661–673

Friml J, Vieten A, Sauer M, Weijers D, Schwarz H, Hamann T, Offringa R, Jürgens G (2003) Efflux-dependent auxin gradients establish the apical-basal axis of Arabidopsis. Nature **426**: 147–153

Friml J, Wiśniewska J, Benková E, Mendgen K, Palme K (2002b) Lateral relocation of auxin efflux regulator PIN3 mediates tropism in Arabidopsis. Nature **415**: 806–809

Fukuda H (2004) Signals that control plant vascular cell differentiation. Nat Rev Mol Cell Biol **5**: 379–391

Gao X, Nagawa S, Wang G, Yang Z (2008) Cell Polarity Signaling : Focus on Polar

Auxin Transport. Molecular Plant **1**:899–909

Garay-Arroyo A, De La M, Garcia-Ponce B, Azpeitia E, Alvarez-Buylla ER (2012) Hormone symphony during root growth and development. Dev Dyn **241**: 1867–1885

Gebbie LK, Burn JE, Hocart CH, Williamson RE (2005) Genes encoding ADP-ribosylation factors in Arabidopsis thaliana L. Heyn.; genome analysis and antisense suppression. J Exp Bot **56**: 1079–1091

Geldner N, Richter S, Vieten A, Marquardt S, Torres-Ruiz RA, Mayer U, Jürgens G (2003a) Partial loss-of-function alleles reveal a role for GNOM in auxin transport-related, post-embryonic development of Arabidopsis. Development **131**: 389–400

Geldner N, Anders N, Wolters H, Keicher J, Kornberger W, Muller P, Delbarre A, Ueda T, Nakano A, Jürgens G (2003b) The Arabidopsis GNOM ARF-GEF Mediates Endosomal Recycling , Auxin Transport , and Auxin-Dependent Plant Growth. Cell **112**: 219–230

Geldner N, Dénervaud-Tendon V, Hyman DL, Mayer U, Stierhof YD, Chory J (2009) Rapid, combinatorial analysis of membrane compartments in intact plants with a multicolor marker set. Plant J **59**: 169–178

Geldner N, Friml J, Stierhof YD, Jürgens G, Palme K (2001) Auxin transport inhibitors block PIN1 cycling and vesicle trafficking. Nature **413**: 425–428

Grunewald W, Friml J (2010) The march of the PINs: Developmental plasticity by dynamic polar targeting in plant cells. EMBO J **29**: 2700–2714

Heilmann I (2016) Phosphoinositide signaling in plant development. Development **143**: 44–55

Hess MW, Müller M, Debbage PL, Vetterlein M, Pavelka M (2000) Cryopreparation provides new insight into the effects of brefeldin A on the structure of the HepG2 Golgi apparatus. J Struct Biol **130**: 63–72

Hou H, Erickson J, Meservy J, Schultz EA (2010) FORKED1 encodes a PH domain protein that is required for PIN1 localization in developing leaf veins. Plant J **63**: 960–973

Jackson CL, Casanova JE (2000) Turning on ARF: The Sec7 family of guanine-nucleotide-exchange factors. Trends Cell Biol **10**: 60–67

John LC, Grisafi PL, Fink GR (1995) A pathway for lateral root formation of *Arabidopsis thaliana*. Genes Dev **9**: 2131–2142

Jonsson K, Boutté Y, Singh RK, Gendre D, Bhalerao RP (2017) Ethylene Regulates Differential Growth via BIG ARF-GEF-Dependent Post-Golgi Secretory Trafficking in Arabidopsis. Plant Cell **29**: 1039–1052

Jürgens G (2004) Membrane Trafficking in Plants. Annu Rev Cell Dev Biol **20**: 481–504

Keuskamp DH, Pollmann S, Voesenek LACJ, Peeters AJM, Pierik R (2010) Auxin transport through PIN-FORMED 3 (PIN3) controls shade avoidance and fitness during competition. Proc Natl Acad Sci **107**: 22740–22744

Kitakura S, Adamowski M, Matsuura Y, Santuari L, Kouno H, Arima K, Hardtke CS, Friml J, Kakimoto T, Tanaka H (2017) BEN3/BIG2 ARF GEF is involved in brefeldin a-sensitive trafficking at the trans-golgi network/early endosome in arabidopsis thaliana. Plant Cell Physiol **58**: 1801–1811

Kleine-Vehn J, Friml J (2008) Polar Targeting and Endocytic Recycling in Auxin-Dependent Plant Development. Annu Rev Cell Dev Biol **24**: 447–473

Klepikova A V, Kasianov AS, Gerasimov ES, Logacheva MD, Penin AA (2016) A high resolution map of the Arabidopsis thaliana developmental transcriptome based on RNA-seq profiling. Plant J **88**: 1058–1070

Koizumi K, Naramoto S, Sawa S, Yahara N, Ueda T, Nakano A, Sugiyama M, Fukuda H (2005) VAN3 ARF-GAP-mediated vesicle transport is involved in leaf vascular network formation. Development **132**: 1699–1711

Kong X, Liu G, Liu J, Ding Z (2018) The Root Transition Zone: A Hot Spot for Signal Crosstalk. Trends Plant Sci **23**: 403–409

Lam SK, Cai Y, Tse YC, Wang J, Law AHY, Pimpl P, Chan HYE, Xia J, Jiang L (2009) BFA-induced compartments from the Golgi apparatus and trans-Golgi network/early endosome are distinct in plant cells. Plant J **60**: 865–881

Langowski L, Wabnik K, Li H, Vanneste S, Naramoto S, Tanaka H, Friml J (2016) Cellular mechanisms for cargo delivery and polarity maintenance at different polar domains in plant cells. Cell Discov. **2**: 1–18

Lee MCS, Miller EA, Goldberg J, Orci L, Schekman R (2004) Bi-Directional Protein Transport Between the Er and Golgi. Annu Rev Cell Dev Biol **20**: 87–123

Lemmon M Pleckstrin Homology (PH) Domains and Phosphoinositides (2007) Biochem Soc Symp. **93**: 81–93

Li SW, Xue L, Xu S, Feng H, An L (2009) Hydrogen peroxide acts as a signal molecule in the adventitious root formation of mung bean seedlings. Environ Exp Bot **65**: 63–

Ljung K, Bhalerao RP, Sandberg G (2001) Sites and homeostatic control of auxin biosynthesis in Arabidopsis during vegetative growth. Plant J **28**: 465–474

Luschnig C, Vert G (2014) The dynamics of plant plasma membrane proteins : PINs and beyond. Development **1**: 2924–2938

Malinowski R (2013) Understanding of Leaf Development—the Science of Complexity. Plants **2**: 396–415

Maloof JN (2004) Plant development: Slowing root growth naturally. Curr Biol **14**: 395–396

Matheson LA, Suri SS, Hanton SL, Chatre L, Brandizzi F (2008) Correct targeting of plant ARF GTPases relies on distinct protein domains. Traffic **9**: 103–120

Mattsson J, Sung ZR, Berleth T (1999) Responses of plant vascular systems to auxin transport inhibition. Development **126**: 2979–2991

Mockaitis K, Estelle M (2008) Auxin Receptors and Plant Development: A New Signaling Paradigm. Annu Rev Cell Dev Biol **24**: 55–80

Mravec J, Skůpa P, Bailly A, Hoyerová K, Křeček P, Bielach A, Petrášek J, Zhang J, Gaykova V, Stierhof YD, et al (2009) Subcellular homeostasis of phytohormone auxin is mediated by the ER-localized PIN5 transporter. Nature **459**: 1136–1140

Naramoto S, Dainobu T, Tokunaga H, Kyozuka J, Fukuda H (2016) Cellular and developmental function of ACAP type ARF-GAP proteins are diverged in plant cells. Plant Biotechnol **33**: 309–314

Naramoto S, Kleine-Vehn J, Robert S, Fujimoto M, Dainobu T, Paciorek T, Ueda T, Nakano A, Van Montagu MCE, Fukuda H, et al (2010) ADP-ribosylation factor machinery mediates endocytosis in plant cells. Proc Natl Acad Sci **107**: 21890–21895

Naramoto S, Otegui MS, Kutsuna N, Rycke R De, Dainobu T, Karampelias M, Fujimoto M, Feraru E, Miki D, Fukuda H, et al (2014) Insights into the Localization and Function of the Membrane Trafficking Regulator GNOM ARF-GEF at the Golgi Apparatus in Arabidopsis. Plant Cell **26**: 3062–3076

Naramoto S, Sawa S, Koizumi K, Uemura T, Ueda T, Friml J, Nakano A, Fukuda H (2009) Phosphoinositide-dependent regulation of VAN3 ARF-GAP localization and activity essential for vascular tissue continuity in plants. Development **136**: 1529–1538

Nebenfuhr A, Ritzenthaler C, Robinson DG (2002) Brefeldin A: deciphering an enigmatic inhibitor of secretion. Plant Physiol **130**: 1102–1108

Negroni L, Balliau T (2006) Proteomic Analysis of Different Mutant Genotypes of Arabidopsis Led to the Identification of 11 Proteins Correlating with Adventitious Root Development. Plant Physiol **140**: 349–364

Nomura K, DebRoy S, Lee YH, Pumplin N, Jones J, He SY (2006) A Bacterial Virulence Protein Suppresses Host Innate Immunity to Cause Plant Disease. Science **313**: 220–213

Nomura K, Mecey C, Lee YH, Alice L, Chang JH, He SY (2011) Effector-triggered immunity blocks pathogen degradation of an immunity-associated vesicle traffic regulator in Arabidopsis. Proc Natl Acad Sci **108**: 10774-10779

Overvoorde P, Fukaki H, Beeckman T (2010) Auxin control of root development. Cold Spring Harb Perspect Biol **2**: 1–16

Paciorek T, Zažímalová E, Ruthardt N, Petrášek J, Stierhof YD, Kleine-Vehn J, Morris DA, Emans N, Jürgens G, Geldner N, et al (2005) Auxin inhibits endocytosis and promotes its own efflux from cells. Nature **435**: 1251–1256

Peer WA, Blakeslee JJ, Yang H, Murphy AS (2011) Seven things we think we know about auxin transport. Mol Plant **4**: 487–504

Perrot-Rechenmann C (2010) Cellular responses to auxin: division versus expansion. Cold Spring Harb Perspect Biol **2**: 1–15

Peter BJ, Kent HM, Mills IG, Vallis Y, Butler PJG, Evans PR, McMahon HT (2004) BAR Domains as Sensors of Membrane Curvature: The Amphiphysin BAR Structure. Science **303**: 495–499

Petersson S V, Johansson AI, Kowalczyk M, Makoveychuk A, Wang JY, Moritz T, Grebe M, Benfey PN, Sandberg G, Ljung K (2009) An Auxin Gradient and Maximum in the Arabidopsis Root Apex Shown by High-Resolution Cell-Specific Analysis of IAA Distribution and Synthesis. Plant Cell **21**: 1659–1668

Petrasek J, Friml J (2009) Auxin transport routes in plant development. Development **136**: 2675–2688

Petrásek J, Mravec J, Bouchard R, Blakeslee JJ, Abas M, Seifertová D, Wisniewska J, Tadele Z, Kubes M, Covanová M, et al (2006) PIN proteins perform a rate-limiting function in cellular auxin efflux. Science **312**: 914–918

Petricka JJ, Winter CM, Benfey PN (2012) Control of *Arabidopsis* Root Development. Annu Rev Plant Biol **63**: 563–590

Pimpl P (2003) The GTPase ARF1p Controls the Sequence-Specific Vacuolar Sorting Route to the Lytic Vacuole. Plant Cell **15**: 1242–1256

Prabhakaran Mariyamma N, Clarke KJ, Yu H, Wilton EE, Van Dyk J, Hou H, Schultz EA (2008) Members of the *Arabidopsis FORKED1-LIKE* gene family act to localize PIN1 in developing veins. J Exp Bot accepted manuscript

Prabhakaran Mariyamma N, Hou H, Carland FM, Nelson T, Schultz EA (2017) Localization of Arabidopsis FORKED1 to a RABA-positive compartment suggests a role in secretion. J Exp Bot **68**: 3375–3390

Reed JW (2001) Roles and activities of Aux/IAA proteins in Arabidopsis. Trends Plant Sci **6**: 420–425

Reinhardt D, Pesce ER, Stieger P, Mandel T, Baltensperger K, Bennett M, Traas J, Friml J, Kuhlemeier C (2003) Regulation of phyllotaxis by polar auxin transport. Nature **426**: 255–260

Richter S, Geldner N, Schrader J, Wolters H, Stierhof YD, Rios G, Koncz C, Robinson DG, Jürgens G (2007) Functional diversification of closely related ARF-GEFs in protein secretion and recycling. Nature **448**: 488–492

Richter S, Kientz M, Brumm S, Nielsen ME, Park M, Gavidia R, Krause C, Voss U, Beckmann H, Mayer U, et al (2014) Delivery of endocytosed proteins to the cell-division plane requires change of pathway from recycling to secretion. eLIFE **3**: 1–16

Robinson DG, Scheuring D, Naramoto S, Friml J (2011) ARF1 Localizes to the Golgi and the Trans-Golgi Network. Plant Cell **23**: 846–849

Roth-Nebelsick A, Uhl D, Mosbrugger V, Kerp H (2001) Evolution and function of leaf venation architecture: a review. Ann Bot **87**: 553–566

Ruegger M, Dewey E, Gray WM, Hobbie L, Turner J, Estelle M (1998) The TIR1 protein of *Arabidopsis* functions in auxin response and is related to human SKP2 and yeast GRR1p. Genes Dev **12**: 198–207

Rymen B, Sugimoto K (2012) Tuning growth to the environmental demands. Curr Opin Plant Biol **15**: 683–690

Sabatini S, Heidstra R, Wildwater M, Scheres B (2003) SCARECROW is involved in positioning the stem cell niche in the Arabidopsis root meristem. Genes Dev 354–358

Sachs, T (1981). The control of patterned differentiation of vascular tissues. Adv Bot Res **9**: 151-262.

Samaj J, Baluska, FrantisekVoigt B, Schlicht M, Volkmann D, Menzel D (2004) Endocytosis, Actin Cytoskeleton, and Signaling. Plant Physiol **135**: 1150–1161

Sancho-Andrés G, Soriano-Ortega E, Gao C, Bernabé-Orts JM, Narasimhan M, Müller AO, Tejos R, Jiang L, Friml J, Aniento F, et al (2016) Sorting Motifs Involved in the Trafficking and Localization of the PIN1 Auxin Efflux Carrier. Plant Physiol **171**: 1965–1982

Sawchuk MG, Scarpella E (2013) Polarity, continuity, and alignment in plant vascular strands. J Integr Plant Biol **55**: 824–834

Scarpella E, Marcos D, Friml J, Berleth T (2006) Control of leaf vascular patterning by polar auxin transport. Genes Dev **20**: 1015–1027

Scheffzek K, Ahmadian MR, Wiesmüller L, Kabsch W, Stege P, Schmitz F, Wittinghofer A (1998) Structural analysis of the GAP-related domain from neurofibromin and its implications. EMBO J **17**: 4313–4327

Sieburth LE, Muday GK, King EJ, Benton G, Kim S, Metcalf KE, Meyers L, Seamen E, Van Norman JM (2006) SCARFACE Encodes an ARF-GAP That Is Required for Normal Auxin Efflux and Vein Patterning in Arabidopsis. Plant Cell **18**: 1396–1411

Simon MLA, Platre MP, Assil S, Van Wijk R, Chen WY, Chory J, Dreux M, Munnik T, Jaillais Y (2014) A multi-colour/multi-affinity marker set to visualize phosphoinositide dynamics in Arabidopsis. Plant J **77**: 322–337

Stefano G, Renna L, Rossi M, Azzarello E, Pollastri S, Brandizzi F, Baluska F, Mancuso S (2010) AGD5 is a GTPase-activating protein at the trans-Golgi network. Plant J **64**: 790–799

Steinmann T, Geldner N, Grebe M, Mangold S, Jackson CL, Paris S, Gälweiler L, Palme K, Jürgens G (1999) Coordinated polar localization of auxin efflux carrier PIN1 by GNOM ARF GEF. Science **286**: 316–318

Steynen Q, Schultz EA (2003) The FORKED genes are essential for distal vein meeting in Arabidopsis. Development **130**: 4695–4708

Sukumar P, Legué V, Vayssières A, Martin F, Tuskan GA, Kalluri UC (2013) Involvement of auxin pathways in modulating root architecture during beneficial plant-microorganism interactions. Plant, Cell Environ **36**: 909–919

Swarup R, Friml J, Marchant A, Ljung K, Sandberg G, Palme K, Bennet M (2001) Localization of the auxin permease AUX1suggests two functionally distinct hormone transport pathways operate in the Arabidopsis root apex. Genes Dev **15**:

2648–2653

Szopa J, Sikorski F (1995) ARF-protein antisense potato displays stable ADP-ribosylation of 40 kDa protein. J Plant Physiol **145**: 383–386

Takai Y, Sasaki T, Matozaki T (2001) Small GTP-binding proteins. Physiol Rev **81**: 153–208

Takhtajan A (Ed.) (2009) *Flowering Plants*. Dordrecht: Springer Netherlands.

Tanaka H, Kitakura S, De Rycke R, De Groodt R, Friml J (2009) Fluorescence Imaging-Based Screen Identifies ARF GEF Component of Early Endosomal Trafficking. Curr Biol **19**: 391–397

Tanaka H, Nodzyński T, Kitakura S, Feraru MI, Sasabe M, Ishikawa T, Kleine-Vehn J, Kakimoto T, Friml J (2014) BEX1/ARF1A1C is required for BFA-sensitive recycling of PIN auxin transporters and auxin-mediated development in arabidopsis. Plant Cell Physiol **55**: 737–749

Tejos R, Sauer M, Vanneste S, Palacios-Gomez M, Li H, Heilmann M, Van Wijk R, Vermeer JEM, Heilmann I, Munnik T, et al (2014) Bipolar Plasma Membrane Distribution of Phosphoinositides and Their Requirement for Auxin-Mediated Cell Polarity and Patterning in Arabidopsis. Plant Cell **26**: 2114–2128

Trivett, ML, Pigg KB (1996) A survey of reticulate venation among fossil and living land pants. In Flowering Plant Origin, Evolution and Phylogeny (ed. D. W. Seldin and L. J. Hickey), pp. 8-31. New York: Chapman and Hall.

Tse YC, Mo B, Hillmer S, Zhao M, Lo SW, Robinson DG, Jiang L (2004) Identification of Multivesicular Bodies as Prevacuolar Compartments in Nicotiana tabacum BY-2 Cells. Plant Cell **16**: 672–693

Ueda T, Uemura T, Sato MH, Nakano A (2004) Functional differentiation of endosomes in Arabidopsis cells. Plant J **40**: 783–789

Vanneste S, Friml J (2009) Auxin: A Trigger for Change in Plant Development. Cell **136**: 1005–1016

Vasco A, Thadeo M, Conover M, Daly DC (2014) Preparation of Samples for Leaf Architecture Studies, A Method for Mounting Cleared Leaves. Appl Plant Sci **2**: 1-4

Verbelen JP, De Cnodder T, Le J, Vissenberg K, Baluška F (2006) The root apex of arabidopsis thaliana consists of four distinct zones of growth activities: Meristematic zone, transition zone, fast elongation zone and growth terminating zone. Plant Signal Behav **1**: 296–304

Vernoud V, Horton AC, Yang Z, Nielsen E (2003) Analysis of the Small GTPase Gene Superfamily of Arabidopsis. Plant Physiol **131**: 1191–1208

Verstraeten I, Schotte S, Geelen D (2014) Hypocotyl adventitious root organogenesis differs from lateral root development. Front Plant Sci **5**: 1–13

Vieten A, Vanneste S, Wisniewska J, Benkova E, Benjamins R, Beeckman T, Luschnig C, Friml J (2005) Functional redundancy of PIN proteins is accompanied by auxin-dependent cross-regulation of PIN expression. Development **132**: 4521–4531

Viotti C, Bubeck J, Stierhof Y-D, Krebs M, Langhans M, Van Den Berg W, Van Dongen W, Richter S, Geldner N, Takano J, et al (2010) Endocytic and Secretory Traffic in *Arabidopsis* Merge in the Trans-Golgi Network/Early Endosome, an Independent and Highly Dynamic Organelle. Plant Cell **22**: 1344–1357

Weijers D, Schlereth A, Ehrismann JS, Schwank G, Kientz M, Jürgens G (2006) Auxin triggers transient local signaling for cell specification in Arabidopsis embryogenesis. Dev Cell **10**: 265–270

Woodward AW, Bartel B (2005) Auxin: Regulation, action, and interaction. Ann Bot **95**: 707–735

Xu J, Scheres B (2005) Dissection of Arabidopsis ADP-RIBOSYLATION FACTOR 1 Function in Epidermal Cell Polarity. Plant Cell **17**: 525–536

Yorimitsu T, Sato K, Takeuchi M (2014) Molecular mechanisms of Sar/Arf GTPases in vesicular trafficking in yeast and plants. Front Plant Sci **5**: 1–12

APPENDIX I

LB liquid medium (1 L)
10 g Bacto-tryptone
5 g Yeast extract
10 g NaCl

LB medium (1 L)
10 g Bacto-tryptone
5 g Yeast extract
10 g NaCl
7 g Agar

Infiltration buffer for Agrobacterium injection
20 mM trisodium phosphate
500 mM 2-(N-morpholino) ethanesulfonic acid
200 mM acetosyringone in dimethyl sulfoxide
5 mg glucose/ml

Total DNA extraction buffer
1 Volume DNA extraction buffer*
1 Volume nucleic lysis buffer**
0.4 Volume 5% Sarkosyl
*DNA extraction buffer (500 mL)
31.8 g Sorbitol
6 g Trizma
0.84 g EDTA
Add HCl until pH reaches 7.5
**Nucleic lysis buffer
2 Volume 1M Trizma
1 Volume 0.5M EDTA
4 Volume 5M NaCl
2 Volume distilled water
20 g CTAB
Add HCl until PH reaches 7.5

APPENDIX II

Table AII: Cotyledon vein characteristics of different Arabidopsis genotypes after 10 days of growth on plates with or without BFA. Values reported are means ± standard deviations. Sample size is indicated within the parenthesis. Differences indicated by "a" are against 0 μM BFA treatment, and indicated by "b" are differences between 10 μM and 20 μM treatments. Sample size shown in brackets is the same for all characteristics, and is thereby only indicated in the first table. Values are means ± standard deviation.

Genotype	# VI (0 μM BFA)	# VI (10 μM BFA)	# Vascular Islands (20 BFA)
WT	0 (50)	0.02 ± 0.14 (54)	0.18 ± 0.46[a,b] (34)
fkd1	0.07 ± 0.26 (56)	0.04 ± 0.19 (27)	0 (12)
fl1	0.04 ± 0.19 (53)	0.04 ± 0.20 (48)	0.04 ± 0.19 (28)
fl2	0 (64)	0.07 ± 0.26[a] (41)	0.52 ± 0.89[a,b] (46)
fl3	0 (65)	0.06 ± 0.25[a] (63)	0.31 ± 0.75[a,b] (36)
fkd1/fl1-2	0.04 ± 0.20 (50)	0 (25)	0 (26)
fkd1/fl2	0.04 ± 0.19 (57)	0.1 ± 0.3 (40)	0.32 ± 0.61[a,b] (41)
fkd1/fl3	0.02 ± 0.13 (60)	0.12 ± 0.50 (43)	0.19 ± 0.54[a] (16)
fkd1/fl2/fl3	0.25 ± 0.53 (71)	0.27 ± 0.66 (52)	0.42 ± 0.61 (52)
fkd1/fl1-2/fl2/fl3	0.98 ± 0.95 (49)	1.24 ± 0.14 (61)	1.40 ± 1.16[a] (73)
fkd2	0 (92)	0.02 ± 0.14 (54)	0.03 ± 0.16 (39)
fkd1/fkd2	0.46 ± 0.67 (61)	0.60 ± 0.69 (43)	0.52 ± 0.65 (25)
arfa1a/b/d/e	0.02 ± 0.12 (66)	0.13 ± 0.33[a] (48)	0 (7)
cvp2/cvl1	4.14 ± 1.82 (74)	5.48 ± 2.18[a] (56)	4.96 ± 2.42[a] (45)

Genotype	# Secondary Veins (0 μM BFA)	# Secondary Veins (10 μM BFA)	# Secondary Veins (20 μM BFA)
WT	4.02 ± 0.25	3.96 ± 0.39	3.97 ± 0.52
fkd1	3.14 ± 0.77	3.19 ± 0.79	3.17 ± 0.83
fl1	3.51 ± 0.64	3.54 ± 0.65	3.39 ± 0.74
fl2	3.84 ± 0.44	3.78 ± 0.57	3.76 ± 0.64
fl3	3.94 ± 0.46	3.90 ± 0.50	3.61 ± 0.73[a,b]
fkd1/fl1-2	3.64 ± 0.66	3.08 ± 0.70[a]	3.23 ± 0.91[a]
fkd1/fl2	3.35 ± 0.69	3.45 ± 0.71	3.05 ± 0.84[b]
fkd1/fl3	2.67 ± 0.63	2.81 ± 0.82	2.75 ± 0.77
fkd1/fl2/fl3	2.14 ± 0.35	2.17 ± 0.43	2.21 ± 0.46
fkd1/fl1-2/fl2/fl3	2.06 ± 0.56	1.85 ± 0.48	1.96 ± 0.59
fkd2	2.28 ± 0.50	2.39 ± 0.56	2.28 ± 0.51
fkd1/fkd2	2.11 ± 0.37	2.07 ± 0.34	1.96 ± 0.2
arfa1a/b/d/e	3.86 ± 0.52	3.71 ± 0.46	3.71 ± 0.49
cvp2/cvl1	2.45 ± 0.62	2.16 ± 0.56[a]	2.47 ± 0.89[b]

Genotype	# Non-meeting Veins (0 μM BFA)	# Non-meeting Veins (10 μM BFA)	# Non-meeting Veins (20 μM BFA)
WT	0.94 ± 0.82	0.89 ± 0.69	1.18 ± 0.76
fkd1	2.54 ± 1.08	2.26 ± 1.02	2.75 ± 1.06
fl1	1.15 ± 0.74	0.92 ± 0.85	0.96 ± 0.69
fl2	1.09 ± 0.75	0.93 ± 0.69	1.20 ± 0.83
fl3	1.02 ± 0.80	1.13 ± 0.71	1.11 ± 0.82
fkd1/fl1-2	3.26 ± 0.94	2.52 ± 0.87[a]	3 ± 0.98[b]
fkd1/fl2	2.82 ± 0.83	2.85 ± 0.92	2.61 ± 1.05
fkd1/fl3	2.33 ± 0.77	2.50 ± 0.74	2.44 ± 1.03
fkd1/fl2/fl3	2.06 ± 0.44	2.08 ± 0.39	2.12 ± 0.51
fkd1/fl1-2/fl2/fl3	1.98 ± 0.63	1.85 ± 0.48	1.95 ± 0.57
fkd2	0.90 ± 0.74	0.94 ± 0.71	0.97 ± 0.87
fkd1/fkd2	2.07 ± 0.44	2.05 ± 0.30	1.88 ± 0.33[b]
arfa1a/b/d/e	1.20 ± 0.77	1.23 ± 0.75	0.86 ± 0.90
cvp2/cvl1	2.32 ± 0.62	2.13 ± 0.57	2.44 ± 0.92[b]

Genotype	# Meeting Veins (0 μM BFA)	# Meeting Veins (10 μM BFA)	# Meeting Veins (20 μM BFA)
WT	3.08 ± 0.80	3.07 ± 0.64	2.79 ± 0.73
fkd1	0.61 ± 0.71	0.93 ± 0.62[a]	0.42 ± 0.67[b]
fl1	2.36 ± 0.68	2.63 ± 0.76	2.43 ± 0.74
fl2	2.75 ± 0.76	2.85 ± 0.73	2.57 ± 0.65
fl3	2.92 ± 0.74	2.78 ± 0.66	2.5 ± 0.61[a,b]
fkd1/fl1-2	0.38 ± 0.57	0.56 ± 0.58	0.23 ± 0.43[b]
fkd1/fl2	0.53 ± 0.63	0.60 ± 0.67	0.44 ± 0.71
fkd1/fl3	0.33 ± 0.60	0.33 ± 0.47	0.31 ± 0.48
fkd1/fl2/fl3	0.08 ± 0.28	0.10 ± 0.36	0.10 ± 0.36
fkd1/fl1-2/fl2/fl3	0.08 ± 0.34	0	0.01 ± 0.12
fkd2	1.38 ± 0.64	1.44 ± 0.66	1.31 ± 0.69
fkd1/fkd2	0.05 ± 0.22	0.02 ± 0.15	0.08 ± 0.28
arfa1a/b/d/e	2.67 ± 0.77	2.48 ± 0.74	2.86 ± 0.90
cvp2/cvl1	0.12 ± 0.62	0.04 ± 0.27	0.02 ± 0.15

APPENDIX III

Supplementary graph: Total root length and lateral root density of different Arabidopsis genotypes after 9 days of growth. [a] indicates significantly different from WT, [bi] indicates significantly different from the corresponding single mutant labelled as [*bi*], [c] indicates significantly different from both single mutants, [d] indicates significantly different from the other member labelled as [*d*], [e] indicates significantly different from all other *fl* members. See Table 10 for values and additional root parameters. Error bars indicate the standard error.